# Characterization of an Encapsulation Platform for pH-sensitive Delivery to the Colon

by Madison Miller

B.Eng., University of Victoria, 2021

A Thesis Submitted in Partial Fulfillment of the Requirements for the Degree of

MASTER OF APPLIED SCIENCE in the Department of Mechanical Engineering

# Characterization of an Encapsulation Platform for pH-sensitive Delivery to the Colon

by Madison Miller

B.Sc., University of Victoria, 2021

Supervisory Committee

Dr. Mina Hoorfar, Supervisor

Department of Mechanical Engineering

Dr. Mohsen Akbari, Departmental Member

Department of Mechanical Engineering

# Abstract

Targeted delivery of bioactive molecules to specific locations within the GI tract allows for better orally delivered therapies, as the molecules will only be released upon reaching the desired absorption or delivery location. Targeted delivery aids in protecting the bioactivity of sensitive cargo as it traverses the GI tract, allows for smaller dosages to be administered and, in some cases, can reduce side effects. In this study, a microfluidic droplet generation platform is designed for production of pH-sensitive microcapsules for targeted delivery of bioactive molecules to the colon. Optical microscopy is used to compare the size distributions of microcapsules generated on-chip and those generated through a simple bulk double emulsion. Scanning electron microscopy is used to characterize the microcapsule morphology. To test the pH-sensitive nature of the microcapsules, they are loaded with dyed microparticles to mimic micron-sized bioactive cargo being interlocked in the polymeric capsule matrix. Their release in acidic and neutral solution is then analyzed, to simulate exposure to the stomach and colon. A preliminary study is then completed using E. coli DH5 alpha as the capsule payload. Results show that a maximum of $7.8 \pm 2.0\%$ of the encapsulated microparticles are released in acidic medium, while a maximum of $70.7 \pm 3.7\%$ are released in neutral solution after 6 hours of exposure, thus confirming the pH-sensitive characteristics of the microcapsules (based on results across 3 trials). Finally, capsules were loaded with E. coli and exposed to both neutral and acidic solution. After 6 hours, 0 viable CFU/ml were recorded, and in neutral solution $5.56 \times 10^6 \pm 0.9 \times 10^6$, $2.6 \times 10^7 \pm 1.8 \times 10^6$ and $2.2 \times 10^8 \pm 2.4 \times 10^7$ CFU/ml were released across 3 trials, corresponding to a maximum viability of $1.37 \pm 0.15\%$. These results were supported by a zeta potential study, which also showed targeted release in neutral solution, and minimal change in zeta potential for capsules in acidic solution. Although these results support the pH-sensitive properties of the microcapsules, they indicate incompatibility of the platform with live cargo. Future work for this study includes testing the capsules with other bioactive cargo, such as vitamins, minerals, and pharmaceuticals, and altering the capsule structure for better compatibility with live bacteria.

# Table of Contents


***Supervisory Committee*** ..... ***ii***

***Abstract*** ..... ***iii***

***Table of Contents*** ..... ***iv***

***List of Figures*** ..... ***vi***

***List of Tables*** ..... ***vii***

***List of Abbreviations*** ..... ***viii***

***Acknowledgements*** ..... ***ix***

***Dedication*** ..... ***x***

***Chapter 1: Introduction*** ..... ***1***

**1.1 Motivation: Applications of pH-Targeted Delivery to the GI tract** ..... **1**

1.1.1 Pharmaceuticals ..... 1

1.1.2 Nutraceuticals and Food Supplements ..... 1

1.1.3 Bacteria/probiotics ..... 2

**1.2 Review of Literature on pH-Targeted Drug Delivery Systems** ..... **2**

1.2.1 Principles of pH-targeted Delivery to the GI Tract ..... 3

1.2.2 Material Selection for pH-Targeted Delivery to the Small Intestine and Colon ..... 4

1.2.3 Past Works in pH-Sensitive Encapsulation of Bioactive Molecules ..... 8

**1.3 Challenges and Limitations of Existing pH-Targeted Delivery** ..... **12**

**1.4 Microfluidics for Controlled and Precise Encapsulation** ..... **13**

1.4.1 Principles of Microfluidic Droplet Generation ..... 13

1.4.2 Common Channel Structures for Microfluidic Droplet Generation ..... 15

**1.5 Review of Capsule Structures** ..... **19**

1.5.1 Continuous Droplets (Beads) ..... 19

1.5.2 Single Core-shell ..... 19

1.5.3 Multilayer Structures ..... 20

**1.6 Thesis Objective** ..... **20**

***Chapter 2: Materials and Methods*** ..... ***21***

**2.1 Material Selection for pH-Sensitive Encapsulation** ..... **21**

2.1.1 In-depth look into Eudragit Polymers ..... 21

2.1.2 Preliminary Tests of Selected Formulations ..... 23

**2.2 Design of a Microfluidic Droplet Generation Platform for Targeted Delivery to the Colon** ..... **26**

2.2.1 Microfluidic Droplet Generation Platform Chip Design ..... 26

2.2.2 Microfluidic Droplet Generation Platform Fabrication ..... 27

2.2.3 Treatment to Generate Hydrophilic Channels for Double Emulsion ..... 29

2.2.4 Functionality of the Microfluidic Droplet Generation Platform ..... 30

***Chapter 3: Characterization of Microcapsules Generated On-Chip*** ..... ***32***

**3.1 Optical Microscopy Imaging** ..... **32**

3.1.1 Size Distribution ..... 32

3.1.2 Sphericity Analysis ..... 34

**3.2 SEM Imaging** ..... **35**

*Chapter 4: In vitro Release Study of pH-sensitive Characteristics – Proof of Concept* ..... *37*
**4.1 Overview of *In Vitro* Release Procedure** ..... **37**
**4.2 *In Vitro* pH-Sensitive Release Results and Discussion** ..... **38**
4.2.1 Results ..... 38
4.2.2 Discussion ..... 42
*Chapter 5: Case Study – Encapsulation and pH-sensitive Release of E. Coli* ..... *43*
**5.1 Confirmation of Bacterial Compatibility with the Encapsulation Process** ..... **43**
**5.2 Overview of Bacterial Encapsulation Procedure** ..... **44**
**5.3 In vitro pH-sensitive Release Results and Discussion** ..... **45**
5.3.1 Results ..... 45
5.3.2 Discussion ..... 49
*Chapter 6: Conclusions and Future Work* ..... *52*
**6.1 Conclusions** ..... **52**
**6.2 Future Work** ..... **53**
**6.3 Contributions** ..... **53**
*Chapter 7: References* ..... *54*
*Appendix A : Spot Plating Protocol* ..... *A-1*
*Appendix B : Microparticle Detection Python Code* ..... *B-1*
**B.1: Particle Counting Function** ..... **B-1**
**B.2: Snippet of Function Call** ..... **B-2**
**B.3: Example of Particle Detection** ..... **B-2**

# List of Figures

Figure 1: Overview of human GI tract environment by Hua et al (2020, 2015) [1], [11]. ..... 3
Figure 2: T-junction flow profile [93] ..... 16
Figure 3: Multi-emulsion T-junction microfluidic device [85] ..... 16
Figure 4: Flow-focusing junction geometry example by Fu et al. [97] ..... 18
Figure 5: Overview of three common encapsulation structures; (a) microbeads, (b) single core-shell, and (c) multilayer core-shell. ..... 19
Figure 6: Comparison of different polymers for encapsulation ..... 21
Figure 7: Release location and pH triggers for Eudragit polymers (made in Biorender) ..... 22
Figure 8: Depiction of Eudragit S100 cross-linking for phage encapsulation by Vinner et al [66]. ..... 23
Figure 9: Cross-chip channel design and dimensions (mm) ..... 27
Figure 10: T-junction chip channel design and dimensions (mm) ..... 27
Figure 11: Completed resin mold ..... 28
Figure 12: (a-c) Hydrophilic channel treatment procedure by Bauer et al. [89], (d) Treated channel in finalized T-junction chip. ..... 29
Figure 13: Graphical depiction of double emulsion pre- and post-crosslinking ..... 30
Figure 14: Double emulsion formulation on-chip ..... 31
Figure 15: (a) Microcapsules generated on-chip, 10X magnification; (b) Size distribution from microfluidic particles; (c) Microcapsules generated through bulk emulsion, 10X magnification; (d) Size distribution from bulk particles. ..... 32
Figure 16: Bulk vs microfluidic histogram for size distribution ..... 34
Figure 17: Bulk vs microfluidic sphericity histogram ..... 35
Figure 18: SEM images of microcapsules formulated (a) on microfluidic chip and (b) through bulk emulsion. ..... 36
Figure 19 (a-c): Release of encapsulated microparticles in acidic and neutral solution across three trials. ..... 38
Figure 20: Release of dyed microparticles in neutral (left) and acidic (right) solution. ..... 39
Figure 21: Microparticle release in acidic, neutral and basic solution ..... 40
Figure 22: P-value denoting statistical difference between 3 trials. ..... 41
Figure 23: F-statistic denoting statistical difference between 3 trials. ..... 41
Figure 24: Bacterial compatibility with Eudragit S100 and L100-55 polymers ..... 43
Figure 25: Zone of inhibition study (0.1 M HCl applied to spread-plated E. coli) ..... 44
Figure 26 (a-c): Released CFU/ml in neutral and acidic solution across three trials (log scale). ..... 47
Figure 27 (a-c): Percent of encapsulated bacteria released in neutral and acidic solution across three trials. ..... 48
Figure 28: Zeta potential analysis results grouped by pH ..... 49

Figure B 1: Full-size image ..... B-3
Figure B 2: Cropped image ..... B-3
Figure B 3: Cropped image with median brightness subtracted off ..... B-4
Figure B 4: Gaussian smoothing to generate relative brightness ..... B-4
Figure B 5: Image with Gaussian blur removed ..... B-5
Figure B 6: Binary image with detected particles based on threshold ..... B-5
Figure B 7: Detected particles (circled in red) based on size and shape parameters ..... B-6

# List of Tables

Table 1: Past works in pH-targeted delivery of bioactive molecules with natural polymers. .....8
Table 2: Past works in controlled delivery of bioactive molecules using synthetic polymers. .....9
Table 3: Advantages and disadvantages of bulk capsule formulation techniques .....12
Table 4: Microparticle formulation compositions .....23
Table 5: Comparison of microparticles formulated from different polymer compositions. .....24
Table 6: Microfluidic chip flow rates .....30
Table 7: Microfluidic vs bulk particle size distribution parameters .....33
Table 8: Calculation of maximum released bacteria for each experiment .....46
Table 9: Calculation of encapsulation efficiency .....46
Table 10: Zeta potential study results .....48

# List of Abbreviations

| | |
|---|---|
| ANOVA | Analysis of variance |
| CFU | Colony-forming unit |
| DI | Deionized (water) |
| DOX | Doxorubicin |
| GI | Gastro-intestinal |
| LB | Lysogeny broth |
| MP | Microparticle |
| PAA | Poly(acrylic acid) |
| PAH | Poly(allylamine hydrochloride) |
| PBS | Phosphate buffered saline |
| PCL | Poly(caprolactone) |
| PEG | Poly(ethylene glycol) |
| PEI | Poly(ethylenimine) |
| PEM | Poly-electrolyte multilayer |
| PG | Poly(glycerol) |
| PLGA | Poly(lactic-co-glycolic acid) |
| PSS | Poly(4-styrene sulfonate) |
| PTFE | Poly(tetrafluoroethylene) |

# Acknowledgements

First and foremost, I would like to thank my supervisor, Dr. Mina Hoorfar, for her continued support and encouragement throughout my graduate degree. It is due to her support that I was able to pursue a project I am passionate about and extend its scope into entrepreneurship. I would also like to thank Nishat Tasnim for her support as a colleague and mentor, and for accompanying me during late bacterial culture experiments. Finally, I would like to thank Emily Earl and Dr. Somayeh Fardindoost for their assistance and encouragement in bringing this project to fruition.

# Dedication

This thesis is dedicated to my family: John, Kathy and Ireland Miller. It is due to their support that I have made it to this point in my academic journey. Their lighthearted humour and encouragement to look forward kept me afloat during difficult times.

My thesis is also dedicated to my partner Dori Blakely. I could not have completed this degree without his support: scientific, moral, and emotional. As two students starting our graduate degrees, I could not have imagined a better culmination of two years of hard work than the life we share today.

# Chapter 1: Introduction

## 1.1 Motivation: Applications of pH-Targeted Delivery to the GI tract

The use of pH-sensitive polymers as taste-masking, enteric or colonic coatings is very common in drug delivery. The following section outlines some applications of pH-sensitive polymers for delivery of bacteria, pharmaceuticals, and nutraceuticals to the stomach, small intestine, or colon.

### 1.1.1 Pharmaceuticals

pH-targeted delivery has been used extensively for orally administered pharmaceuticals. Targeted delivery is typically used to bypass the digestive enzymes and acidic environment of the stomach with minimal drug loss and degradation. The small intestine is the most common location for targeted delivery of pharmaceuticals to be delivered systemically; most nutrient and drug absorption occurs here due to the organ's large surface area [1]. One example of this is pH-mediated delivery of insulin to the small intestine for treatment of diabetes mellitus [2].

There are also applications where targeted delivery of pharmaceuticals to the stomach or colon would be highly beneficial. In the case of the stomach, targeted drug delivery could be applied for H. pylori infection therapies, antacids and treatments for gastric ulcers, such as misoprostol [3]. Drugs that can benefit from targeted delivery to the colon include inflammatory bowel disease (IBD) therapies (mesalazine, sulfasalazine and other prodrugs) and colorectal cancer therapies [4].

### 1.1.2 Nutraceuticals and Food Supplements

As stated by Puri et al., "nutraceuticals include pro- and pre-biotic foodstuff and food for special medical uses; and food supplements includes single or combinations of mineral, vitamins, protein supplements, functional foods and herbal products" [5]. They represent concentrated versions of nutrients that can be consumed through a well-balanced diet [6]. Most nutraceuticals are absorbed in the small intestine, again owing to its large surface area. A common problem with delivery of these compounds is degradation and loss of bioactivity prior to reaching the absorption site within the gastrointestinal (GI) tract, due to their plant-based origin [6]. This category of food-sourced products with health benefits could thus highly benefit from the use of pH-targeted delivery to preserve the bioactivity of the active ingredients. Although these compounds are not traditional drugs, they have shown promising positive effects on disease treatment, including omega-3 fatty acids for treatment of cardiovascular diseases, curcumin for cancer therapies and carotenoids for protective skin treatments [5]. Product efficiency and in vivo absorption can be maximized by

applying pH-sensitive coatings to protect the above compounds through the harsh gastric environment.

### 1.1.3 Bacteria/probiotics

Oral delivery of live bacterial cells has been explored at length for therapeutic purposes. The GI tract of mammals is populated with a number of bacterial strains, which maintain a carefully regulated flora to promote the host's health [7]. However, this balance can be disturbed by infection or disease and thus can require treatment to restore the natural flora. The colon, specifically, can benefit from the delivery of therapeutic bacteria. Colon-targeted bacteria-based therapies have been explored to treat "Crohn's disease (ileitis or enteritis), diverticulitis, ulcerative colitis, irritable bowel syndrome (IBS), colonic dysmotility, and colon cancer" [7]. Inflammatory bowel diseases (IBD) in general have increasingly become cause for concern in North America, with prevalence amongst the population surpassing 0.3%, adding substantial costs to the healthcare system [8]. With oral dosage deemed the best administration method for live cells for IBD therapies, delivery vehicles for IBD treatment are thus an important topic of research [7].

Although bacteria and probiotics are covered under the umbrella of nutraceuticals, there are important considerations to be taken for live cargo that differ from the requirements for other functional foods or bioactive compounds. Live bacteria can be administered orally for many health-related reasons, with lactic acid bacteria (LAB) most commonly used as probiotics [7], [9]. In addition to the colonic diseases outlined above, probiotics have been studied to treat rotavirus diarrhea, H. pylori-caused gastric ulcers and collagenous colitis [7]. Specific pH-targeted delivery is advantageous for these applications as the bacteria can be locally delivered to the region where therapy is needed.

Cell viability is an important concern in therapeutic administration of bacterial cells. The transit through the GI tract involves exposure to highly acidic fluid, digestive enzymes and other mechanical and chemical stressors that can kill free bacteria before they reach the desired therapeutic location. It is thus necessary to incorporate protective measures within the delivery vehicles (capsules) to preserve cell viability. One way to do this is utilizing a pH-sensitive material within the capsules to limit stomach acid exposure, and to trigger bacteria release from the capsule in response to reaching the desired pH level of the target release location.

## 1.2 Review of Literature on pH-Targeted Drug Delivery Systems

The following sections provide a review of the important considerations involved in the design and selection of pH-targeted drug delivery systems. The highly variable environment of the GI tract is first explained, and an overview is provided for a variety of natural and synthetic materials

that are suitable for pH-sensitive drug delivery. Finally, past works and research in the field of targeted drug delivery are listed.

### 1.2.1 Principles of pH-targeted Delivery to the GI Tract

To successfully reach a specific region in the GI tract, the orally administered capsule must remain intact throughout each of the distinct environments within the GI tract prior to its target. The capsule will first traverse the mouth and esophagus. It then reaches the stomach, where the pH can range between 0-2 in a fasted state and the ingested contents can remain in the stomach between 0-2 hours [1]. However, in a fed state these values increase to a pH range of 2-6 and transit time of 2-6 hours [1]. The capsule will then enter the small intestine, with a pH ranging from 6-7.4 [1]. Here, transit takes 2-6 hours (typically 3-4 hours) and the majority of nutrient and drug absorption occurs; thus, it is a common target location for drug delivery [1], [10]. Finally, the capsule travels to the colon (pH ranging from 5-7), where water absorption and remaining nutrient absorption will take place during the highly variable 6-70 hour transit time [1]. The general environmental conditions experienced at each region of the GI tract are illustrated in Figure 1 below.

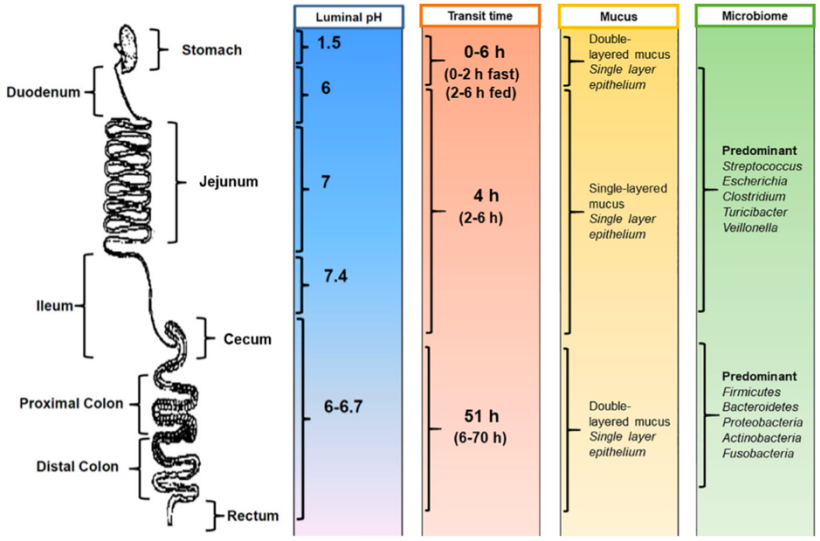


*Figure 1: Overview of human GI tract environment by Hua et al (2020, 2015)* [1], [11].

One well-understood challenge of formulating pH-responsive capsules for targeted delivery is achieving this targeted delivery to a specific location. Due to the variability of pH levels throughout the GI tract, both inherent with the system itself and variability amongst different individuals, it is difficult to select a material that can deliver its payload to the exact desired location [12]. For example, the optimal dissolution pH for successful colonic delivery is 6.4 [12], but the true pH of the colon can vary between pH values of 5-7 [10]. The variation in gastric emptying time between different individuals also contributes to this issue and increases difficulty in developing a standardized coating [13]. The presence of digestive enzymes and the long transit time from oral

administration to the colon are also important considerations that can complicate targeted colonic delivery [14].

### 1.2.2 Material Selection for pH-Targeted Delivery to the Small Intestine and Colon

Protective materials play a significant role in therapeutic efficacy to shield the capsule payload from the harsh conditions experienced throughout the GI tract. To deliver the payload to specific locations within the GI tract, the protective material must be tuned to degrade in response to a certain stimulus unique to the desired delivery location. In the case of GI delivery, this stimulus is often a specific pH level. Each protective material thus has favorable aspects and limitations in different pH levels, each requiring a specific design. Among various materials, polymers that degrade at a specific pH have been recognized as the most attractive, mainly due to their potential for solid formulations with long shelf lives, sustained delivery, ease of administration and biocompatibility. The following section reviews different protective materials as well as the advantages and disadvantages of each one.

#### *1.2.2.1 Overview of Common Natural Polymers*

Natural polymers are materials that are derived from naturally occurring sources, such as algae, crustaceans, and other various plant, seed and animal sources [15]. Some examples of such materials include carboxymethyl hexanoyl chitosan, hydroxyapatite, whey proteins or calcium carbonate [16]–[19]. These materials have a wide range of structures, with proteins and polysaccharides most used as encapsulating matrices. The following sections provide an overview of some common polysaccharides and proteins used for encapsulation of orally delivered bioactive molecules.

**Polysaccharides**

Polysaccharides are complex carbohydrate structures that can be derived from a variety of sources. They share the advantageous properties of biocompatibility and relative low cost, and some polysaccharides exhibit pH-dependent dissolution. Some polysaccharides commonly employed in targeted delivery applications are discussed below.

**Alginate**

Alginate, an anionic polysaccharide derived from brown algae, is composed of D-mannuronic acid (M) and L-guluronic acid (G) blocks and will cross-link ionically when exposed to divalent cations [20]. It is a popular selection for controlled delivery applications due to its biocompatibility, pH sensitivity and mucoadhesive properties [20]–[24]. The pH sensitivity of alginate causes the polymer to shrink at low pH levels and swell at neutral or slightly alkaline pH levels, releasing the encapsulated agent as the hydrogel swells [25]. However, in targeted delivery applications, alginate

is typically used in tandem with another polymer, as its highly hydrophilic nature can result in payload loss during encapsulation [26]. Further, due to the polymer's pKa value of 3.5, premature degradation could occur in the stomach if the pH is increased in a fasted state [26].

**Chitosan**

Chitosan is a cationic polysaccharide that can be obtained through the deacetylation of chitin, which is the primary material of the exoskeleton of crustaceans, cuticles of insects and cell wall of fungi [23], [27]. Due to its positive charge, it can be cross-linked with negatively charged cross-linking agents, such as tripolyphosphate (TPP), citrate, sulfate, and phosphate [20]. It also exhibits pH-dependent solubility and biocompatible mucoadhesive properties, making it suitable for oral delivery of active molecules. Chitosan is particularly suitable for drug delivery to the stomach, as it will degrade in response to the protonation of its amino groups that occurs at a lower pH range ($pH < 6$) [28], [29]. However, significant research has also been pursued in formulations combining chitosan with other polymers for drug delivery to the intestine, to retain the advantageous mucoadhesiveness, antimicrobial and low immunogenicity properties of chitosan [28].

**Cellulose**

Cellulose is a rigid, polar polysaccharide found in the cell wall of plants, composed of D-glucose residues [20]. Cellulose-based polymers are particularly useful for colonic delivery of active molecules as they are readily degraded in the colon by the residing cellulolytic bacteria [30]. However, native cellulose molecules are insoluble in water and cannot be digested within the human GI tract, and thus are not suitable for applications requiring a degrading matrix [20], [31]. Native cellulose can only be degraded in strong acidic or alkaline aqueous solutions, and thus cellulose-based polymers have been derived to produce a degradable formulation [32]. Some common cellulose derivatives that have been used for targeted oral delivery of active molecules are carboxymethyl cellulose (CMC), methylcellulose (MC) and hydroxypropyl methylcellulose (HPMC) copolymers [20], [33].

**Gums**

Gums, derived from a variety of plant sources, are polysaccharides that have been widely used in controlled oral drug delivery applications, either alone as the encapsulating matrix or as a component of a composite material. Guar gum, is highly stable through the pH range of approximately 3.5-9, but can be readily degraded by microbes residing in the large intestine, making it suitable for colonic delivery [34]. Similarly, xanthan gum remains intact in the stomach and small intestine, but is degraded by the colonic microflora [35]. Gums can also be combined with other polymers to generate pH-sensitive properties, such as Zhang et al.'s work in reacting xanthan gum and cysteamine tetra-hydrazine to create a pH and redox-sensitive nanogel [36].

Although alone they lack pH-sensitive properties, gum Arabic [37], gellan gum [38], [39], xanthan gum [40] and guar gum [41], [42] have also all been incorporated in oral drug delivery applications.

**Proteins**

Proteins, and protein-based polymer composites, are biocompatible, non-toxic, naturally-sourced encapsulation materials that have been widely used in biomedical applications [43]. Both animal-sourced (collagen, gelatin, fibrin, keratin, silk) and plant-sourced proteins (soy protein, whey protein, zein) have shown promise in encapsulation-based applications [43]. Although native protein molecules do not demonstrate pH-responsive swelling, protein-based polymers and hydrogels have shown promise in the area, such as a keratin-based smart hydrogel, where the maximum swelling is observed at a pH of 8 [44].

**Gelatin**

Gelatin is an animal-derived protein composed of a variety of polypeptide chains that exhibits temperature-dependent gelation, gelling at temperatures below 40ºC and becoming a viscous fluid at higher temperatures [20]. It has also been cross-linked using physical methods beyond temperature such as pH or UV irradiation, and various chemical or biological agents including formaldehyde, glutaraldehyde, genipin and enzymes [45]. Although gelatin will not exhibit pH-sensitive degradation on its own, it can be combined with different monomers such as poly-acrylic acid to produce this degradation profile [46].

**Whey Protein**

Whey protein is derived from milk, and is primarily composed of β-lactoglobulin and 6α-lactalbumins [47]. Whey protein isolate (protein content exceeding 90%) has commonly been used to encapsulate hydrophobic drugs, and can enhance the bioavailability of poorly soluble drugs due to its mucoadhesive properties [48]. Although whey protein does not exhibit pH-dependent solubility, its main component β-lactoglobulin is resistant to pepsin (an enzyme in the stomach) and thus whey protein-based particles can protect their payload from the harsh gastric environment [49].

### *1.2.2.2 Overview of Common Synthetic Polymers*

Synthetic polymers are another potential selection for controlled oral delivery of active molecules and are advantageous due to the customizability of their properties during formulation. Some common synthetic polymers used for encapsulation are polyethers, with PEG being the most popular, and a variety of acrylate or acrylic acid-based polymers [50]–[52].

**Polyethers**

Polyethers refer to the wider group of polymers that have ether functional groups in their backbone. The most common and popular polyether in drug delivery applications, poly(ethylene glycol) (PEG), provides some important benefits for oral drug delivery applications, including being non-toxic, biocompatible, and water-soluble [53]. In fact, "PEGylation" of microparticles is very common to enhance absorption and avoid undesired interactions in vivo, often coined the stealth effect [53]. However, as the polymer does not degrade in the body, it can accumulate within organs as the molar mass of the polymer increases [53]. Other alternative polyethers that have been used for drug delivery applications are poly(propylene glycol) (PPG) and poly(glycerol) (PG) [53].

**Poly(methacrylate)-based polymers: Eudragit**

Eudragit® polymers are a family of methacrylate-based polymers suited for controlled release of drugs or other particle payloads [50]. For pH-triggered delivery, there are three main categories of the polymer family. Eudragit E, a cationic polymer, dissolves at pH levels below 5.5 and is suitable for applications in taste-masking as it is soluble in the gastric fluid of the stomach [50]. Eudragit L is an anionic polymer that dissolves at pH levels above 6, making it suitable for drug delivery to the intestines through oral administration [50]. Similarly, Eudragit S is an anionic polymer with a dissolution pH of 7 and above, making it suitable for colonic delivery applications [50]. The different Eudragit grades can also be combined at different ratios to produce a polymer that degrades at a specific desired pH between the degradation pH of the two components [54], [55].

This family of polymers can be applied through several fabrication methods. As mentioned above, there are specific formulations that can be used to deliver payloads to the stomach, small intestine and colon based on pH changes. One known issue, however, is variation in pH and gastric emptying time between different patients, as the solubility of the polymer will vary based on exposure time and the pH of the environment [13]. To overcome this issue researchers have paired Eudragit (S and FS-30D, respectively) with starch [56] or guar gum [57] for microbial degradation to occur alongside pH-based dissolution [13].

**Poly(acrylic acid)**

Poly (acrylic acid) (PAA) is an anionic polymer that has been widely used in medical, pharmaceutical, food processing and cosmetic applications [58]. The pH-sensitive nature of the polymer is caused by protonation of carboxyl groups at acidic pH, leading to strong hydrogen bonding, and deprotonation at neutral pH results in polymer swelling and payload release [58]. Another beneficial property of PAA is its bioadhesiveness; it can stick to the mucosal lining within the small intestine, which can optimize delivery and absorption of therapeutic molecules [59].

**Kollicoat® MAE Polymer Series**

Kollicoat, a series of polymers sold by BASF Pharma, also have a dedicated series of enteric polymers (MAE 100P, MAE 100-55 and MAE DP) [60]. These polymers allow for targeted drug delivery, with the polymers degrading at pH levels exceeding 5.5 [60]. The polymers are anionic and allow for payload protection through the stomach and dissolution in the small intestine. They can be made as aqueous or organic dispersions and are commonly used in film-coating applications for enteric delivery [61].

### 1.2.3 Past Works in pH-Sensitive Encapsulation of Bioactive Molecules

Table 1 provides a summary of some relevant encapsulation-based applications of a variety of natural polymers with pH-sensitive properties and different coating methods.

*Table 1: Past works in pH-targeted delivery of bioactive molecules with natural polymers.*

| Technique | Coating Method | Encapsulated substance | Matrix substance | Shell material | Application | Source |
|---|---|---|---|---|---|---|
| Microfluidic | Microfluidic droplet and electrostatic droplet formation | Diclofenac in alginate core | Ampiphillin-loaded chitosan | - | Dual-loaded oral drug delivery | Yang 2014 [62] |
| | Microfluidic emulsification | Gelatin + Vitamin A | Sodium alginate | - | Oral drug delivery to intestine | Huang 2014 [24] |
| Bulk emulsion | Emulsion cross-linking | Bovine serum albumin | Guar gum and methacrylic acid | - | Controlled oral delivery to colon | Sharma 2013 [41] |
| | Emulsion cross-linking | Budesonide | Guar gum | - | Controlled oral delivery to colon | Liu 2015 [42] |
| | Ionotropic gelation and sonication | Rifampicin | Sodium alginate + cellulose nanocrystals | - | Controlled oral delivery within GI tract | Thomas 2018 [63] |
| Extrusion | Ionotropic gelation | Progesterone | Low methoxy amidated pectin and sodium | - | Controlled oral delivery to colon | Gadalla 2016 [64] |

| | | | | | | |
|---|---|---|---|---|---|---|
| | | | carboxymethyl cellulose (LMAP/NaCMC) | | | |
| | Ionotropic gelation | Progesterone | Zinc pectinate and chitosan | - | Controlled oral delivery to colon | Gadalla 2015 [65] |
| Use of external forces | Electrospinning then electrospraying | DOX and *withania coagulans* | Chitosan | Starch | Controlled delivery of hydrophobic and hydrophilic agents to the SI or colon | Sampath kumar 2018 [6] |
| Tablet coating | Dried macroscale gel tablets | Caffeine | Whey protein concentrate | Sodium alginate | pH-controlled release of bioactive agents | Gunasekaran 2006 [19] |

Table 2 provides an overview of a variety of methods in which synthetic polymers were applied to deliver small molecules through the digestive tract.

*Table 2: Past works in controlled delivery of bioactive molecules using synthetic polymers.*

| **Technique** | **Coating method** | **Encapsulated substance** | **Matrix substance** | **Shell material** | **Application** | **Source** |
|---|---|---|---|---|---|---|
| **Microfluidic** | W/O emulsion | Clostridium difficile bacteriophages | Eudragit S100 | - | pH-triggered delivery of phages to colon | Vinner 2017 [66] |
| | W/O emulsion followed by spraying | TNF-alpha antisense oligonucleotide | GelMA | Eudragit FS30D | pH-triggered release of ASO to colon for IBD treatment | Gan 2021 [67] |
| | Two-stage W/O/W emulsion | Hydrophobic anti-cancer drugs | Hydrophobically- | Eudragit FS30D | Colon-targeted oral delivery of | Hasani-Sadrabadi 2016 [68] |

| | | | | | | |
|---|---|---|---|---|---|---|
| | | | modified chitosan | | anticancer drugs | |
| | Ultrasonic enhanced microfluidic system | Repaglinide | Ethylcellulose and Eudragit RSPO | - | Controlled oral delivery of diabetes drugs to GI tract | Shrimal 2022 [69] |
| **Loaded particle coating** | Lyophilization | Lactase | Eudragit L100-55 | Eudragit EPO (cationic coating) | Controlled oral drug delivery to intestine | Homayun 2018 [70] |
| | Multi-emulsion solvent evaporation | Insulin | Porous PLGA | Eudragit L30D | Controlled oral delivery of insulin to small intestine | Naha 2008 [71] |
| | Emulsion followed by solvent evaporation | Metronidazole | Chitosan | Eudragit L100 or S100 | Controlled oral drug delivery to colon | Chourasia 2004 [72] |
| | Multi-emulsion followed by solvent evaporation | Aceclofenac | Chitosan | Eudragit L100 or S100 | Controlled oral drug delivery to colon | Umadevi 2010 [73] |
| | Emulsion-dehydration and solvent evaporation | Metronidazole | Pectin | Eudragit S100 | Controlled oral drug delivery to colon | Vaidya 2009 [74] |
| | Complex coacervation, extrusion into cross-linker and fluidized bed coating | Oxytetracycline | Alginate/chitosan | Acryl-EZE® MP | Controlled oral drug delivery to GI tract | Kleinubing 2014 [75] |
| | Dual-step spray drying | Budesonide | Chitosan and alginate | Eudragit S100 | Controlled drug delivery to | Crcarevska 2009 [76] |

| | | | | | | |
|---|---|---|---|---|---|---|
| | | | | | colon for IBD treatment | |
| | Pan coating | Prednisolone | Zein | Zein + Kollicoat ® MAE 100P | Controlled oral delivery to colon | Nguyen 2019 [54] |
| | Extrusion-spheronization then fluidized bed coating | Metronizadole | Chitosan and cellulose | Kollicoat SR 30 D, Kollicoat 30 and Kollicoat MAE 30 DP | Controlled oral drug delivery to colon | Ferrari 2013 [77] |
| **Tablet coating** | Spray coating | Mesalazine | lactose monohydrate | Eudragit L100-55 & Eudragit S100 | Controlled oral drug delivery to colon | Khan 2000 [55] |
| | Compression coating then dip coating | Mesalamine | Talc, magnesium stearate, dibasic calcium phosphate dihydrate, sodium starch glycolate | Hydroxypropyl methylcellulose, then Eudragit L100 | Controlled oral drug delivery to colon | Patel 2008 [12] |
| | Wet granulation and compression followed by fluidized bed coating | Aceclofenac | Xanthan gum | Eudragit L100 & Eudragit S100 | Controlled oral drug delivery to colon | Ramasamy 2011 [35] |
| | Dip-coating (2-4x) | Ibuprofen | Mesoporous silica tablet | Eudragit S100 | Controlled oral drug delivery to small intestine | Xu 2011 [78] |

## 1.3 Challenges and Limitations of Existing pH-Targeted Delivery

The most common ways these polymers are utilized in industry are in spray or film coating of macroscale tablets containing active pharmaceutical ingredients (APIs), which is commonly done using a fluidized bed apparatus [61]. However, the applications and compatibilities of pH-sensitive materials and coatings are limited in production at industrial scale. For example, the cost of implementing and applying a pH-sensitive coating is sometimes more expensive than loading a larger dosage into a capsule, and thus companies opt to administer higher dosages knowing that the entire payload will not be absorbed. This results in an inefficient product that can cause uncomfortable side effects for the user.

Industrial techniques for encapsulating different medications or active molecules within pH-sensitive polymers operate under the governing principles of efficient production and high throughput. These factors (characteristic of bulk production techniques) allow companies to maximize profit but do not provide the same level of specificity and control and the monodisperse product offered by microfluidic techniques. Table 3 compares some common formulation methodologies used in industry to create protective, pH-sensitive capsules for orally delivered active molecules.

*Table 3: Advantages and disadvantages of bulk capsule formulation techniques*

| Formulation method | Advantages | Disadvantages |
|---|---|---|
| **Extrusion** | • Requires relatively simple equipment<br>• Typically inexpensive<br>• Gentle - compatible with sensitive payloads | • Low throughput<br>• Not suitable for all fluid types<br>• Can subject encapsulated agent to mechanical stress |
| **Spray chilling** | • High yield<br>• Inexpensive after one-time purchase of apparatus<br>• Avoids the use of high temperatures and harsh chemicals<br>• Particles have a smooth, spherical surface | • Variation amongst produced capsules<br>• Payload can be expelled during spray chilling process<br>• Not suitable for encapsulated agents sensitive to low temperatures<br>• Limited encapsulation materials |
| **Spray drying** | • High yield<br>• Inexpensive after one-time purchase of apparatus<br>• Fast encapsulation | • Exposes encapsulated agents to high temperatures.<br>• Loss of product along chamber walls<br>• Variation amongst produced capsules<br>• Limited encapsulation materials<br>• Can create particles with an irregular porous surface |

| | | |
|---|---|---|
| | | • Non-uniform conditions in drying chamber |
| **Fluidized bed** | • Suitable for a wider variety of coating materials than spray drying/chilling<br>• Lower temperatures than spray drying<br>• Coating thickness is easily controlled with process parameters<br>• Relatively high yield and fast production<br>• Low cost after initial purchase | • Difficult to avoid particle agglomeration (clumping)<br>• Geographic conditions can affect encapsulation efficiency (Weather effect) [79] |
| **Bulk emulsion** | • Higher throughput than microfluidic emulsions<br>• There is a variety of different methods available and suitable for many applications<br>• Can form a wide range of particle sizes | • Particle size cannot be precisely controlled<br>• Restricted to immiscible fluids<br>• Some methods require harsh chemicals (solvent evaporation) |
| **Dip/Film/Spray Coating** | • Good control over coating layer thickness<br>• Compatible with a wide range of coating materials<br>• Multiple coatings can easily be added sequentially | • Not suitable for formulating particles<br>• Can only be used for solid particles (not droplets)<br>• No control over individual (micro/nanoscale) particles |

## 1.4 Microfluidics for Controlled and Precise Encapsulation

This section provides a review of important equations, concepts, and considerations in microfluidics-based encapsulation.

### 1.4.1 Principles of Microfluidic Droplet Generation

Microfluidics involves the manipulation of microscale volumes of fluids, in the context of this thesis, as a method of formulation of small droplets. Fluids are typically pumped into microscale channels and the resultant fluid dynamics on-chip will passively produce microscale capsules. External forces, such as electrical fields or acoustic vibrations can be applied to the apparatus to actively formulate the particles. However, to create microcapsules through this process, the fluids must not mix, which can be accomplished through fluid emulsification.

An emulsion involves the combination of two immiscible fluids to form droplets. The carrier fluid is typically referred to as the continuous phase, while the fluid composing the droplet is called the

dispersed phase. In the case of microfluidic emulsions, the respective phases are fed in through different channels with specified flow rates based on intended capsule size. Different channel configurations can be designed, and various flow regimes can be realized based on the desired product. Some common channel geometries and flow regimes are discussed in the following sections.

The performance of microfluidic devices is highly dependent on geometrical properties, fluid flow rates, and the wettability of microfluidic channels [80]. The Reynolds, capillary and Weber numbers can be employed to characterize flow profiles. First, the Reynolds number is defined as the ratio of inertial fluid forces to viscous forces:

$$Re = \frac{\rho v l}{\eta},$$

*Equation 1: Reynolds Number*

where $\rho$ is the density of the fluid, $v$ is the velocity, l is the characteristic length scale of the channel and $\eta$ is the fluid viscosity [81]. The Reynolds number describes the flow as being either laminar or turbulent, with the transition from laminar to turbulent flow commonly defined to occur between Re ~ 2100 [82]. However, for microfluidic applications, the Reynolds number is typically on the order of 10 or smaller, thus inducing laminar flow [83]. The capillary number measures the viscous forces the fluid experiences with respect to interfacial surface tension [81]. It is defined as

$$Ca = \frac{\eta U}{\gamma},$$

*Equation 2: Capillary number*

where $\eta$ is the fluid viscosity, U is the fluid velocity and $\gamma$ is the interfacial tension force [81]. The capillary number is especially important in microfluidic applications for characterizing the interactions between the dispersed and continuous phases entering a chip.

Finally, the Weber number provides a ratio of the inertial forces with respect to the interfacial tension experienced by two fluids in contact. The Weber number can be described by the following equation,

$$We = \frac{\rho L U^2}{\gamma}$$

*Equation 3: Weber number*

Where $\rho$ is the fluid density, L is the characteristic length scale, U is the fluid velocity and $\gamma$ is the interfacial tension [84].

Another important consideration for microfluidic-based emulsions is the surface properties of the channels. Emulsions, having distinct dispersed and continuous phases, require the dispersed phase

to be carried down the center of the channel, and thus the channel hydrophobicity or hydrophilicity must be compatible with that of the carrier fluid. There are hydrophobic (PDMS) and hydrophilic (glass, quartz) options for the chip material, but typically both hydrophobic and hydrophilic regions are needed on a single chip. A controlled patterning method and suitable material is thus required. One example of a hydrophobic treatment is silane coupling on the hydrophilic Pyrex glass [85]. Hydrophilic modification of PDMS is a more difficult procedure due to its inert nature, but can be accomplished through a "plasma polymerized acrylic acid (PPAA) coating method", "a photoreactive sol-gel coating, in combination with grafted poly(acrylic acid)" or "layer-by-layer deposition of polyelectrolytes" [86]–[89].

Emulsion on microfluidic chip as an encapsulation technique provides the advantages of, first, high precision and control with regards to flow rates, input volumes, pressures, and chip geometry [81], [90]. This high level of control results in highly monodisperse products with little variation amongst the capsules. Microfluidic experiments are also highly tailorable, as reagents can be swapped out easily and chip geometry can be quickly altered using modelling software. Further, in microfluidics the produced particles are not limited to solely spherical droplets; research has been pursued in producing "moon-shaped, dendritic and toroidal particles" as well [91]. Given that droplets are produced one at a time through a single stream, modules can also be added to image each individual droplet and view its contents and morphology. This also contributes to the high level of control over individual droplets. Other additions, such as a camera counting droplet production or equipment added to sense certain droplet parameters are highly effective in microfluidic applications. However, one inherent disadvantage of classic microfluidic devices is their low production volume and speed, encompassing both chip fabrication and droplet formulation [92]. For industrial applications, the high throughput of bulk techniques will often outweigh the high specificity and monodisperse production of microfluidic techniques. Adjustments such as parallel chip operation can be made to increase production, but throughput will still be lower than production through bulk encapsulation techniques.

### 1.4.2 Common Channel Structures for Microfluidic Droplet Generation

There are a variety of suitable methods and materials to be used for chip fabrication and droplet generation, but some selections have an abundance of proof of functionality in the literature and are thus preferred. For example, PDMS is a common material selection due to its cost-effective and inert nature, and the ease of manufacturing. Further, T-junction and flow-focusing channel structures are both well-defined common selections for a PDMS-based microfluidic chip. The following sections review these channel structures.

### *1.4.2.1 T-Junction*

A T-junction microfluidic device involves the dispersed phase meeting the continuous phase at a 90-degree angle, as shown in Figure 2. The geometry of the channels can be fully defined based on three parameters: the width of the continuous phase channel (w), the width of the dispersed phase channel ($w_{in}$) and the height of all channels (h) [93]. The size of the formed droplets is thus highly dependent on this geometry as well as both the pressure gradient and the flow rates of the two fluids [93]. One advantage of the use of T-junction microfluidic junctions is that only two channels interact at the junction, as opposed to three in flow-focusing geometries, thus resulting in a less complex meeting of the input fluids.

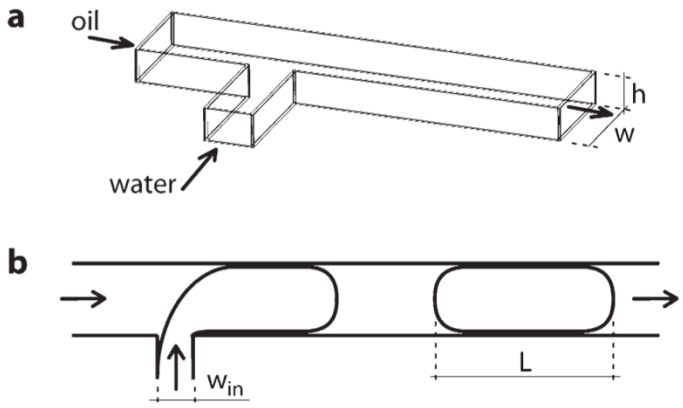


*Figure 2: T-junction flow profile* [93]

T-junction-based microfluidic devices can also be used to create multiple emulsions by implementing sequential T-shaped intersections. Okushima et al. formulated double emulsions using a sequential T-junction chip, as shown in Figure 3. The apparatus allowed for the formulation of either single or multiple-core droplets, and showed the importance of channel surface treatments in microfluidic applications [85].

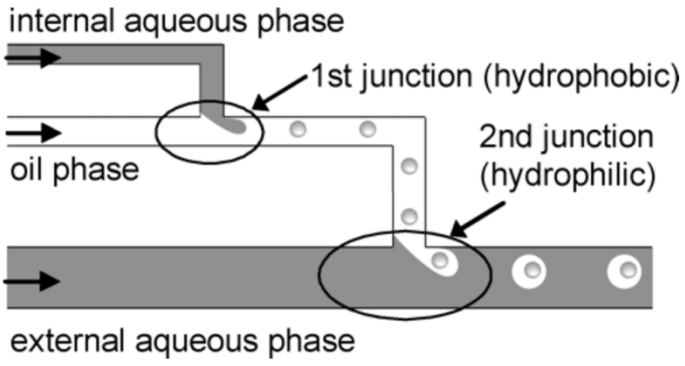


*Figure 3: Multi-emulsion T-junction microfluidic device* [85]

Three distinct flow regimes can be observed for a T-junction channel structure: squeezing, dripping and jetting [81]. In the squeezing regime, the continuous phase flow rate (henceforth referred to as $Q_c$) is low, and the hydrodynamic (or static) pressure will increases with inflow of the dispersed phase [81]. This pressure will squeeze off a droplet of the dispersed phase from its inflow channel, creating a plug whose dimensions are dependent on the flow rate ratio of the dispersed phase and continuous phase ($Q_d/Q_c$) [81].

In comparison, the dripping regime will begin once the capillary number of the continuous phase (denoted as $Ca_c$) reaches a critical value. This value is dependent on "channel size, flow rate ratio and viscosity ratio" of the two phases, and literature has shown the critical $Ca_c$ value can range from 0.003-1 [81]. Where in the squeezing flow droplet break-off is induced by pressure drop, in the dripping regime shear stress will induce droplet formation from the dispersed phase inflow. Also, the produced droplet size is highly dependent on viscosity ratio and decreases with $Ca_c$ [81].

Finally, the jetting regime denotes parallel flow of the two streams, and can be produced by increasing both flow rates and tailoring the flow rate ratio [81]. The droplets will be pinched off from the dispersed phase further downstream from the junction compared to squeezing and dripping flow profiles as the jetted stream is relatively stable until Rayleigh instability causes its break-off [81].

#### *1.4.2.2 Flow-focusing*

A flow-focusing system, as shown in Figure 4, involves the use of a small orifice to induce droplet formation as both the dispersed phase and two continuous phase inputs flow through it [81]. The droplet will be pinched off from the dispersed phase stream either within or past the narrow junction, with the two continuous phase streams meeting the dispersed phase at a 90º angle [81]. Different orientations of the three input channels can be employed, such as three parallel channels flowing towards the orifice, as demonstrated by Zhu et al. [94]. Moon et al. used a flow focusing system with a simple cross-shaped junction, without a small orifice, to produce water-in-water, aqueous two phase system droplets [95].

Flow-focusing systems can also be used to create multiple emulsions by adding focusing junctions in sequence, each introducing a fluid immiscible with the previous fluid to the device. For example, Abate et al. successfully produced up to quintuple emulsions using a sequence of flow-focusing junctions with water and (HFE-7500) fluorocarbon oil as alternating inputs [96]. Each droplet was successfully encapsulated at the following junction as the junctions were "hydrodynamically coupled using triggered droplet formation", meaning that "[each nozzle] is slightly narrower than the incoming emulsion from the previous drop maker" to block the nozzle until the new droplet is formed [96].

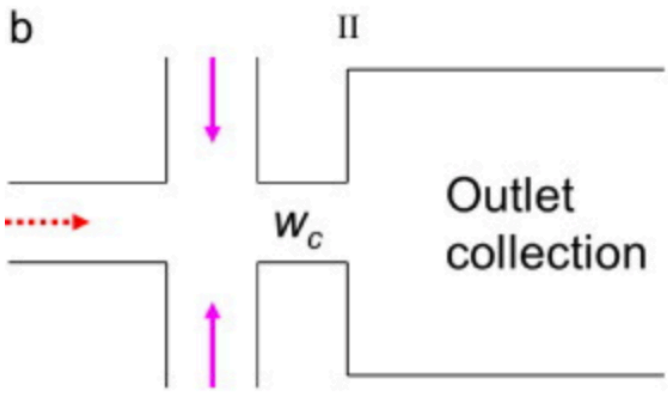


*Figure 4: Flow-focusing junction geometry example by Fu et al.* [97]

The $Ca_c$ can be used to characterize the droplet breakup and flow characteristics of the device. Again, three distinct flow profiles can be observed as the $Ca_c$ value is changed: squeezing, dripping or jetting [81]. A fourth method of droplet breakup, as observed by Anna et al., was called "thread formation", or "tip-streaming", which is controlled by device geometry and occurs at low capillary numbers [98]. In the squeezing regime, the dispersed phase will fully fill the narrow junction, with the lack of space for the continuous phase causing a high pressure past the junction. This pressure forces a droplet to be broken off at the junction [81].

In the dripping case, which corresponds to a higher $Ca_c$, the formed droplets are smaller than the narrow junction diameter and the dispersed phase does not fully fill the junction. It is instead focused through the center of the junction, allowing a stream of the continuous phase to flow on either side. This breakup can be attributed to both Rayleigh instability and shear forces, and the droplets will break off from the stream once it is sufficiently elongated [81].

Finally, in the jetting regime, the $Ca_c$ is increased beyond the dripping regime and the droplet breakup occurs further downstream from the junction. The jetting regime is characterized by a longer dispersed phase stream due to the higher velocity, and the breakup is due to Rayleigh instability, which occurs when "the length of the jet increases to be comparable to its radius" [81].

Zhu et al. (2015) observed a fifth method of droplet breakup, which they named "tip-multi-breaking" [94]. In this method, several droplets are observed to break off from the inner phase stream, with the number of droplets dependent on the capillary number for both phases. Their device also employed vibration as a perturbation to the inner phase tubing prior to injection into the device to observe how vibration amplitude and frequency affects droplet breakup. Their device combined both flow-focusing and co-flow geometries by injecting the dispersed phase through a capillary into a focusing orifice alongside the continuous phase [99].

Bazban-Shotorbani et al. used a flow-focusing device to formulate alginate microdroplets for controlled oral drug delivery, and found that by manipulating flow rates and channel lengths they

were able to tune the pore size of alginate to enhance its drug retention [100]. Their work showed that the implications of selected flow ratios extended beyond just particle size.

## 1.5 Review of Capsule Structures

This section reviews some suitable capsule particle structures for emulsion-based encapsulation and targeted drug delivery. Figure 5 provides an illustration of the three main droplet structures described below.

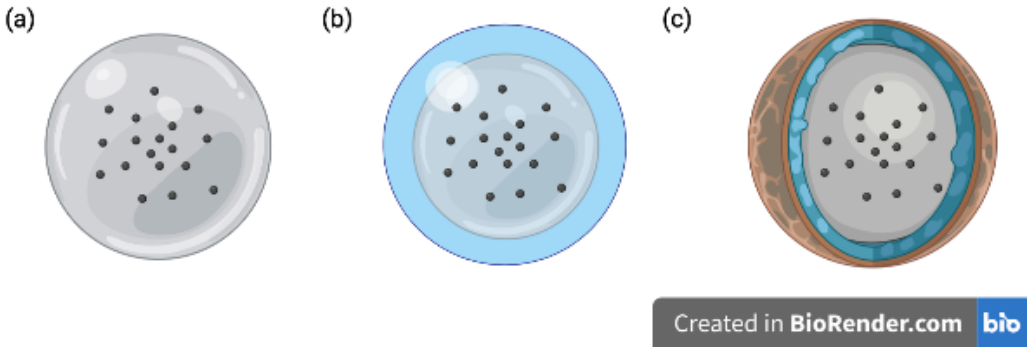


*Figure 5: Overview of three common encapsulation structures; (a) microbeads, (b) single core-shell, and (c) multilayer core-shell.*

### 1.5.1 Continuous Droplets (Beads)

Continuous droplets, or beads, are structures where the desired final product is a spherical droplet with the same composition throughout the matrix. Different materials can be used to compose the droplet, and active molecules can be dispersed throughout the matrix, but the droplet composition must be the same throughout the entire structure. Examples of relevant previous controlled delivery applications using continuous droplet structures include stimuli-responsive microgels loaded with proteins [101] and bacteriophages dispersed throughout a pH-sensitive polymer droplet for delivery to the colon to therapeutic purposes [66].

### 1.5.2 Single Core-shell

Single-layer core-shell structures are characterized by a distinct shell protecting an inner core from its surrounding environment. These particles can be formed through droplet microfluidics, emulsions, fluidized bed encapsulation, spray drying, spray chilling, and several other methods. For emulsion-based methods, the two fluids combined must be immiscible to avoid accidental mixing of the core and shell. For formulation through droplet microfluidics, a dual-emulsion is created, such as water-in-oil-in-water, oil-in-water-in-oil or a selection of immiscible aqueous fluids as used in two-phase aqueous systems. The structure may have a single inner core per outer shell, or multiple cores encapsulated in each droplet. Qi et al. developed a “self-double-

emulsifying drug delivery system", where water-in-oil-in-water double emulsions are spontaneously formed through a mixture of "hydrophilic surfactants and water-in-oil emulsions" upon entering the acidic environment of the stomach [102]. Drugs are encapsulated in the inner aqueous phase and either single or multiple aqueous cores per oil shell can be synthesized [102]. Yang et al. synthesized microcapsules of a similar structure, utilizing a chitosan shell to encapsulate alginate microparticles. The alginate core(s) were loaded with diclofenac and the chitosan shell was loaded with ampicillin, and the cationic nature of chitosan facilitated drug release in the acidic environment of the stomach [62].

### 1.5.3 Multilayer Structures

Multilayer core-shell structures, in contrast, have a distinct inner core that is enveloped by multiple shell layers. For capsules with multiple cores, the cores are often suspended within an inner matrix, with additional layers surrounding this matrix. For single core, multilayer structures, the core is enveloped within multiple shells of varying thicknesses. These multilayer structures can be fabricated through multi-step emulsions (for example, $W_1/O_1/W_2/O_2$) using bulk techniques, microfluidic techniques [96], [103], [104] or through sequential coating methods such as fluidized beds. Research has also been pursued to formulate all-aqueous particles through multiple emulsions [105]. Further, they are not required to solely be composed of liquid phases. Chen et al. fabricated gas-in-oil-in-water-in-oil emulsified particles where the drug release can be triggered by ultrasonic stimuli due to the gaseous core [106]. Both hydrophobic or hydrophilic drugs can be loaded within the sequential fluidic layers of the particle, allowing for the triggered delivery of multiple active agents by a single particle [106].

## 1.6 Thesis Objective

The objective of this work is to design an encapsulation platform for controlled delivery of bioactive compounds to the colon. Targeted delivery to the colon was pursued as most nutraceuticals and pharmaceuticals are delivered to and absorbed by the small intestine, resulting in a significant number of studies in the area. Colonic delivery is less common, but still presents a desirable target for controlled delivery, especially for cargo such as bacteria, or therapies for colonic diseases. Capsules are generated through an emulsion-based technique on microfluidic chip to explore the advantages and drawbacks of microfluidic formulation over traditional bulk encapsulation techniques. Materials are selected to enact targeted delivery to the colon, utilizing the inherent pH variation of the GI tract as a stimulus for particle dissolution and release. An *in vitro* release study is conducted to confirm the targeted release capabilities of the capsules. Finally, a case study is pursued where E. coli alpha is loaded into the capsules, to present a potential use case for the encapsulation platform in industry.

# Chapter 2: Materials and Methods

Chapter 2 reviews the materials selected for pH-sensitive encapsulation, the tests performed to support this selection, and the methodology employed through the microfluidic chip design, fabrication and troubleshooting process.

## 2.1 Material Selection for pH-Sensitive Encapsulation

Three metrics were identified to compare polymers for use in pH-sensitive delivery applications: water solubility, biocompatibility, and variable pH-dependent solubility. The results of this analysis are shown in Figure 6, with poly(acrylic acid) and the Eudragit suite of polymers satisfying all three metrics. From these two choices, the Eudragit polymers were selected for further analysis, given the wide range of products available and their prior use in the field.

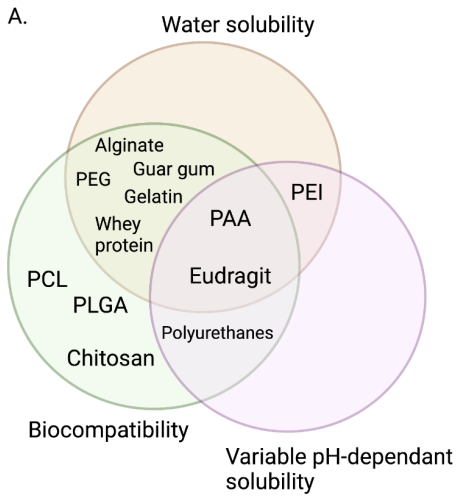


*Figure 6: Comparison of different polymers for encapsulation*

### 2.1.1 In-depth look into Eudragit Polymers

After the Eudragit polymers were selected for further research, the different formulations were analyzed to determine the optimal product for enteric targeting.

To begin, Eudragit E is a cationic copolymer composed of a "dimethylaminoethyl methacrylate, butyl methacrylate, and methyl methacrylate" blend [13]. It is soluble in gastric fluid (up to a maximum pH of 5). Eudragit E thus has applications in taste masking as it can bypass the neutral environment of the mouth and esophagus without degrading. Next, Eudragit L100 and L100-55 are suitable for delivery payloads to the small intestine; they degrade at and above pH levels of 6 and 5.5, respectively. Eudragit S100 is used to target the colon, degrading above pH levels of 7. All Eudragit L and S polymers are anionic, and their formulation ratios are altered to manipulate

the pH trigger point. For example, Eudragit L100 is composed of a 1:1 ratio of methacrylic acid and methyl methacrylate, while Eudragit S100 utilizes the same polymers at a ratio of 1:2 [13]. Eudragit L100-55 uses a 1:1 ratio of methacrylic acid and ethyl acrylate [13]. Figure 7 depicts the dissolution location of the Eudragit polymers within the human GI tract.

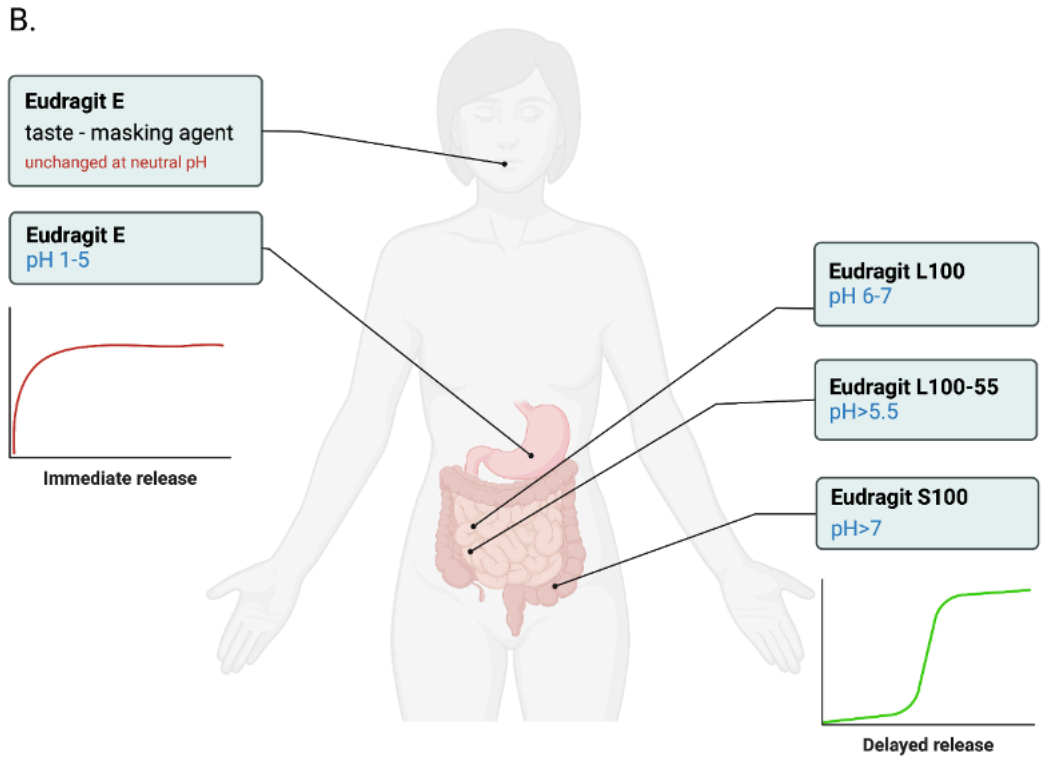


*Figure 7: Release location and pH triggers for Eudragit polymers (made in Biorender)*

The pH-triggered dissolution characteristic is dependent on the presence of carboxylic groups within the polymers. For the enteric polymers, carboxylic groups are converted to carboxylate upon exposure to pH 6 or 7 fluids (for Eudragit L100 and S100, respectively) [13]. This deprotonation lowers the degree of hydrogen bonding which causes the polymer network to disentangle. This process is illustrated in Figure 8, specifically for the Eudragit S100 polymer. The payload depicted is bacteriophages, with the research conducted by Vinner et al [66].

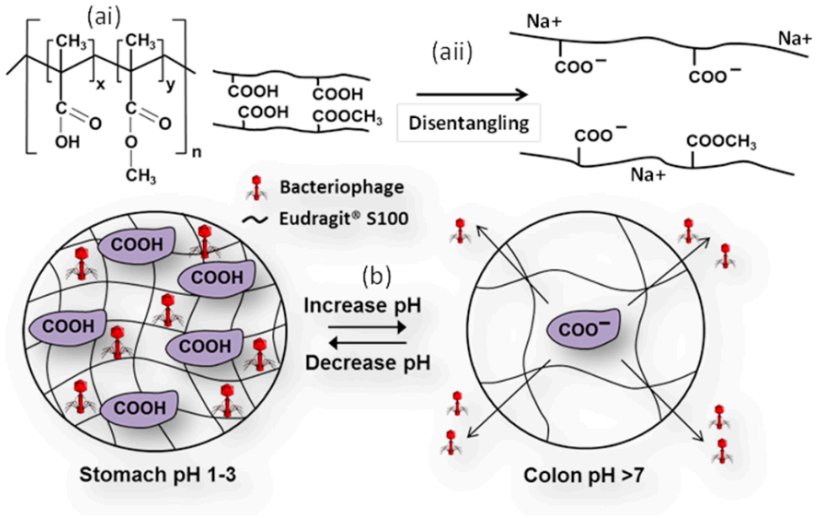


*Figure 8: Depiction of Eudragit S100 cross-linking for phage encapsulation by Vinner et al* [66].

### 2.1.2 Preliminary Tests of Selected Formulations

Several different combinations and concentrations of polymers were quantitatively and qualitatively analyzed to determine the optimal formulation for our approach. As colonic delivery is desired, Eudragit S100 was selected as the desired pH-sensitive material, and alginate was identified as a potential additive based on its mucoadhesive properties and extensive use in tandem with Eudragit polymers. First, the viscosity of several formulations was measured using a viscometer. The results of these tests, and the composition of each formulation, can be seen in Table 4. It should be noted that all formulations are dissolved in DI water.

*Table 4: Microparticle formulation compositions*

| Formulation # | ES100 % | Alginate % | Viscosity (mPa s g/cm3) | Temperature (ºC) |
|---|---|---|---|---|
| 1 | 1 | 2 | 18.32 | 19.66 |
| 2 | 1 | 0 | 7.48 | 20.49 |
| 3 | 2 | 2 | 10.01 | 20.42 |
| 4 | 2 | 0 | 5.58 | 20.2 |
| 5 | 5 | 2 | 43.59 | 20.06 |
| 6 | 5 | 0 | 13.92 | 20.2 |
| 7 | 10 | 2 | 10.24 | 20.34 |
| 8 | 10 | 0 | 34.61 | 20.3 |
| 9 | 20 | 2 | 1077.86 | 20.45 |
| 10 | 20 | 0 | 497.28 | 20.38 |

The formulations were also qualitatively compared based on their ease of preparation. Aqueous suspensions of Eudragit are produced by dissolving the polymer powder in DI water, creating an acidic, opaque liquid. 1 M NaOH is then added slowly until the solution turns clear, indicating that the polymer has fully dissolved, and the pH has been neutralized. However, this process is very difficult for higher concentrations (10% and 20%) of Eudragit as a large volume of NaOH is required to neutralize the solution, thus resulting in a heavily diluted solution with a high pH. The resultant higher pH also inhibits cross-linking with pH 1 HCl for both 10% and 20% solutions. Formulations 7-10 were thus excluded from further consideration.

Polymers were also compared qualitatively based on the ability to formulate and manipulate microcapsules and their appearance post-crosslinking, as shown in Table 5. For this test, particles were formulated through a bulk emulsion. In brief, 20 ml of the inner aqueous phase formulation selected from Table 4 was poured into 100 ml of mineral oil with 2% Span 80. This single emulsion was then left to stir (using a magnetic stir bar) at 200 rpm for five minutes. This emulsion was then poured into 400 ml of 0.1 M HCl with 2% Tween 80 and left to stir at 300 rpm for 15 minutes, thus creating a double (W/O/W) emulsion.

For formulations solely composed of Eudragit, the capsules appeared “filmy” and were difficult to move and manipulate. However, the addition of alginate provided the formulations with more “bulk”, thus providing a more robust, spherical capsules. The Eudragit content of the formulation also influenced cross-linking strength – the lowest concentration of 1% did not fully cross-link. Table 5 shows particles from each formulation (colour was added for easy differentiation between formulations).

*Table 5: Comparison of microparticles formulated from different polymer compositions.*

| | No alginate | 2% alginate |
|---|---|---|
| 1% ES100 | 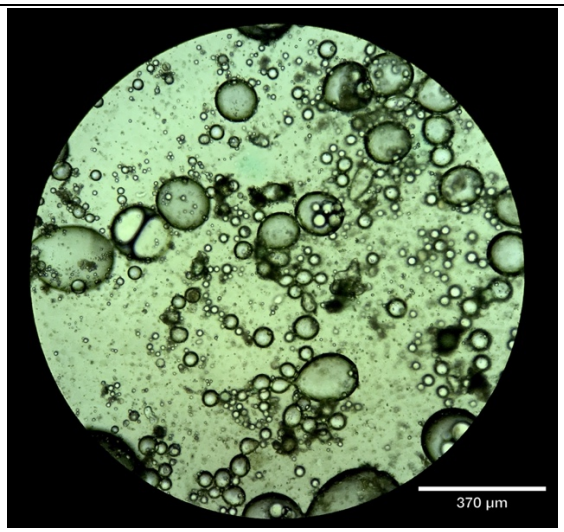 | 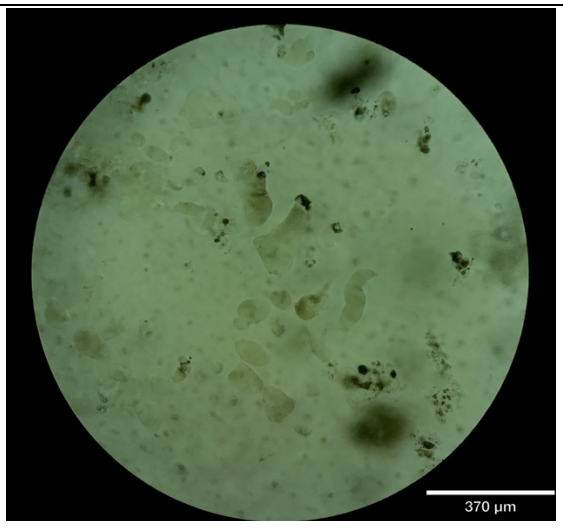 |

| | | |
|---|---|---|
| 2% ES100 | 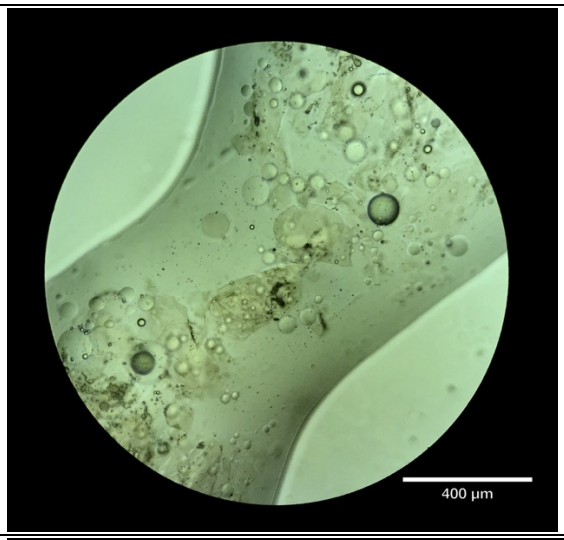 | 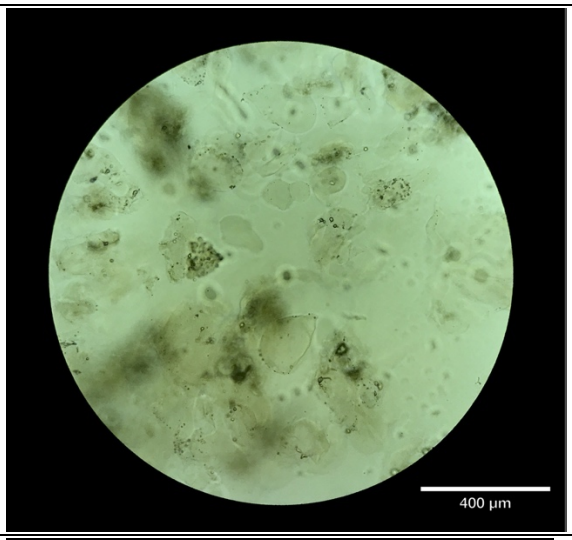 |
| 5% ES100 | 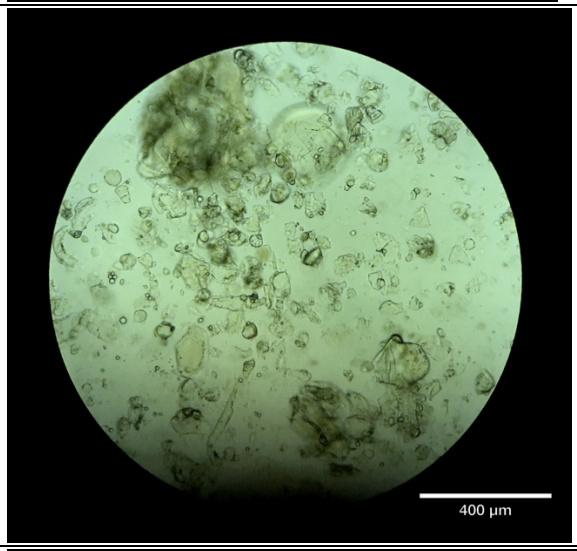 | 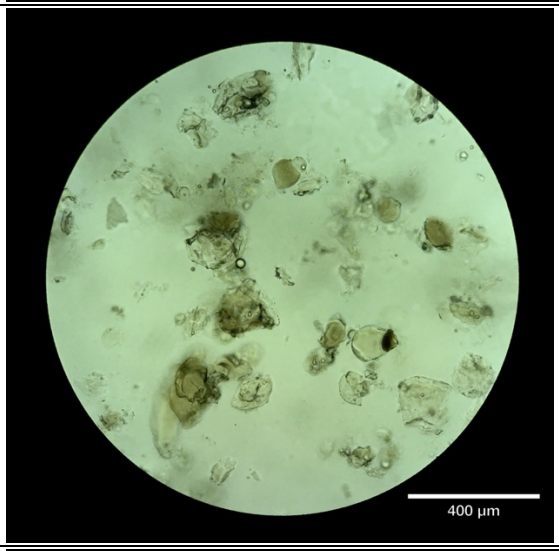 |
| 10% ES100 | 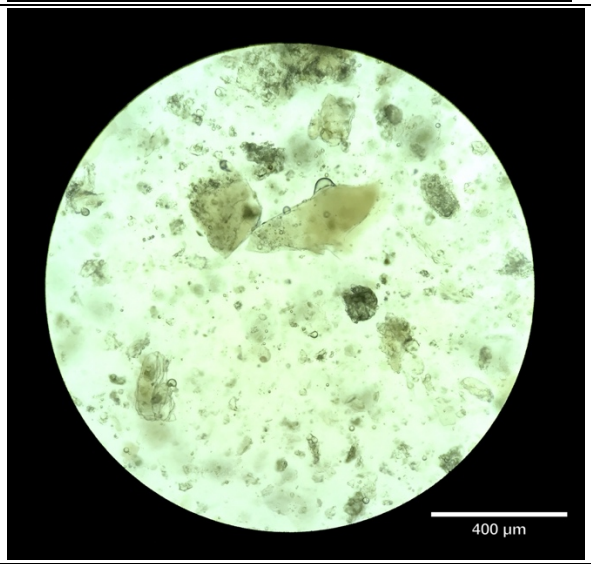 | 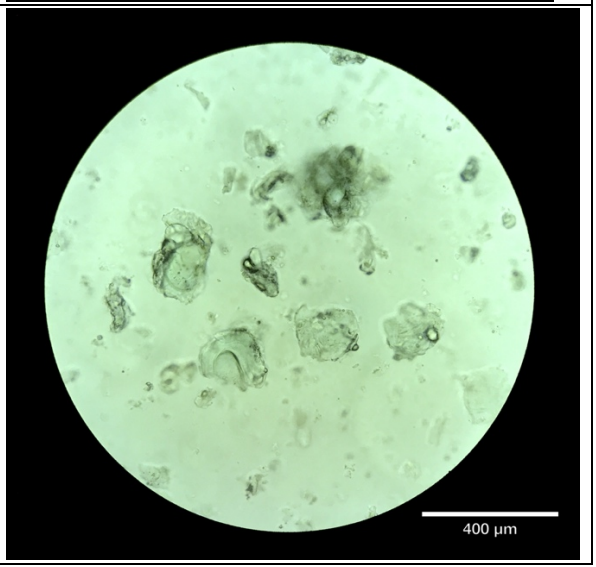 |

| | | |
|---|---|---|
| 20% ES100 | 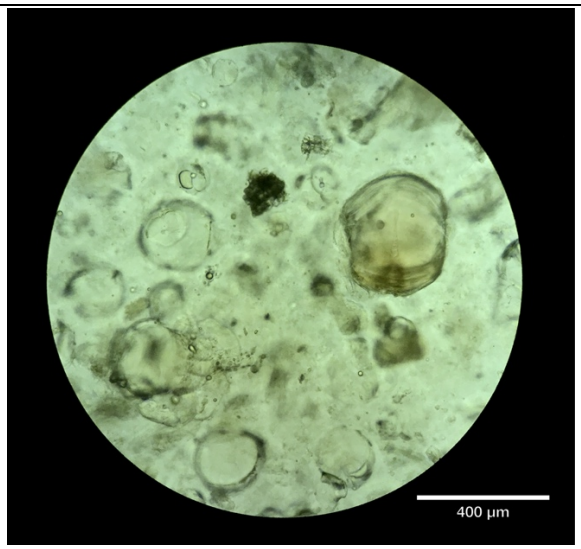 | 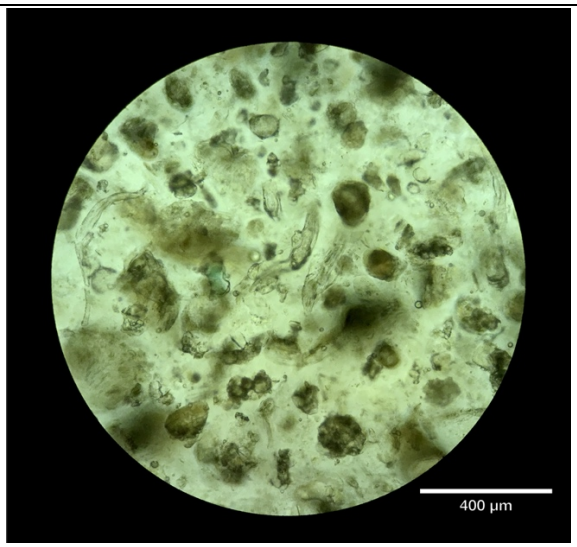 |

Based on the above evaluations, formulations 4 and 6 were determined to be the two best alternatives for pH-sensitive particles. Upon testing on-chip, it was found that the more viscous formulation 6 (5% ES100, 2% alginate) was more prone to jetting and disturbing the synchronized droplet-making junctions. Formulation 4 was thus selected as the optimal formulation for on-chip pH-sensitive capsule generation.

## 2.2 Design of a Microfluidic Droplet Generation Platform for Targeted Delivery to the Colon

This section reviews the design, fabrication and troubleshooting process for the custom microfluidic chip. The performance of the microfluidic chip is then analyzed by comparing the microcapsules produced on chip to those formulated using a bulk emulsion.

### 2.2.1 Microfluidic Droplet Generation Platform Chip Design

The first iteration of the microfluidic chip utilized a cross-junction structure, as shown in Figure 9 (all dimensions in millimetres). The figure depicts channel widths ranging from 50-100 µm, and the channel depth was consistent at 100 µm. This channel design was optimized using the resin molds and finalized with a wafer fabricated using photolithography. Droplets were successfully generated on this chip, but one difficulty encountered was forcing the outer phase to meet and recombine at each junction. This phenomenon also made the hydrophilic channel coating procedure (discussed in section 2.2.3) nearly impossible, as the blocking stream of DI water would mix with the treatment fluids or flow out through the centermost hole, causing the treatment fluids to back into the middle channels.

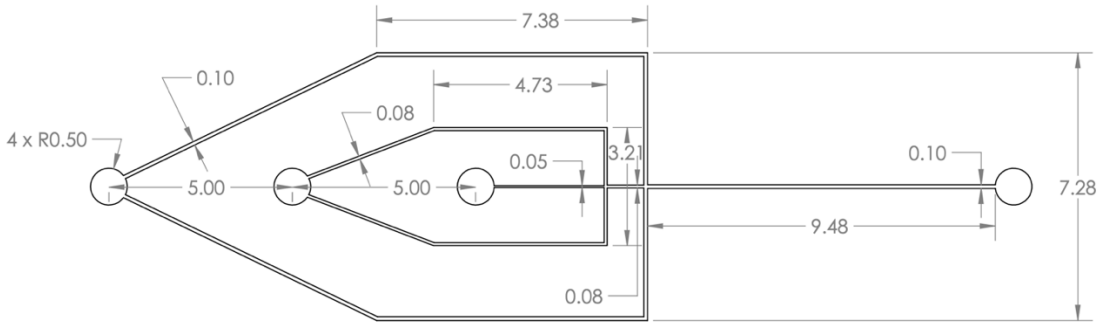


*Figure 9: Cross-chip channel design and dimensions (mm)*

The T-junction chip, shown in Figure 10 (all dimensions in millimetres), was designed in response to difficulties encountered using the cross-chip. The channel widths ranged from 100-150 µm, and the channel depth was again held constant at 100 µm. This channel design successfully generated a $W_1/O/W_2$ double emulsion.

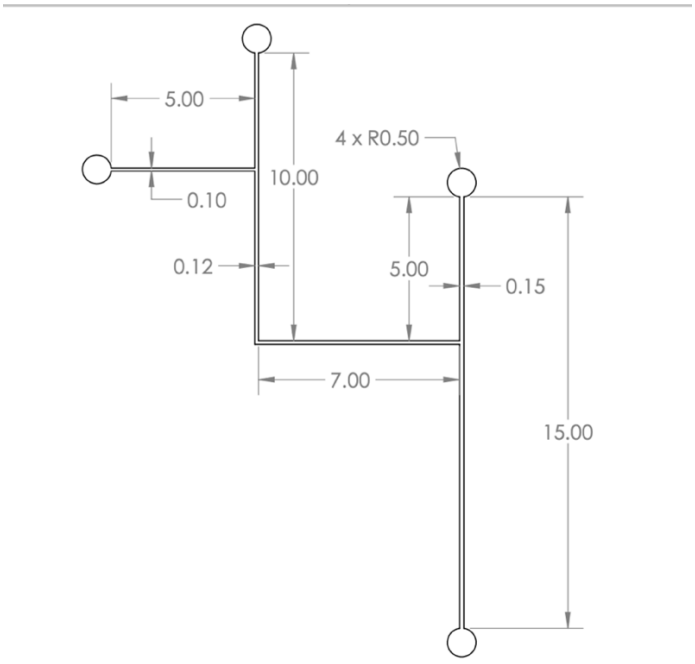


*Figure 10: T-junction chip channel design and dimensions (mm)*

### 2.2.2 Microfluidic Droplet Generation Platform Fabrication

As a low-cost prototyping measure, channel molds were first fabricated using 3D-printed resin molds. The Phrozen Sonic Mini 8K printer was used for prototypes, with the Phrozen Aqua 8K resin. The protocol was derived through iterative testing and by inspecting the quality of the PDMS chips created upon removal from the mold. To begin, the mold designs are drafted using

Solidworks, having a base no more than 2.5 mm in height and channel walls no wider than 2 mm. The resultant .stl file is printed using the Phrozen printer and resin using the 20 µm resolution setting, and the completed prints are carefully scraped off the print bed using a razor blade. The prints are then rinsed with IPA for 20 seconds in a beaker and transferred into a bag containing fresh IPA. The bags are then placed in a sonicator for 2 minutes. The washed molds are removed from the bag and left to dry in a fume hood. Once dry, they are placed in the UV curing apparatus for 15 minutes. Finally, the molds are transferred onto a hot plate set to 120ºC and left for 2 hours. The heat-treated molds are washed with acetone and are then ready to be filled with PDMS. Each mold resembled the one shown in Figure 11, with small alterations to the channel dimensions and design. The mold in Figure 11 will make four identical T-junction chips, with channel dimensions ranging from 100-150 µm. One of the four channel designs in the resin mold is depicted by the red box in Figure 11.

*Figure 11: Completed resin mold*

To create the PDMS chips in the master mold, the PDMS prepolymer and curing agent (Sylgard 184 Silicone Elastomer Base and Curing Agent, Dow Corning) are first mixed at a ratio of 8:1 and are then poured into the treated resin mold. The filled resin mold is then degassed in a benchtop vacuum chamber and is covered with aluminum foil and placed on a hot plate to cure (105ºC, 1 hour and 15 minutes). Next, the cured PDMS is carefully peeled off the master mold, and inlet and outlet holes are punched into the chip using a 1 mm biopsy punch (Miltex). Finally, the prepared chips are bonded to glass slides via plasma treatment (40 second exposure, 18 cc/min $O_2$). The bonded chips are left on a hot plate at 85ºC overnight to fortify the bonding.

Next, the optimized channel designs (found through testing chips fabricated using resin molds) were transferred onto a master mold to manufacture more precise structures using

photolithography. The channel structure is drafted using Solidworks software and transferred to the mold using a photomask supplied by Artnet Pro. The microfluidic device is cast on a soft lithography mold, manufactured using a silicon wafer and SU-8 3025 photoresist (Kayaku Advanced Materials Inc.). The PDMS prepolymer and curing agent are thoroughly mixed at a ratio of 8:1, poured over the patterned silicon wafer and degassed in a benchtop vacuum chamber. The prepared mold is then left to cure for 4 hours on a hot plate set to 85ºC. The cured PDMS chips are removed from the master mold and plasma-bonded following the procedure outlined above.

### 2.2.3 Treatment to Generate Hydrophilic Channels for Double Emulsion

To generate capsules through a double emulsion ($W_1/O/W_2$) on-chip, it was necessary to treat the channel contacting the $W_2$ phase to render this portion of the chip hydrophilic. This was accomplished using the polyelectrolyte multilayer (PEM) coating procedure, treating only the desired channel. Bauer et al.'s protocol, as illustrated in Figures 12 (a-c), was followed for the PEM channel treatment, and the untreated channels were blocked with a continuous stream of DI water, injected using a syringe pump [89]. In brief, 0.1% w/v poly(allylamine hydrochloride) (PAH) and 0.1%w/v poly(styrene sulfonate) were dissolved in DI water. Segments of PAH and PSS were drawn up in PTFE tubing, alternating with 0.1 M NaCl and separated by short air plugs, as displayed in Figure 12 (a). These segments were injected into the chip via syringe pump to coat the desired channel, ensuring each coating step entered the channel for several minutes before NaCl washing. Figure 12 (b) is a graphical representation of the PEM coating procedure, and Figure 12 (c) shows the implications of multiple treatment segments (n) on the coating, analyzed through fluorescence microscopy. The treated channel is highlighted in yellow in Figure 12 (d). The coating was left to stabilize overnight before use.

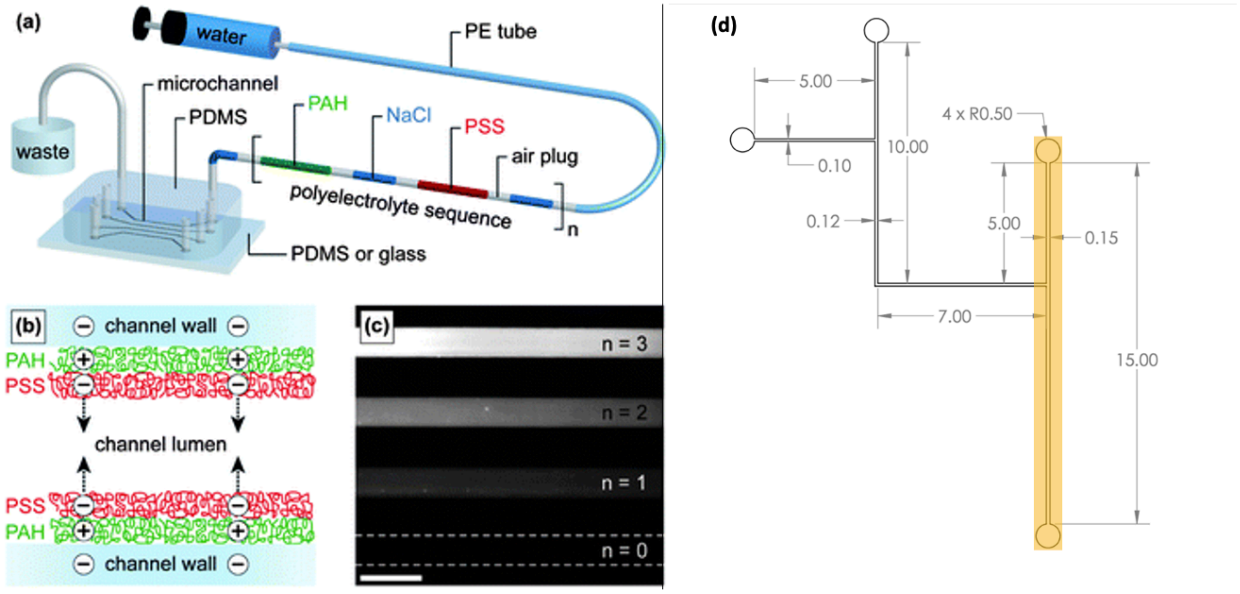


*Figure 12: (a-c) Hydrophilic channel treatment procedure by Bauer et al.* [89]*, (d) Treated channel in finalized T-junction chip.*

### 2.2.4 Functionality of the Microfluidic Droplet Generation Platform

The finalized capsule structure, shown in Figure 13, was formulated as a $W_1/O/W_2$ double emulsion on-chip. The inner aqueous phase consisted of the Eudragit S100 polymer (Evonik) and alginate (Sigma-Aldrich) both dissolved in DI water at concentrations of 2% w/v. This phase was also loaded with fluorescent microparticles (diameter 1 µm, 4.55 x $10^{10}$ particles/ml, Polysciences) at a ratio of 5% v/v. The sacrificial oil phase was composed of mineral oil with 2% v/v Span80 (both from Sigma-Aldrich). Finally, the outer aqueous phase consisted of HCl diluted to 0.1 M (pH=1) in DI water and 2% v/v Tween80 (Sigma-Aldrich). The incorporation of HCl as the outer carrier phase allowed for partial cross-linking on-chip. Span80 and Tween80 are surfactants used to stabilize emulsions by lowering interfacial tension between phases. Fluids are pumped into the chip using three syringe pumps (KD Scientific), disposable 1 mL poly syringes, blunt-end needle tips and PTFE tubing.

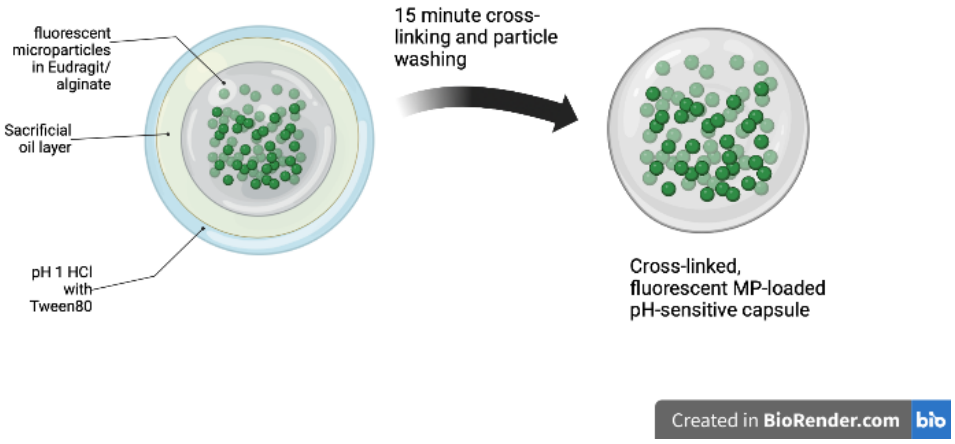


*Figure 13: Graphical depiction of double emulsion pre- and post-crosslinking*

The flow rates for capsule generation were chosen through real-time troubleshooting and testing. It was necessary to synchronize the two droplet generation junctions to avoid mixing of the $W_1$ and $W_2$ phases. Further, the dripping flow regime was desired. The finalized flow rates are listed in Table 6.

*Table 6: Microfluidic chip flow rates*

| Phase | Composition | Flow rate |
|---|---|---|
| $W_1$ | 2% Eudragit S100, 2% alginate, 5% v/v dyed MPs in DI water | 125 µl/hour |
| O | Mineral oil with 2% Span80 | 175 µl/hour |
| $W_2$ | pH 1 HCl with 2% Tween80 | 500 µl/hour |

Figure 14 depicts double emulsions being formulated on-chip. A video was also taken of the droplets being generated to determine the number of particles produced per hour. Based on this analysis, an approximate particle generation rate of 3600 particles/hour was calculated.

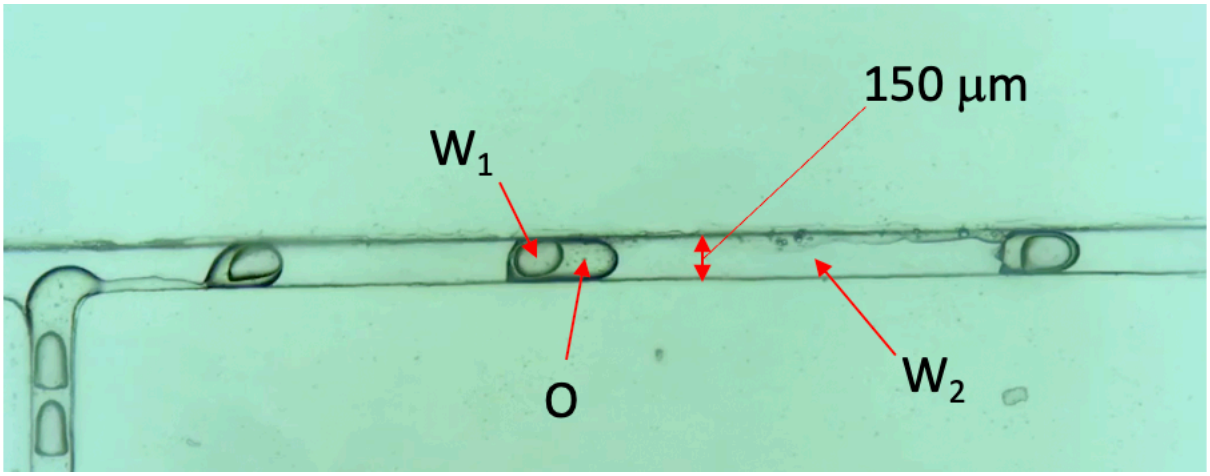


*Figure 14: Double emulsion formulation on-chip*

A recurrent issue with channel coating was limiting the DI water leakage into the treated channel during the PEM treatment. This could mostly be controlled by flow rates, and the performance improved drastically from what was observed on the cross-chip, but some leakage was unavoidable. The hydrophilic channel coating is thus less strong along the channel walls immediately following the droplet-making junction. This can be seen in Figure 14, with the oil phase slightly adhering to the PDMS walls prior to breaking off into a droplet.

This section highlighted the rationale for material selection and chip design, and the functionality and design process of the microfluidic chip.

# Chapter 3: Characterization of Microcapsules Generated On-Chip

Optical microscopy (ECHO Revolve) was used to compare bulk and microfluidic formulations through the generation of a size distribution and sphericity analysis for both samples. SEM imaging (Hitachi S-4800 FESEM) was used to analyze the morphology of both samples of particles. In both cases, samples were diluted to maintain a statistically significant number of particles while limiting particle aggregation. Particles produced through the bulk and microfluidic techniques were compared to determine how formulation technique influences the produced particles. The results of these studies are outlined in sections 3.1 and 3.2.

## 3.1 Optical Microscopy Imaging

### 3.1.1 Size Distribution

Optical microscopy was used to generate size distributions for particles formulated through both microfluidic and bulk techniques, with a sample for each shown in Figures 15 (a) and (c), respectively. Red arrows depict some of the particles shown in the image.

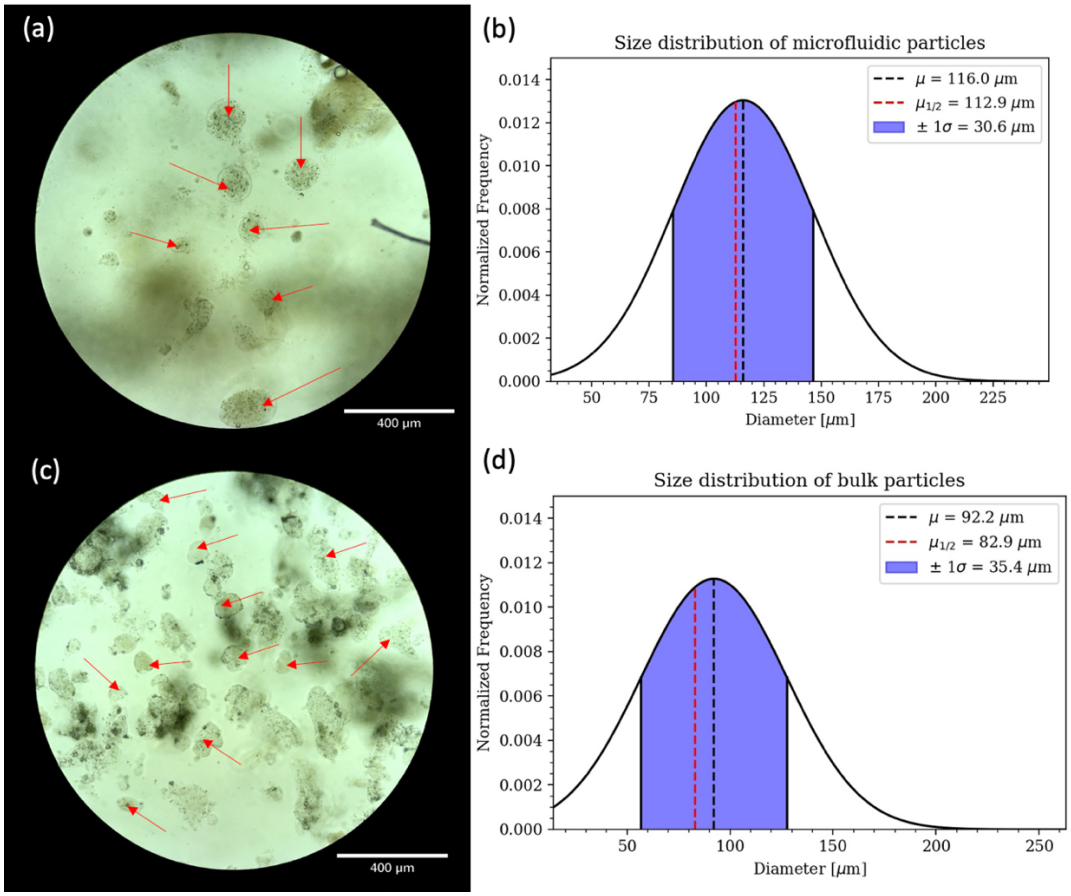


*Figure 15: (a) Microcapsules generated on-chip, 10X magnification; (b) Size distribution from microfluidic particles; (c) Microcapsules generated through bulk emulsion, 10X magnification; (d) Size distribution from bulk particles.*

Figures 15 (b) and (d) show the size distributions of particles formulated through microfluidic and bulk methodologies, respectively. These results show a larger mean particle diameter (116.0 μm) for microfluidic particles and a smaller standard deviation of 30.6 μm, compared to the mean of 92.2 μm and standard deviation of 35.4 μm for bulk particles. It should be noted that, for consistency, all particles were measured along their longest axis.

The mean, median, skew, kurtosis and difference between the mean and median for both populations are summarized in Table 7. The skew values indicate that both populations are positively skewed (or skewed right). However, Bulmer's general rule (in Principles of Statistics) provides some benchmark values indicating the degree of skewness: values between -0.5 to 0.5 are approximately symmetric, values between 0.5 to 1 and -1 to -0.5 are moderately skewed, while skew values less than -1 or greater than 1 are considered highly skewed [107], [108]. Referring to Table 7, it is evident that the microfluidic particle size distribution is moderately skewed, while the bulk size distribution is highly skewed. The positive skew values for both data sets indicates that the distribution has a longer tail on the right, or higher than the mean. In terms of particle sizes, this indicates that both data sets have more particles larger than the mean (as opposed to more particles smaller than the mean), with this effect even more pronounced in the bulk data set.

The polydispersity index (PDI), a metric commonly used to analyze monodispersity of a sample of microparticles, was calculated using Equation 4, below:

$$PDI = (\frac{\sigma}{\mu})^2 \ ,$$

*Equation 4: Polydispersity index*

Where σ is the standard deviation of the sample, and μ is the mean particle size. For polymeric-based particles, a PDI equal to or less than 0.2 is generally considered acceptable and indicative of a monodisperse sample [109]. The calculated PDI values of 0.07 for the microfluidic sample, and 0.15 for the bulk emulsion both fall within the acceptable range; however, the enhanced capability of creating a monodisperse sample presented by the microfluidic device is evident from these results.

*Table 7: Microfluidic vs bulk particle size distribution parameters*

| | **Microfluidic** | **Bulk** |
|---|---|---|
| **Mean (μm)** | 116.0 | 92.2 |
| **Median (μm)** | 112.9 | 82.9 |
| **Mean-median difference** | 3.1 | 9.3 |
| **Standard deviation (μm)** | 30.6 | 35.4 |
| **Skew** | 0.77 | 1.13 |
| **Kurtosis** | 1.38 | 2.07 |
| **Polydispersity index (PDI)** | 0.07 | 0.15 |

Figure 16 below overlays the two histograms representing the size distributions of the particles. When compared in this fashion, it is apparent that the microfluidic sample has a more normal distribution, with a wide, well-defined peak showing the mean particle size. In comparison, the bulk distribution is flatter, with some individual outlying higher peaks lying below the mean particle size. This wider dispersion of sizes can be attributed to the lack of control over individual particles when using bulk formulation techniques. In bulk emulsions, the stirring speed is the only parameter that allows for control over the emulsion (if phase volumes are kept constant between batches). The use of a magnetic stir bar also imparts more shear stress onto the particles than on-chip, which could result in larger particles breaking apart at early stages of the emulsion, thus producing a lower mean particle size.

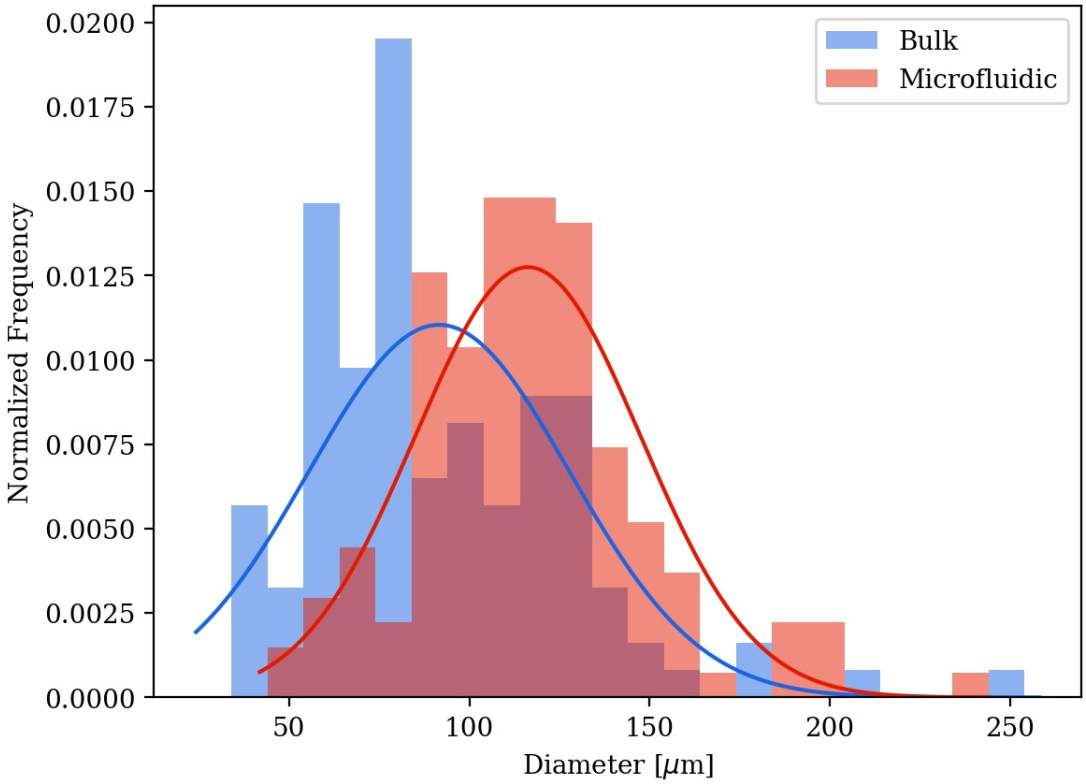


*Figure 16: Bulk vs microfluidic histogram for size distribution*

### 3.1.2 Sphericity Analysis

The sphericity of the formulated particles was also analyzed beyond the qualitative morphology studies outlined in section 3.2. A spherical product is more desirable than an elliptical, or otherwise misshapen product as the dissolution profile of a more consistently spherical product will differ less between batches than the dissolution profile of a more polydisperse, unpredictably shaped product. To calculate sphericity, the particles are measured along their major (longest) and minor (shortest) axes, generating a ratio. This ratio results in a value between zero and one, with a sphericity of one indicating a perfectly spherical product. The same images that were used to

generate the size distribution were used for this study, and again a sample size of 150 particles was selected for both the microfluidic and bulk samples.

Based on this analysis, the bulk sample was found to have an average sphericity of 0.78 ± 0.14, and the microfluidic sample an average sphericity of 0.88 ± 0.09. These results are also presented in Figure 17 as overlaid histograms. In Figure 17, the microfluidic distribution clearly shows that the frequency of measurements peaks for measurements indicating a (nearly) perfectly spherical product. The bulk sample, however, shows a similar frequency of measurements for sphericity values between 0.65 and 1.0. The results clearly indicate the enhanced capabilities of the microfluidic chip in producing a consistent product with good sphericity, and that the microfluidic technique outperforms a traditional bulk emulsion in this regard.

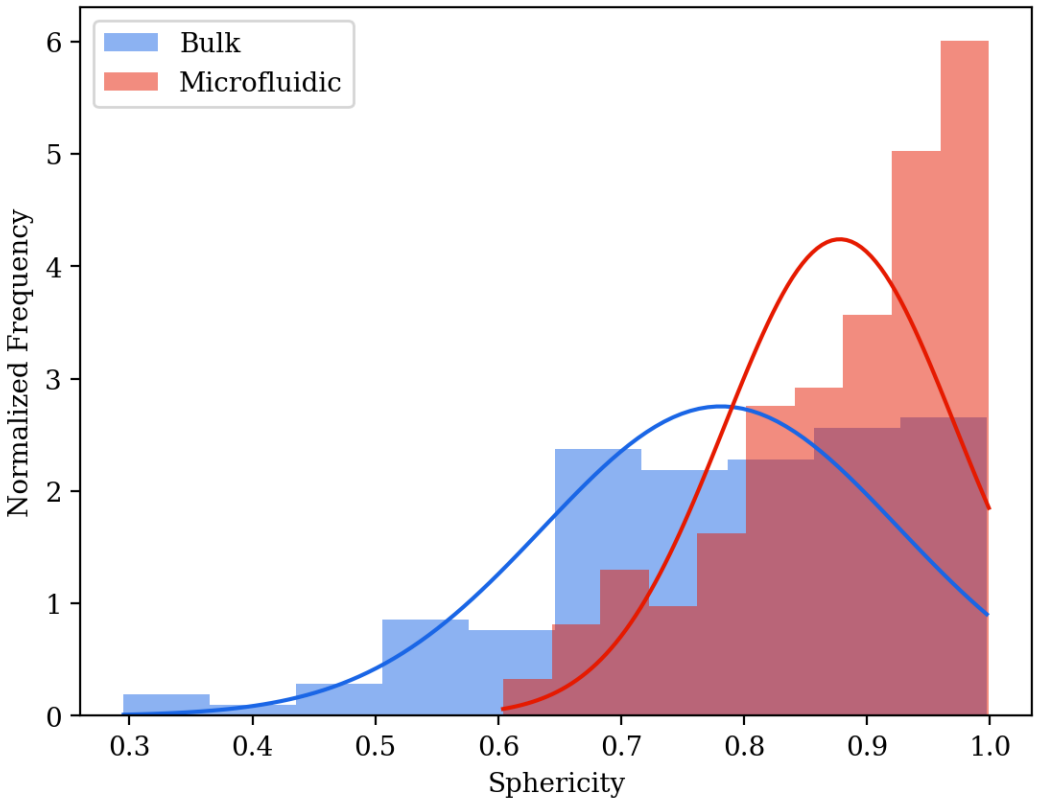


*Figure 17: Bulk vs microfluidic sphericity histogram*

## 3.2 SEM Imaging

SEM imaging was used to compare the particles generated through bulk and microfluidic formulation technique, specifically to analyse particle morphology. Diluted samples of microfluidic and bulk particles are shown in Figures 18 (a) and (b), respectively. Again, a selection of the particles shown in the image are depicted with red arrows. It is clear, from this analysis, that

particles formulated on-chip are smoother and more spherical than particles generated through the bulk emulsion technique. This can likely be attributed to the minimal shear stress particles undergo on-chip, compared to the particles that are subjected to the shear imparted by the stir bar. Further, this could be impacted by time spent in HCl – particles made as a bulk emulsion are cross-linked for 15 minutes and subsequently washed but given the additional time necessary to formulate particles on-chip the first particles generated could spend up to 2 hours in the HCl carrier fluid.

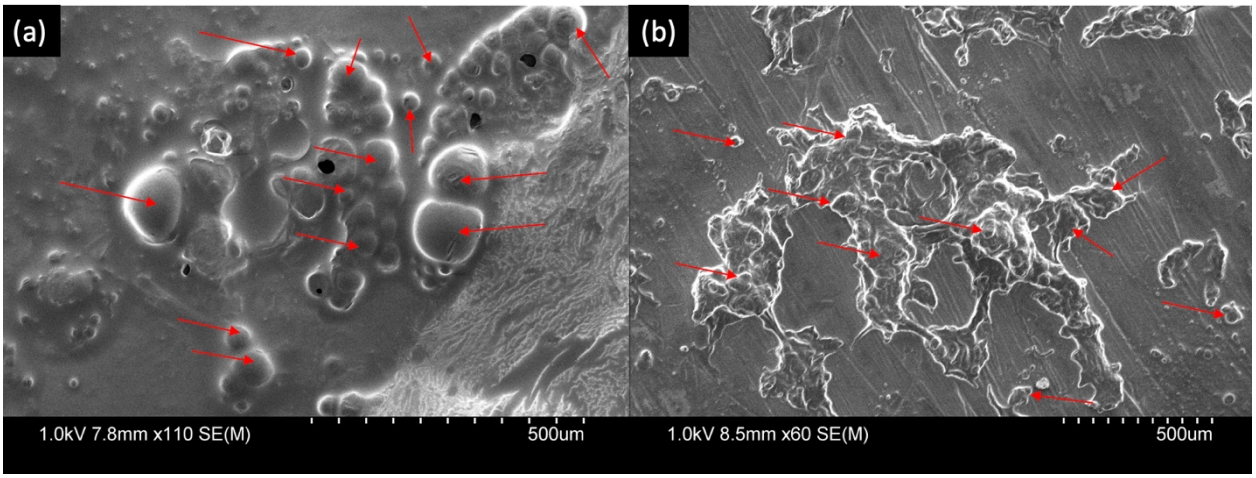


*Figure 18: SEM images of microcapsules formulated (a) on microfluidic chip and (b) through bulk emulsion.*

One known issue with SEM imaging was particle aggregation, which was mostly mitigated by sample dilution prior to drop-casting. As well, since the cross-linked particles still have some water content when drop-cast, some particle collapse was observed through SEM imaging. Thus, the size of each particle may be slightly underestimated due to particle shrinkage. For this reason, SEM imaging was only used for quantitative analysis of morphology, and optical microscopy was implemented to generate size distributions of the particles.

This chapter provides a quantitative analysis to show the enhanced capabilities of microfluidic encapsulation in producing a monodisperse, spherical product with ideal morphology.

# Chapter 4: *In vitro* Release Study of pH-sensitive Characteristics – Proof of Concept

To simulate the release of small particles from the pH-sensitive capsules, green-dyed microparticles 1 μm in diameter were used as a model payload. This release study was conducted to show the difference in release upon exposure of particles to acidic and neutral solutions (simulating the gastric and colonic environments).

## 4.1 Overview of *In Vitro* Release Procedure

To start, the dyed microparticles (MPs) (diameter 1 μm, 4.55 x $10^{10}$ particles/ml, 2.5% aqueous suspension, Polysciences) were added to the inner aqueous phase at a ratio of 5% v/v. Approximately 150 mg of polymeric microcapsules were then generated on-chip and washed three times with DI water using a 20 μm cell strainer (Grenier Bio-One). The washed capsules are then divided in half and added to tubes containing 1ml of pH 2 (acidified with HCl) or pH 7.4 PBS. These tubes were left on a shaker, and at predetermined time points of 5 minutes, 30 minutes, 1, 2, 3, 4, 5 and 6 hours an aliquot of the suspending solution was taken from each tube to determine the released concentration of dyed MPs. Time points were selected based on past works as they represent relevant physiological time frames.

Dyed MP concentration, and consequently percent release, was determined using a custom contour detection algorithm written in Python. The code utilizes the packages OpenCV, NumPy, SciPy and Matplotlib, and can be found in Appendix B [110]–[113]. Three aliquots of 0.2 μl were taken from both samples at each time point and deposited on a glass slide. A second glass slide was used to flatten the droplet and the overall surface area of the flattened droplet was measured. Images were taken at 20X magnification to view the number of particles within a given area of the droplet. A scale bar representing 200 μm x 200 μm was used to isolate a known area of the flattened droplet, and the number of dyed MPs in this region was calculated. Three images of each droplet were taken, resulting in a total of 9 images of an isolated area for each time point (in both acidic and neutral solutions). The particle content in each isolated area was extended to percent concentration, taking into consideration the dilution of the stock solution through particle generation and the release, and the small region of the flattened droplet that was examined. Finally, the nine measurements were averaged for each time point and plotted as percent release with respect to time. The experiment was repeated three times.

Multiple ANOVA (analysis of variance) studies were done to analyze statistical significance of the data, by comparing means between different groups of data. The relevant results derived from these tests are a P-value and an F-statistic. The P-value is the value of interest, where values below

0.05 indicate there is a statistically significant difference between the group means. The F-statistic denotes the ratio of the variance between group means and the mean of variance within a group and is typically used for analysis when the P-value indicates statistical significance between groups.

## 4.2 *In Vitro* pH-Sensitive Release Results and Discussion

The following sections outline and discuss the results achieved in the microparticle release trials.

### 4.2.1 Results

#### *4.2.1.1 Microparticle Release in Neutral and Acidic Solution*

Three replicates of the release experiment were completed, with the total percent release depending on the weight of microparticles added to each tube for each experiment (ranging from 41.8 mg to 66.5 mg). The results of each experiment are shown in Figure 19 (a-c).

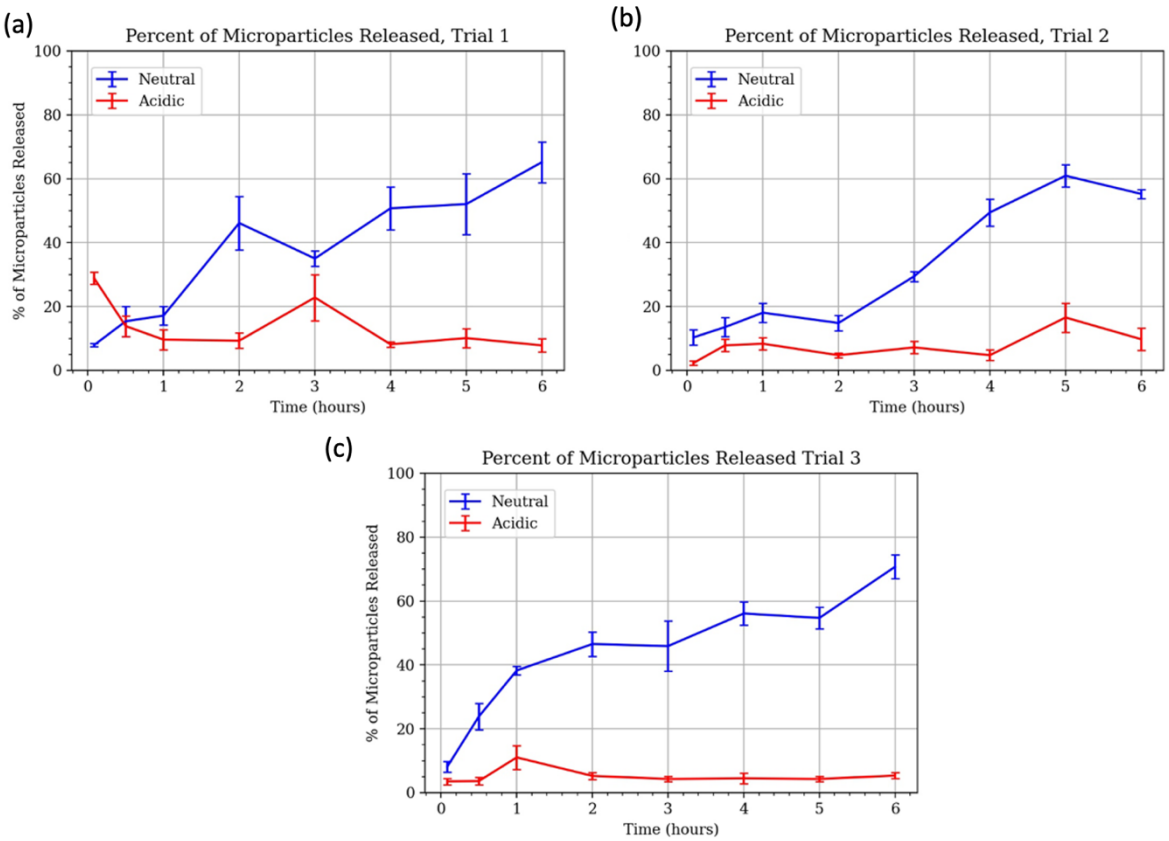


*Figure 19 (a-c): Release of encapsulated microparticles in acidic and neutral solution across three trials.*

After 6 hours of exposure, maximum release percentages of 7.8 ± 2.0%, 9.8 ± 3.5%, 5.4 ± 0.9% and 65.2 ± 6.4%, 55.3 ± 1.4%, 70.7 ± 3.7% were found in acidic and neutral solution, respectively,

across three trials. Visually, the difference in dissolution between neutral and acidic solution was apparent, as shown in Figure 20.

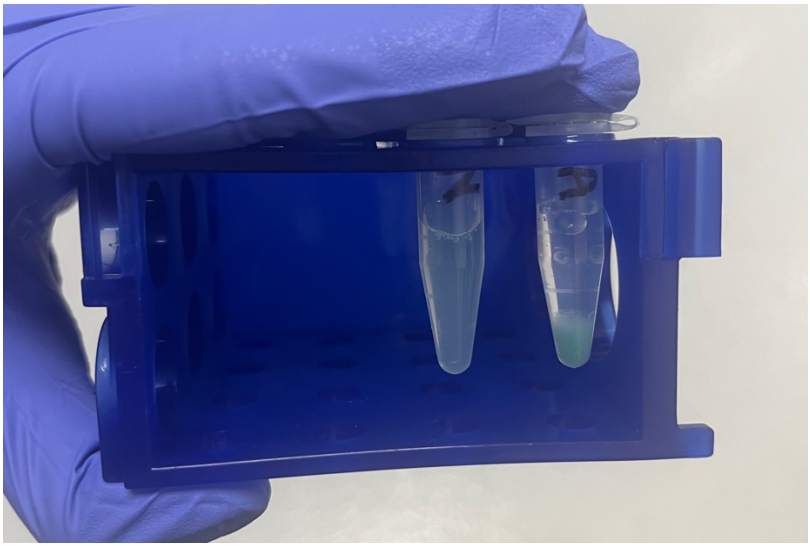

*Figure 20: Release of dyed microparticles in neutral (left) and acidic (right) solution.*

### *4.2.1.2 Microparticle Release in Basic Solution*

As shown in section 4.2.1.1, this experiment proved the pH-sensitive nature of the microparticles. The neutral release results of 65.2 ± 6.4%, 55.3 ± 1.4%, and 70.7 ± 3.7% indicated preferential dissolution in neutral solution (as intended) but near-100% dissolution was not observed for any of the three trials. It was thus necessary to analyze whether the discrepancy in expected MP release was due to incomplete dissolution of the polymeric microcapsules or a limit of detection in the code. To accomplish this, during trial three a third release experiment was conducted simultaneously in pH 12 NaOH. It is known that the microcapsules will completely dissolve upon exposure to highly basic solution, validated through exposing small amounts of microcapsules to basic solution under fluorescent microscopy and observing their immediate dissolution. The number of MPs observed in this release study can thus represent 100% release. The results of this study can be seen in Figure 21.

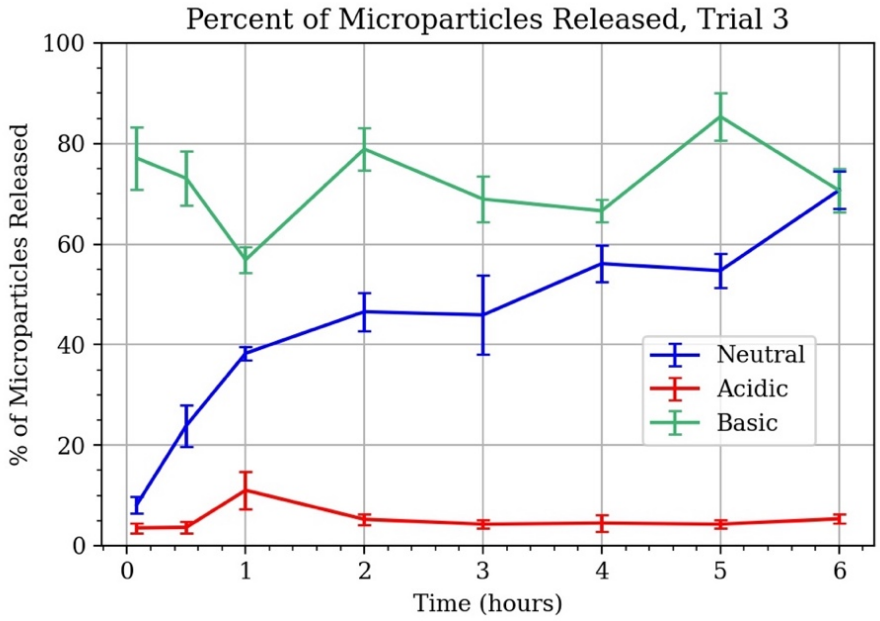


*Figure 21: Microparticle release in acidic, neutral and basic solution*

In this study, release percentages of 5.4 ± 0.92%, 70.7 ± 3.7% and 70.6 ± 4.3% were observed for acidic, neutral and basic solutions, respectively after 6 hours of exposure. Given that capsules dissolve immediately upon exposure to basic solution, variations in the basic data line indicate differences in MP content between 0.2 µl aliquots and not increase in release with respect to time. Minimum and maximum release percentages of 56.9 ± 2.5% and 85.4 ± 4.7% were observed for basic data, with an average release percentage of 72.2 ± 2.7% in basic solution across all time points. These results indicate that polymeric microcapsules are completely dissolving in neutral solution and fully releasing their payload, but an approximate maximum of 72.2% of the dyed MPs are detected.

An ANOVA study was conducted to analyze the statistical significance of release differences between acidic, neutral and basic solution after 6 hours of exposure. Through this study, a P-value of $5.4 \times 10^{-13}$ and an F-statistic of 114.3 were found, showing, as expected, that there is a significant difference between the groups. A T-test was then done to compare the neutral and basic groups, which were hypothesized to have both released the entirety of their payload after 6 hours. A P-value of 0.989 was found, alongside a T-statistic of 0.0138. These results indicate that the means of the neutral and basic release results after 6 hours are approximately equal, confirming that 100% of the payload was released after 6 hours of exposure to neutral solution.

#### *4.2.1.3 Analysis of Variation Between Trials*

One final ANOVA study was done to analyze any difference between trials (conducted on three different days). Individual studies were done for acidic and neutral solutions at each time point

(leading to 16 ANOVA studies total). The P-value and F-statistic across these time points are plotted in Figures 22 and 23, respectively.

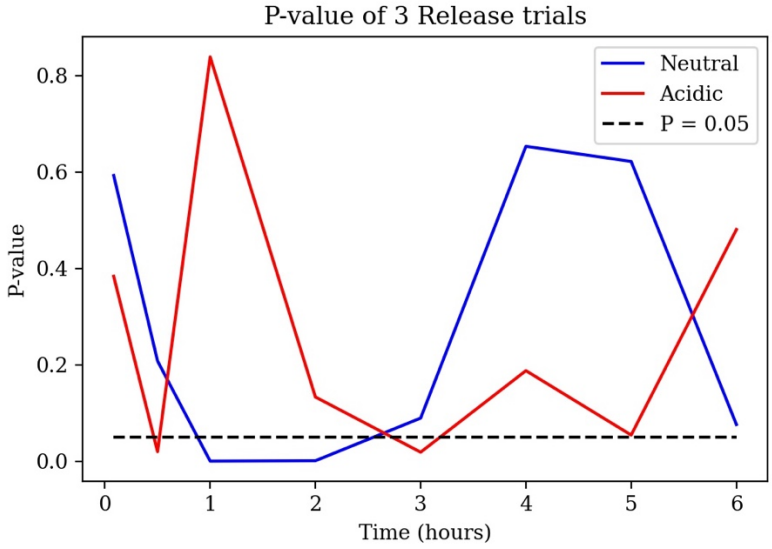


*Figure 22: P-value denoting statistical difference between 3 trials.*

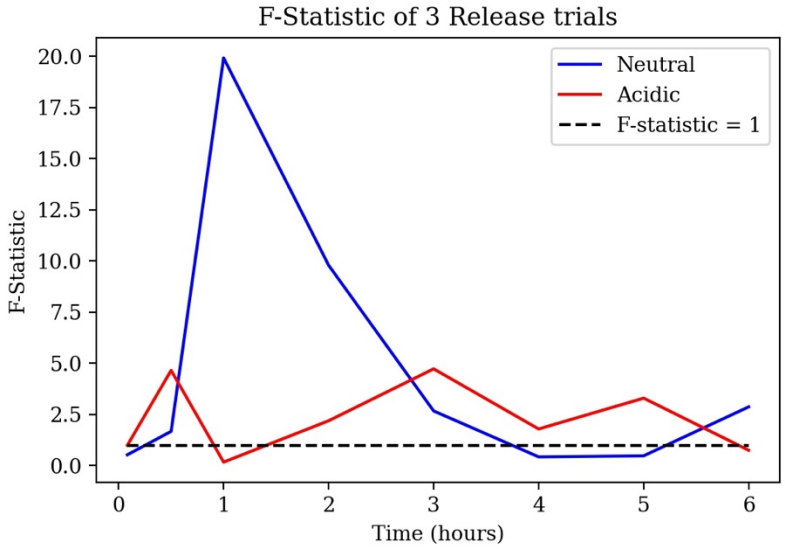


*Figure 23: F-statistic denoting statistical difference between 3 trials.*

In Figure 22, P-values above the dashed black line (denoting the threshold value of 0.05) indicate no statistical difference amongst group means at that time point. 4/16, or 25% of the ANOVA analyses indicate that there is a statistically significant difference between group means (thus showing a difference between the three trials). Naturally, the F-statistic trends further away from a value of 1 at these same time points, as shown in Figure 23. The significance of these results is further discussed in the next section.

### 4.2.2 Discussion

As discussed in the results, one issue with the MP release and detection procedure is the inability to accurately detect 100% of released MPs. When all MPs were known to be released (in basic solution), an average detection limit of 72% was found. One reason for the low maximum detection threshold for the released microparticles is that the code has difficultly distinguishing multiple MPs within clusters of MPs. Although the dyed MPs do not usually cluster, this can affect results by underestimating the number of released MPs. Further, the test tubes are shaken prior to sampling the suspending fluid to avoid collection of dyed MPs at the bottom of the tube, but samples are only taken from the top half of the test tube to avoid picking up polymeric microparticles. Some collection at the bottom of the tube could still be occurring. Finally, this image analysis technique is considered "semi-quantitative", and 100% release and detection was not expected. The observed results demonstrate the pH sensitivity of the polymeric microcapsules and show the capsule's capabilities of protecting small cargo from release while traversing the acidic gastric environment. However, they also indicate that the particle detection method could be improved, potentially by using DLS studies for enumeration instead.

One additional issue with the particle detection imaging process is variation in droplet surface area. Droplets that are simply deposited on a glass slide are convex and thus throughout the thickness of the droplet different particles come into focus. Droplets must be compressed between two glass slides to contain all the dyed MPs to a single viewing plane that can be focused on. However, when the top glass slide is placed on the droplet, the spreading pattern and final area is unpredictable, even though the volume is consistent at 0.2 µl. The area of each compressed droplet was recorded using ECHO microscope software, but ultimately the average area across each trial was calculated and used for all subsequent calculations, to account for variations in spreading patterns.

Finally, the ANOVA results in section 4.2.1.3 indicate no statistically significant difference between group means in general. However, 25% of the analyzed time points did show difference between group means. Upon further examination of the results, statistical significance between means was observed for neutral release after 1 and 2 hours, and acidic release after 30 minutes and 3 hours. It is difficult to pinpoint exact reasons for these variations, but some variation between samples is unavoidable. For example, some droplets have more bubbles than others, which can take up more space in the captured image or obscure microparticles that are close to their border. Differences could also be attributed to particles settling to the bottom of the test tube if it was not shaken prior to taking a sample, or to taking samples from different depths of the sample solution within the tube. In general, these results show little statistically significant difference between trials, and where differences are shown they can be attributed to unavoidable deviations between samples.

# Chapter 5: Case Study – Encapsulation and pH-sensitive Release of E. Coli

This section describes a case study for encapsulation of E. coli within the polymeric microcapsules as a demonstration of a potential payload.

## 5.1 Confirmation of Bacterial Compatibility with the Encapsulation Process

To successfully encapsulate live bacteria, it was necessary to first confirm the compatibility of the Eudragit L100-55 and S100 polymers with bacterial growth. The Eudragit polymers were thus dissolved in LB (lysogeny broth) at concentrations of 2% w/v and inoculated with a live culture. The inoculated cultures were then incubated, and bacterial growth was tracked over the next 20 hours, compared to a control sample of pure LB inoculated with E. coli DH5 alpha. The growth was enumerated using the standard spot plating method (detailed protocol can be found in Appendix A), and the time frame was chosen as a relevant interval for the culture to pass through exponential, stable and death phases of bacterial growth. The results from this test can be seen in Figure 24. All samples show clear exponential and stable phases of growth, exhibiting the compatibility of the polymers with E. coli.

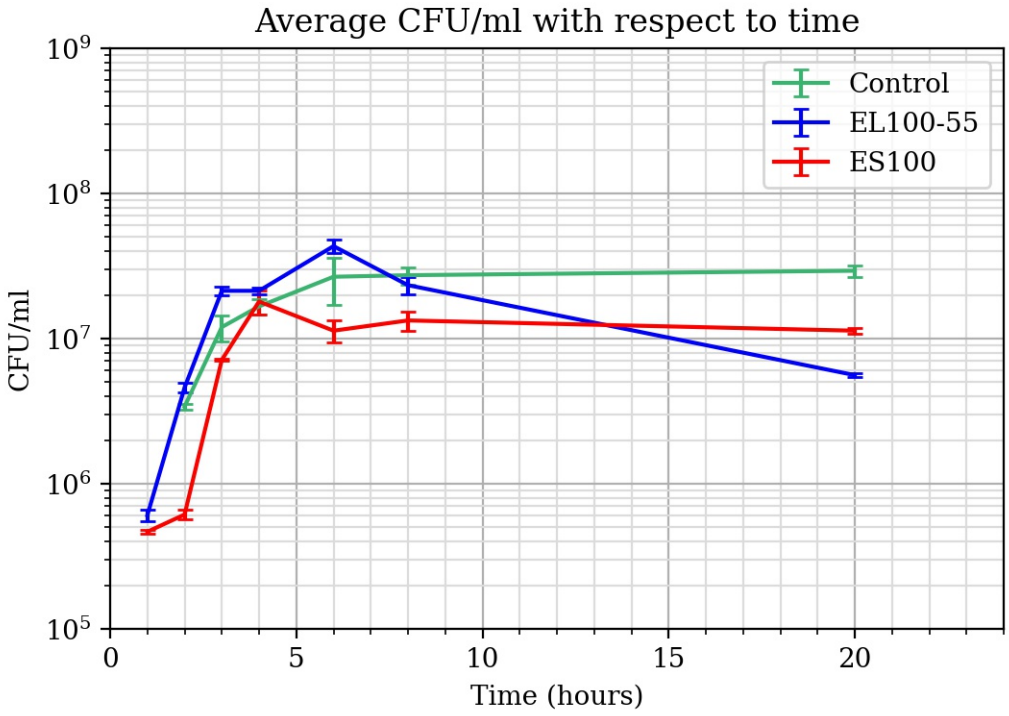


*Figure 24: Bacterial compatibility with Eudragit S100 and L100-55 polymers*

It was also essential to make sure that bacteria were compatible with all chemicals used in this study. The bacterial growth study from 5.1 proved the compatibility of the Eudragit polymers with E. coli. The compatibility of E. coli with pH 1 HCl was done using a zone of inhibition study. E. coli was spread across a petri dish, and a 100 µl droplet of 0.1 M HCl was applied to the surface of the plate. After 24 hours, the bacterial lawn was examined, and no inhibition of bacterial growth was observed in the area where the HCl was applied. This proved that the acid did not cause a drop in bacterial viability. The results from this test can be seen in Figure 25. The droplet of HCl was applied in the location indicated by the black dot in the center of the petri dish.

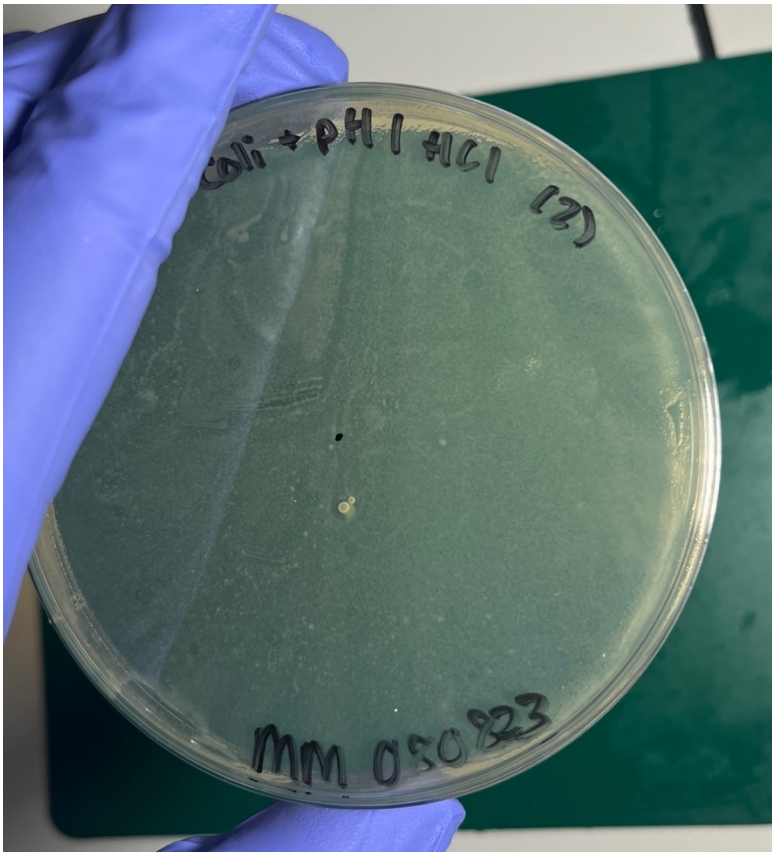


*Figure 25: Zone of inhibition study (0.1 M HCl applied to spread-plated E. coli)*

## 5.2 Overview of Bacterial Encapsulation Procedure

After the pH-sensitive payload release of the capsules was validated in Chapter 4, a preliminary E. coli release study was pursued. The protocol used was similar to the one outlined in 4.1, with slight variations in the material preparation and a different enumeration technique. The new $W_1$ formulation is 2% Eudragit S100 and 2% alginate suspended in LB instead of DI water, to provide the live bacteria with adequate nutrients.

To begin, an overnight culture of bacteria must first be prepared a day prior to encapsulation. This is done by adding a colony-forming-unit (CFU) from an agar plate into 4 mL of LB. This is then stored at 37ºC for 24 hours. Next, a subculture is done to restart the bacterial growth, where 400 µl of the overnight culture is added to 4 mL of fresh LB. This fresh culture is left to incubate for 6 hours.

After 6 hours of incubation, the fresh culture is centrifuged (10 minutes, 4000 rpm) to isolate the biomass within the tube. The supernatant is pipetted off, and the tube is refilled to an identical volume with the $W_1$ phase (2% Eudragit S100, 2% alginate in LB broth). Particles are then formulated on-chip and washed as was outlined in section 4.1. A target weight of 150 mg (true weight was recorded for each experiment) of particles is added to 1 ml of either acidic or neutral PBS and is left on a shaker set to 200 rpm at room temperature to release. 20 µl aliquots of each suspending solution are taken at the time points outlined in section 4.1, and the released payload is enumerated using the standard spot plating method (Appendix A). The volume taken at each time point is replenished with fresh acidic or neutral PBS. This study was repeated three times to validate reproducibility and determine statistical significance and deviations.

To support and validate the spot plating results, an additional zeta potential study was done to analyze bacterial viability and release. Zeta potential can be used to identify relative amounts of viable bacteria in solution, as the intact cell membrane forms a surface charge where it contacts surrounding media. Zeta potential measurements were taken of capsules immediately after addition to neutral and acidic solution, and to the same samples after 6 hours of release. A reference zeta value was also taken for free cells diluted ten times in water. It should be noted that, for this experiment, water and pH 2 HCl were used as suspending media instead of PBS to avoid erosion of the gold electrodes in the zeta cuvettes. Three consecutive zeta potential measurements were taken for each sample, and the average of these trials is used as the final measurement value.

## 5.3 In vitro pH-sensitive Release Results and Discussion

In this section, results of the bacterial release experiment are presented and discussed.

### 5.3.1 Results

To determine the absolute number of bacteria encapsulated and released, the bacterial growth was tracked during the encapsulation procedure, and the dilutions throughout the encapsulation and release were also taken into consideration. Given that bacteria can still grow and divide at room temperature, a small aliquot of the bacteria/LB/polymer solution was kept at room temperature while capsules were generated on-chip. Once capsules were washed and added to either acidic or neutral PBS, a sample of this aliquot was immediately taken, and spot plated to account for any additional growth at room temperature during encapsulation.

In this experiment, the PBS sample taken for spot plating was diluted from known CFU/ml in the $W_1$ phase. The exact weight of particles formulated and added to each tube was recorded, and the CFU content of each aliquot was determined using the known density (1.03 g/ml) of the $W_1$ phase. The resultant maximum CFU/ml released for each experiment (corresponding to 100% payload release) is shown in Table 8.

*Table 8: Calculation of maximum released bacteria for each experiment*

| Experiment Number | Starting maximum CFU/ml (measured) | Maximum Released CFU/ml (calculated, acidic) | Maximum Released CFU/ml (calculated, neutral) |
|---|---|---|---|
| 1 | $3.00x10^{10}$ | $4.50x10^{9}$ | $1.50x10^{9}$ |
| 2 | $1.78x10^{10}$ | $3.88x10^{9}$ | $3.56x10^{9}$ |
| 3 | $2.11x10^{11}$ | $1.26x10^{10}$ | $1.62x10^{10}$ |

Encapsulation efficiency was also calculated, by sampling and spot plating the suspending fluid discharged alongside the particles formulated on-chip. This value was compared to the known encapsulated CFU/ml. The encapsulation efficiency, as calculated for each experiment, is shown in Table 9.

*Table 9: Calculation of encapsulation efficiency*

| Experiment Number | Encapsulated CFU/ml | Suspending fluid post-encapsulation CFU/ml | Encapsulation efficiency (%) |
|---|---|---|---|
| 1 | $3.00x10^{10}$ | $1.67x10^{7}$ | 99.99% |
| 2 | $1.78x10^{10}$ | $1.50x10^{8}$ | 99.15% |
| 3 | $2.11x10^{11}$ | $3.33x10^{6}$ | 99.98% |

Figure 26 (a-c) shows the released bacteria in both neutral and acidic solutions across three different six-hour trials. Values are expressed as CFU/ml detected in the suspending solution. Note that the graphs shown in Figure 26 are displayed with a log-scale y axis, and data points that drop below the minimum y value correspond to a value of 0 CFU/ml. Figure 27 (a-c) shows the same data expressed as a percent of total viable bacteria released (based on the encapsulated CFU/ml calculated in Table 8).

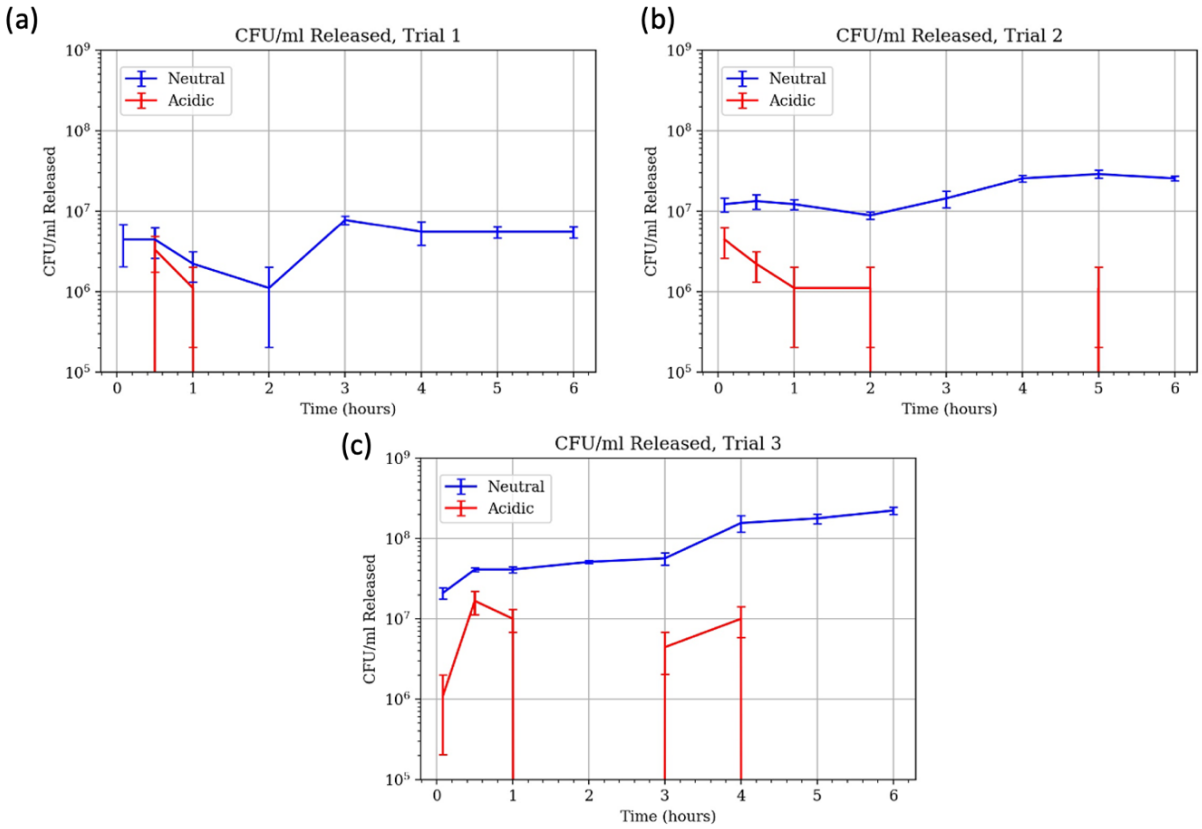


*Figure 26 (a-c): Released CFU/ml in neutral and acidic solution across three trials (log scale).*

After 6 hours of release, 0% of encapsulated viable cells were observed across all three trials of release in acidic solution. Meanwhile, in neutral solution, the recorded CFU/ml released was 5.56 x $10^6$ ± 0.9 x $10^6$ , 2.6 x $10^7$ ± 1.8 x $10^6$ and 2.2 x $10^8$ ± 2.4 x $10^7$ CFU/ml. As shown in Figure 27 (a-c), this corresponds to a percent release of 0.37 ± 0.06%, 0.66 ± 0.05% and 1.37 ± 0.15%.

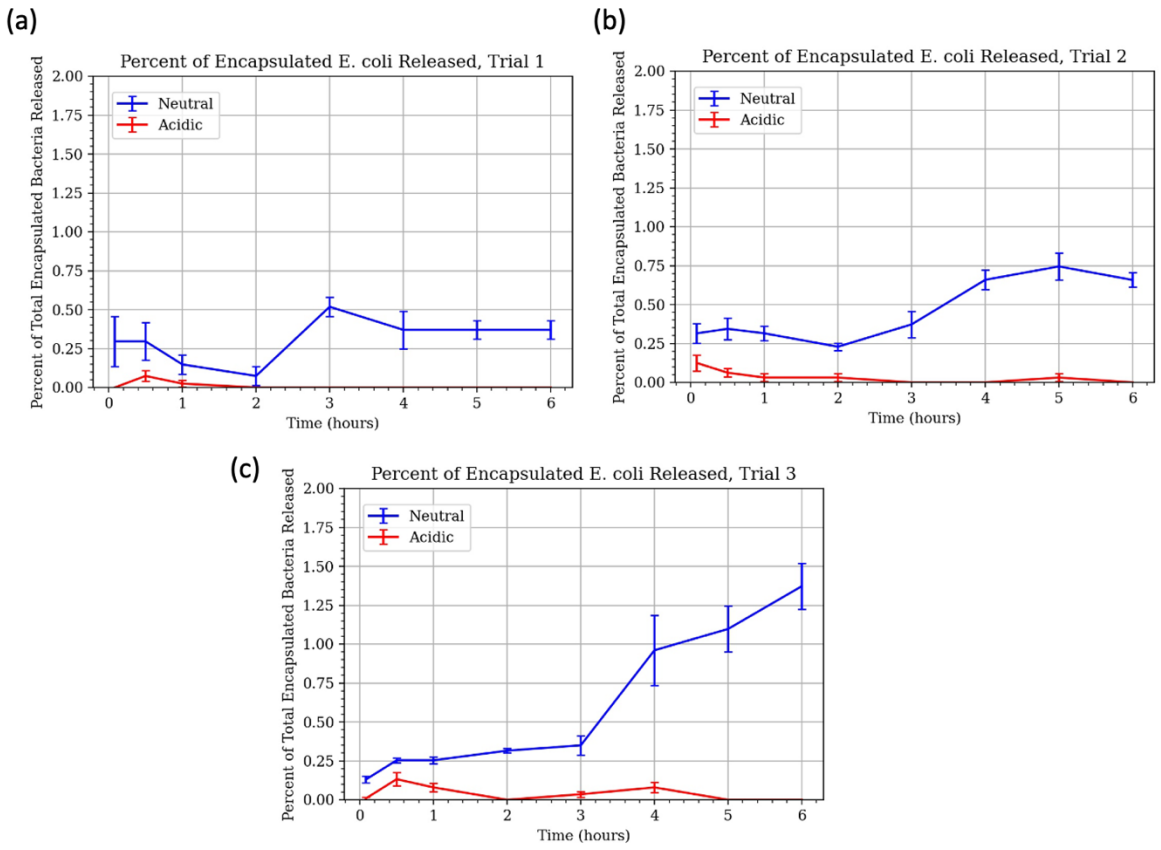


*Figure 27 (a-c): Percent of encapsulated bacteria released in neutral and acidic solution across three trials.*

A final release trial was conducted to validate the spot plating results, using a zeta potential study to analyze bacterial viability and release. The results of the zeta potential study can be seen in Table 10 and Figure 28.

*Table 10: Zeta potential study results*

| Sample | Zeta Potential (mV) |
|---|---|
| Free cells (10X diluted) in water | -35.7 ± 1.4 |
| Microcapsules in water (5 min) | -22.8 ± 0.6 |
| Microcapsules in pH 2 HCl (5 min) | -5.8 ± 0.2 |
| Microcapsules in water (6 hr) | -41.8 ± 3.8 |
| Microcapsules in pH 2 HCl (6 hr) | -7.1 ± 1.0 |

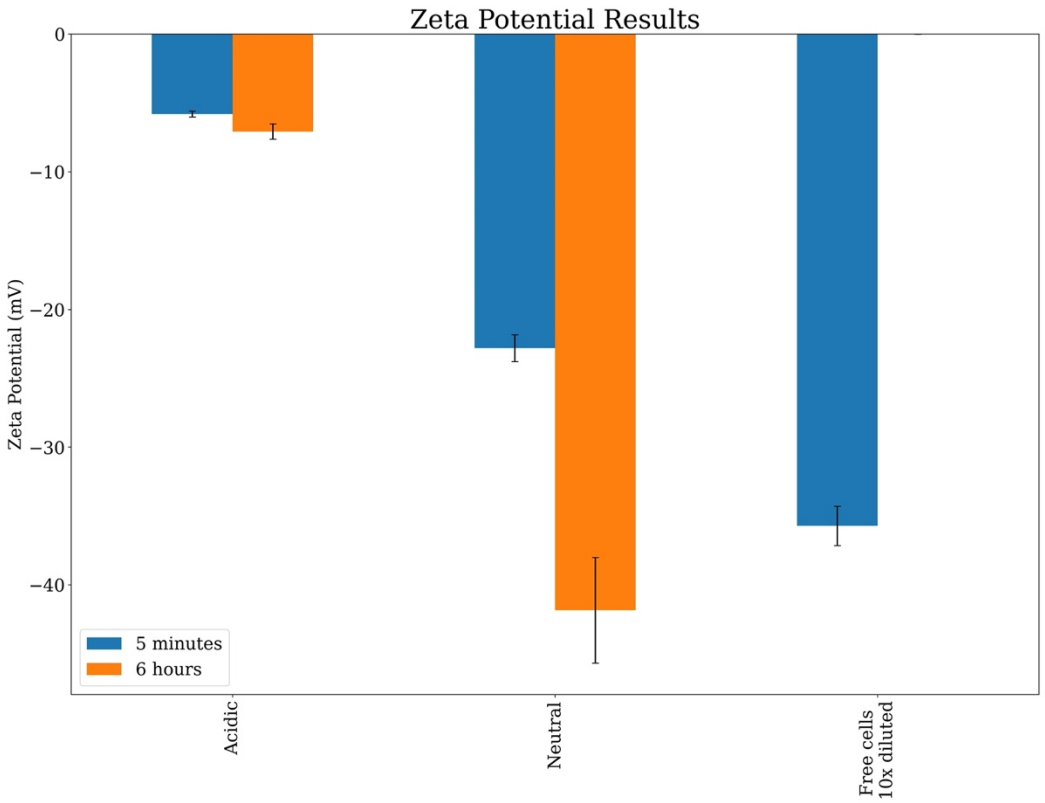


*Figure 28: Zeta potential analysis results grouped by pH*

The important parameters for analysis from the zeta study are the differences between acidic release and neutral release before and after the 6 hours of microcapsule dissolution and release. In acidic solution, a change of -1.269 mV is observed after 6 hours of release, while a difference of -19.033 mV is observed across the 6 hours of exposure in neutral solution. This correlates with expectations: minimal release should be seen for acidic solution, while the number of free bacteria should increase after 6 hours of release in neutral solution, leading to a distinct change in recorded zeta potential.

### 5.3.2 Discussion

First and foremost, the results displayed in section 5.1 demonstrate that the bacteria are selectively released in neutral fluid and capsules remain intact in acidic solution. However, the determined released percentages of 0.37%, 0.66%, and 1.37% in neutral fluid show that although the capsules selectively dissolve and release their payload at neutral pH, bacteria are dying within the capsules prior to release. In fact, based on the values presented in Table 8 and Figure 26, an approximate log 2 viability decrease can be seen in the bacterial populations. Encapsulation efficiency was exceptional, with values of 99.94%, 99.15% and 99.98% found across three trials. This metric

represents the viable cells that were missed during the encapsulation process and were left suspended in the cross-linking pH 1 HCl.

Across all three trials, there were multiple measurements in acidic solution where the detected number of viable cells was 0 CFU/ml. This is due to the limit of detection of the spot plating procedure (Appendix A). For example, for the values in Trial 1, if a spot plating experiment is done, and a single colony appears in the first dilution column (for 1/3 triplicates), this corresponds to $1.11 \times 10^6$ CFU/ml detected. There are still viable cells being released, but at low enough concentrations that colonies will not grow on the spot plates. For this reason, a zeta potential study was subsequently done to validate the results of the spot plating procedures.

In the zeta potential study, the main metric of interest was the difference between zeta values observed for acidic and neutral release before and after particle dissolution (5 minutes, and 6 hours). As discussed above, differences of -1.269 mV and -19.033 mV were observed across the 6 hours of exposure in acidic and neutral solution, respectively. It is known that live bacterial cells have a distinct zeta potential charge, while dead cells show zero zeta potential due to their ruptured membrane. It is hypothesized that encapsulated cells show a different zeta potential value than the released cells. The small change in the acidic samples can be attributed to the minimal release of bacteria from the pH-sensitive microcapsules. The initial neutral reading ($-22.804 \pm 0.558$ mV) was taken second, and ultimately spent approximately one hour in solution prior to the reading, so some release was expected. The value can be attributed to the presence of both encapsulated and released viable bacteria. The value recorded after 6 hours ($-41.837 \pm 3.840$ mV) is close to the value recorded for free cells, and the significant increase in zeta potential can be attributed to the known release of bacteria from the capsules, as exhibited by the spot plating studies. However, it is possible that upon release the exposure to the polymeric capsule changes the zeta potential of the bacteria, and thus it cannot be conclusively determined that the zeta potential of the cells released in neutral solution after 6 hours should match that of the diluted free cells. This zeta study confirmed the spot plating results by illustrating a distinct change in zeta potential in only neutral solution, displaying selective release of bacteria based on pH.

One limitation of zeta potential studies is the settling and sinking of sample contents to the bottom of the zeta cuvette. For this reason, three studies are done and averaged, and measurements are taken immediately after loading the sample into the cuvette. Another limitation of conducting zeta potential studies in tandem with spot plating is sample loss. Given the small volume of particles generated (and the spot plating limitation described above), a volume of 1 ml is selected for the release fluid, which is also the approximate capacity of the zeta cuvette. Through loading and unloading the cuvette it is impossible to fully inhibit sample loss, and thus some microcapsules and release fluid were lost in this process.

Bacterial encapsulation is a far more difficult task than the proof-of-concept microparticle encapsulation due to the inherent variability of bacterial cultures. When a new culture (or subculture) is started, there is unavoidable variation that occurs for the maximum CFU/ml observed at stable growth phase. For this reason, bacterial release was also enumerated as a percent of total encapsulated bacteria, rather than absolute CFU/ml. Bacteria can also continue to grow when removed from the incubator and left at room temperature, and the temperature of the laboratory can also affect bacterial growth rates. One measure taken to mitigate bacterial growth within the capsules is encapsulating the bacteria when they reach a stable growth phase. An optimal time point of 6 hours was determined through the bacterial growth analysis outlined in section 5.1. Further, contamination must be avoided, but some exposure to the environment is unavoidable (ex. while capsules are being formulated on chip). Sterility measures, such as wiping down all surfaces with ethanol and using sterile tubing and syringes were taken, but this was another complication compared to the MP encapsulation procedure.

Finally, results indicated that although capsules were successful in encapsulating bacteria and releasing their payload selectively, storage within the particles caused a dramatic drop in bacterial viability. As mentioned above, a log 2 decrease in CFU/ml is seen throughout the microfluidic encapsulation and release process, while storage at various temperatures (37ºC, 20ºC, 4ºC and -20ºC) overnight results in near-complete eradication of the viable bacteria. Encapsulated bacteria are often frozen or lyophilized (typically with a cryoprotectant added) as they will become dormant and not continue to grow. The proposed encapsulation system was also tested by freezing particles with or without glycerol as a suspending fluid (in a standard -20ºC freezer or flash-frozen in dry ice). Glycerol was selected as it is a common cryoprotectant for E. coli. Minimal growth was observed upon resuspending the frozen capsules in acidic and neutral PBS and spot plating the suspending fluid. It should be noted that capsules were also tested with the polymer/bacteria solution containing glycerol, but this formulation caused phase separation upon centrifugation to separate particles, and thus no capsules could be produced. Given the drop in viability across all storage temperatures, the immediate log 2 drop in viability following the encapsulation process, and the proven compatibility with the chemicals involved, it can be concluded that the cross-linking process is incompatible with live cargo.

Future work should focus on developing a new structure for the capsules that retains their pH sensitivity while protecting the live cargo from the cross-linking process. One alternative could be the implementation of a core-shell structure, to avoid having the bacteria dispersed throughout a cross-linked matrix. Upon confirmation that this new structure is compatible with live cargo, shelf life and suitable storage conditions for the capsules should be tested.

# Chapter 6: Conclusions and Future Work

## 6.1 Conclusions

In this work, a custom formulation of pH-sensitive materials was designed and used for targeted delivery of bioactive compounds. This work was pursued to develop a biocompatible microcapsule capable of protecting sensitive cargo from degradation and release through the stomach and small intestine. The custom polymer formulation and a T-junction microfluidic chip were characterized using dyed microparticles as a model payload, and the performance of the microfluidic chip was compared to a conventional bulk emulsion. Through SEM imaging, it was found that particles formulated on-chip are more spherical and noticeably smoother than those made using a bulk emulsion. Sphericity was quantified through optical microscopy, with an average sphericity of 0.78 ± 0.14 calculated for the bulk sample and a value of 0.88 ± 0.09 found for the microfluidic sample. Optical microscopy was used to calculate size distributions for both bulk and microfluidic particles. A mean diameter of 92.2 μm and a PDI of 0.15 was found for bulk particles, while microfluidic particles were larger but more monodisperse, with a mean diameter of 116.0 μm and a PDI of 0.07.

The pH-sensitive nature of the microcapsules was then validated through an in vitro release study, with release quantified through particle concentration detection using a custom Python code. After 6 hours of exposure to either neutral or acidic fluids, ultimate payload release was found to be 65.2 ± 6.4%, 55.3 ± 1.4%, and 70.7 ± 3.7% in neutral fluid, and 7.8 ± 2.0%, 9.8 ± 3.5%, 5.4 ± 0.9% in acidic fluid, over three individual trials. Release was then compared to the known complete dissolution of MPs in highly basic solution, with an average of 72.2 ± 2.7% dyed MP release detected over 6 hours. These studies proved the microcapsules will selectively release their payload in neutral solution and represent a viable option for targeted delivery of bioactive molecules to the colon. However, the results also indicated that the semi-quantitative image analysis procedure could not enumerate all MPs, corresponding to an underestimated release percentage due to limits in detection.

Finally, this characterization study was then extended to bacterial release, with payload release found to be 0.37 ± 0.06%, 0.66 ± 0.05% and 1.37 ± 0.15% in neutral fluid and 0% (across all three trials) in acidic fluid after 6 hours. These results were supported by an additional zeta potential and spot plating study done in tandem, which showed a distinct change in potential observed in neutral solution only, correlating to the release of live bacteria. The observations of these experiments show that although the capsules display the desired targeted release in neutral solution, they are not suitable for the encapsulation and delivery of live cargo. The cross-linking procedure used to formulate the capsules causes a fast (log 2) drop in viability that continues to decline through overnight storage of the capsules.

## 6.2 Future Work

First steps in future work for this project should include identifying suitable bioactive cargo for targeted delivery to the colon. Potential candidates could include prodrugs or immunosuppressants for treatment of IBD, antibiotics or therapeutic drugs to treat colorectal cancer. This work can also easily be extended to targeted delivery of compounds to the small intestine by using the Eudragit L100-55 polymer in place of the Eudragit S100 polymer, where initial work has already been pursued for encapsulation and targeted delivery of iron salts. A more detailed *in vitro* release study could also be pursued by utilizing the TIM model, which simulates sequential transit through the GI tract, including relevant residence times, the presence of enzymes, and accurate absorption measurements.

Another aspect of this work that could be further explored is the hydrodynamics of the capsule formulation procedure conducted on-chip, and the impact of wettability. Although the oil phase is used as a sheath and is not a component of the finalized capsule, the impact of different oil sheath thicknesses on capsule cross-linking and size should be characterized. The surface tension between phases should also be characterized to further analyze its impact on capsule formulation.

Finally, future work for this project should also tackle the issue of encapsulated bacterial cell viability. Based on the conclusion that direct exposure to cross-linking is leading to cell death, a core-shell structure could be research and implemented, to protect the bacteria within an inner core while still cross-linking the Eudragit polymers to envelop this core and accomplish the targeted delivery.

## 6.3 Contributions

The main contribution of this work is a custom aqueous formulation of Eudragit polymers, compatible with loading hydrophilic cargo dispersed throughout a continuous matrix. Although Eudragit polymers are common in industrial targeted drug delivery, they are typically used as a coating for dry tablets. In research, emulsion-based encapsulation using Eudragit is common, but most applications use organic solvents which evaporate to leave solid particles, causing biocompatibility-related concerns and limiting its use with sensitive cargo. Further, the use of on-chip cross-linking through exposure to acidic solution produces smooth, monodisperse particles, which can lead to more consistent drug delivery. Finally, this work showed the capabilities of the encapsulation platform to deliver a model payload, but this can be extended to other bioactive compounds, such as vitamins, minerals and pharmaceuticals.

# Chapter 7: References


[1] S. Hua, "Advances in Oral Drug Delivery for Regional Targeting in the Gastrointestinal Tract - Influence of Physiological, Pathophysiological and Pharmaceutical Factors," *Front. Pharmacol.*, vol. 11, Apr. 2020.

[2] S. Abdella *et al.*, "pH and its applications in targeted drug delivery," *Drug Discov. Today*, vol. 28, no. 1, p. 103414, Jan. 2023.

[3] M. Oth, M. Franz, J. Timmermans, and A. Möes, "The Bilayer Floating Capsule: A Stomach-Directed Drug Delivery System for Misoprostol," *Pharm. Res.*, vol. 09, no. 3, pp. 298–302, 1992.

[4] L. E. McCoubrey, A. Favaron, A. Awad, M. Orlu, S. Gaisford, and A. W. Basit, "Colonic drug delivery: Formulating the next generation of colon-targeted therapeutics," *J. Control. Release*, vol. 353, pp. 1107–1126, Jan. 2023.

[5] V. Puri *et al.*, "A Comprehensive Review on Nutraceuticals: Therapy Support and Formulation Challenges," *Nutrients*, vol. 14, no. 21, p. 4637, Nov. 2022.

[6] K. Sampathkumar and S. C. J. Loo, "Targeted Gastrointestinal Delivery of Nutraceuticals with Polysaccharide-Based Coatings," *Macromol. Biosci.*, vol. 18, no. 4, p. 1700363, Apr. 2018.

[7] S. Prakash, "Colon-targeted delivery of live bacterial cell biotherapeutics including microencapsulated live bacterial cells," *Biol. Targets Ther.*, p. 355, Sep. 2008.

[8] S. C. Ng *et al.*, "Worldwide incidence and prevalence of inflammatory bowel disease in the 21st century: a systematic review of population-based studies," *Lancet*, vol. 390, no. 10114, pp. 2769–2778, Dec. 2017.

[9] S. Salminen, "Demonstration of safety of probiotics — a review," *Int. J. Food Microbiol.*, vol. 44, no. 1–2, pp. 93–106, Oct. 1998.

[10] I. Sensoy, "A review on the food digestion in the digestive tract and the used in vitro models," *Curr. Res. Food Sci.*, vol. 4, pp. 308–319, 2021.

[11] S. Hua, E. Marks, J. J. Schneider, and S. Keely, "Advances in oral nano-delivery systems for colon targeted drug delivery in inflammatory bowel disease: Selective targeting to diseased versus healthy tissue," *Nanomedicine Nanotechnology, Biol. Med.*, vol. 11, no. 5, pp. 1117–1132, Jul. 2015.

[12] M. M. Patel, T. J. Shah, A. F. Amin, and N. N. Shah, "Design, Development and Optimization of a Novel Time and pH-Dependent Colon Targeted Drug Delivery System," *Pharm. Dev. Technol.*, vol. 14, no. 1, pp. 65–72, Jan. 2009.

[13] S. Thakral, N. K. Thakral, and D. K. Majumdar, "Eudragit: a technology evaluation.," *Expert Opin. Drug Deliv.*, vol. 10, no. 1, pp. 131–49, Jan. 2013.

[14] J. Chen, X. Li, L. Chen, and F. Xie, "Starch film-coated microparticles for oral colon-specific drug delivery," *Carbohydr. Polym.*, vol. 191, pp. 242–254, Jul. 2018.

[15] F. J. Rodrigues, M. F. Cedran, J. L. Bicas, and H. H. Sato, "Encapsulated probiotic cells: Relevant techniques, natural sources as encapsulating materials and food applications – A narrative review," *Food Res. Int.*, vol. 137, p. 109682, Nov. 2020.

[16] T.-Y. Liu and Y.-L. Lin, "Novel pH-sensitive chitosan-based hydrogel for encapsulating poorly water-soluble drugs," *Acta Biomater.*, vol. 6, no. 4, pp. 1423–1429, Apr. 2010.

[17] D. R. K. Weerasuriya, W. P. S. L. Wijesinghe, and R. M. G. Rajapakse, "Encapsulation of

anticancer drug copper bis(8-hydroxyquinoline) in hydroxyapatite for pH-sensitive targeted delivery and slow release," *Mater. Sci. Eng. C*, vol. 71, pp. 206–213, Feb. 2017.
[18] G. Begum *et al.*, "In Situ Strategy to Encapsulate Antibiotics in a Bioinspired $CaCO_3$ Structure Enabling pH-Sensitive Drug Release Apt for Therapeutic and Imaging Applications," *ACS Appl. Mater. Interfaces*, vol. 8, no. 34, pp. 22056–22063, Aug. 2016.
[19] S. Gunasekaran, S. Ko, and L. Xiao, "Use of whey proteins for encapsulation and controlled delivery applications," *J. Food Eng.*, vol. 83, no. 1, pp. 31–40, Nov. 2007.
[20] S. Razavi, S. Janfaza, N. Tasnim, D. L. Gibson, and M. Hoorfar, "Microencapsulating polymers for probiotics delivery systems: Preparation, characterization, and applications," *Food Hydrocoll.*, vol. 120, p. 106882, Nov. 2021.
[21] O. Sandoval-Castilla, C. Lobato-Calleros, H. S. García-Galindo, J. Alvarez-Ramírez, and E. J. Vernon-Carter, "Textural properties of alginate–pectin beads and survivability of entrapped Lb. casei in simulated gastrointestinal conditions and in yoghurt," *Food Res. Int.*, vol. 43, no. 1, pp. 111–117, Jan. 2010.
[22] M. Chávarri, I. Marañón, R. Ares, F. C. Ibáñez, F. Marzo, and M. del C. Villarán, "Microencapsulation of a probiotic and prebiotic in alginate-chitosan capsules improves survival in simulated gastro-intestinal conditions," *Int. J. Food Microbiol.*, vol. 142, no. 1–2, pp. 185–189, Aug. 2010.
[23] F. Ansari, H. Pourjafar, V. Jodat, J. Sahebi, and A. Ataei, "Effect of Eudragit S100 nanoparticles and alginate chitosan encapsulation on the viability of Lactobacillus acidophilus and Lactobacillus rhamnosus," *AMB Express*, vol. 7, no. 1, p. 144, Dec. 2017.
[24] K.-S. Huang *et al.*, "Synthesis of uniform core-shell gelatin-alginate microparticles as intestine-released oral delivery drug carrier," *Electrophoresis*, vol. 35, no. 2–3, pp. 330–336, Feb. 2014.
[25] M. George and T. E. Abraham, "pH sensitive alginate–guar gum hydrogel for the controlled delivery of protein drugs," *Int. J. Pharm.*, vol. 335, no. 1–2, pp. 123–129, Apr. 2007.
[26] Deepa Thomas and M.S. Latha, "Alginate Based Nanocarriers for Controlled Drug Delivery Applications," in *Alginate Biomaterial: Drug Delivery Strategies and Biomedical Engineering*, S. Jana and S. Jana, Eds. Signapore: Springer Nature, 2023, pp. 61–84.
[27] Y. Gao *et al.*, "Recent advances in microfluidic-aided chitosan-based multifunctional materials for biomedical applications," *Int. J. Pharm.*, vol. 600, p. 120465, May 2021.
[28] H. Du, M. Liu, X. Yang, and G. Zhai, "The design of pH-sensitive chitosan-based formulations for gastrointestinal delivery," *Drug Discov. Today*, vol. 20, no. 8, pp. 1004–1011, Aug. 2015.
[29] I. A. Sogias, V. V. Khutoryanskiy, and A. C. Williams, "Exploring the Factors Affecting the Solubility of Chitosan in Water," *Macromol. Chem. Phys.*, vol. 211, no. 4, pp. 426–433, Feb. 2010.
[30] J. B. Russell, R. E. Muck, and P. J. Weimer, "Quantitative analysis of cellulose degradation and growth of cellulolytic bacteria in the rumen," *FEMS Microbiol. Ecol.*, vol. 67, no. 2, pp. 183–197, Feb. 2009.
[31] W. Li, L. Liu, H. Tian, X. Luo, and S. Liu, "Encapsulation of Lactobacillus plantarum in cellulose based microgel with controlled release behavior and increased long-term storage stability," *Carbohydr. Polym.*, vol. 223, p. 115065, Nov. 2019.
[32] L. Alves, B. Medronho, F. E. Antunes, D. Topgaard, and B. Lindman, "Dissolution state

of cellulose in aqueous systems. 2. Acidic solvents," *Carbohydr. Polym.*, vol. 151, pp. 707–715, Oct. 2016.
[33] S. Javanbakht and A. Shaabani, "Carboxymethyl cellulose-based oral delivery systems," *Int. J. Biol. Macromol.*, vol. 133, pp. 21–29, Jul. 2019.
[34] A. George, P. A. Shah, and P. S. Shrivastav, "Guar gum: Versatile natural polymer for drug delivery applications," *Eur. Polym. J.*, vol. 112, pp. 722–735, Mar. 2019.
[35] T. Ramasamy, U. D. S. Kandhasami, H. Ruttala, and S. Shanmugam, "Formulation and evaluation of xanthan gum based aceclofenac tablets for colon targeted drug delivery," *Brazilian J. Pharm. Sci.*, vol. 47, no. 2, pp. 299–311, Jun. 2011.
[36] L. Zhang, J. Xu, Q. Wen, and C. Ni, "Preparation of xanthan gum nanogels and their pH/redox responsiveness in controlled release," *J. Appl. Polym. Sci.*, vol. 136, no. 36, p. 47921, Sep. 2019.
[37] A. K. Nayak, B. Das, and R. Maji, "Calcium alginate/gum Arabic beads containing glibenclamide: Development and in vitro characterization," *Int. J. Biol. Macromol.*, vol. 51, no. 5, pp. 1070–1078, Dec. 2012.
[38] F. Yang, S. Xia, C. Tan, and X. Zhang, "Preparation and evaluation of chitosan-calcium-gellan gum beads for controlled release of protein," *Eur. Food Res. Technol.*, vol. 237, no. 4, pp. 467–479, Oct. 2013.
[39] S. D. Ribeiro *et al.*, "Cellulose triacetate films obtained from sugarcane bagasse: Evaluation as coating and mucoadhesive material for drug delivery systems," *Carbohydr. Polym.*, vol. 152, pp. 764–774, Nov. 2016.
[40] N. Kulkarni, P. Wakte, and J. Naik, "Development of floating chitosan-xanthan beads for oral controlled release of glipizide," *Int. J. Pharm. Investig.*, vol. 5, no. 2, p. 73, 2015.
[41] S. Sharma, J. Kaur, G. Sharma, K. K. Thakur, G. S. Chauhan, and K. Chauhan, "Preparation and characterization of pH-responsive guar gum microspheres," *Int. J. Biol. Macromol.*, vol. 62, pp. 636–641, Nov. 2013.
[42] Y. Liu and H. Zhou, "Budesonide-Loaded Guar Gum Microspheres for Colon Delivery: Preparation, Characterization and in Vitro/in Vivo Evaluation," *Int. J. Mol. Sci.*, vol. 16, no. 2, pp. 2693–2704, Jan. 2015.
[43] D. Jao, Y. Xue, J. Medina, and X. Hu, "Protein-Based Drug-Delivery Materials," *Materials (Basel).*, vol. 10, no. 5, p. 517, May 2017.
[44] M. L. Peralta Ramos, J. A. González, L. Fabian, C. J. Pérez, M. E. Villanueva, and G. J. Copello, "Sustainable and smart keratin hydrogel with pH-sensitive swelling and enhanced mechanical properties," *Mater. Sci. Eng. C*, vol. 78, pp. 619–626, Sep. 2017.
[45] M. Foox and M. Zilberman, "Drug delivery from gelatin-based systems," *Expert Opin. Drug Deliv.*, vol. 12, no. 9, pp. 1547–1563, Sep. 2015.
[46] A. I. Raafat, "Gelatin based pH-sensitive hydrogels for colon-specific oral drug delivery: Synthesis, characterization, and in vitro release study," *J. Appl. Polym. Sci.*, vol. 118, no. 5, pp. 2642–2649, Dec. 2010.
[47] M. A. Farooq *et al.*, "Whey protein: A functional and promising material for drug delivery systems recent developments and future prospects," *Polym. Adv. Technol.*, vol. 30, no. 9, pp. 2183–2191, Sep. 2019.
[48] M. S. Islam *et al.*, "Bioadhesive Food Protein Nanoparticles as Pediatric Oral Drug Delivery System," *ACS Appl. Mater. Interfaces*, vol. 11, no. 20, pp. 18062–18073, May 2019.
[49] H.-K. Ha, S. Rankin, M.-R. Lee, and W.-J. Lee, "Development and Characterization of

Whey Protein-Based Nano-Delivery Systems: A Review," *Molecules*, vol. 24, no. 18, p. 3254, Sep. 2019.
[50] V. Nikam *et al.*, "Eudragit a versatile polymer: A review," *Pharmacologyonline*, vol. 1, pp. 152–164, 2011.
[51] H. Pohlit, I. Bellinghausen, M. Schömer, B. Heydenreich, J. Saloga, and H. Frey, "Biodegradable pH-Sensitive Poly(ethylene glycol) Nanocarriers for Allergen Encapsulation and Controlled Release," *Biomacromolecules*, vol. 16, no. 10, pp. 3103–3111, Oct. 2015.
[52] J. Wu, Y. Shen, W. Jiang, W. Jiang, and Y. Shen, "Magnetic targeted drug delivery carriers encapsulated with pH-sensitive polymer: synthesis, characterization and *in vitro* doxorubicin release studies," *J. Biomater. Sci. Polym. Ed.*, vol. 27, no. 13, pp. 1303–1316, Sep. 2016.
[53] C. Englert *et al.*, "Pharmapolymers in the 21st century: Synthetic polymers in drug delivery applications," *Prog. Polym. Sci.*, vol. 87, pp. 107–164, Dec. 2018.
[54] M. N. U. Nguyen, P. H. L. Tran, and T. T. D. Tran, "A single-layer film coating for colon-targeted oral delivery," *Int. J. Pharm.*, vol. 559, pp. 402–409, Mar. 2019.
[55] M. Z. I. Khan, H. P. Štedul, and N. Kurjaković, "A pH-Dependent Colon-Targeted Oral Drug Delivery System Using Methacrylic Acid Copolymers. II. Manipulation of Drug Release Using Eudragit® L100 and Eudragit S100 Combinations," *Drug Dev. Ind. Pharm.*, vol. 26, no. 5, pp. 549–554, Jan. 2000.
[56] V. C. IBEKWE, M. K. KHELA, D. F. EVANS, and A. W. BASIT, "A new concept in colonic drug targeting: a combined pH-responsive and bacterially-triggered drug delivery technology," *Aliment. Pharmacol. Ther.*, vol. 28, no. 7, pp. 911–916, Oct. 2008.
[57] C. Ji, H. Xu, and W. Wu, "In vitro evaluation and pharmacokinetics in dogs of guar gum and Eudragit FS30D-coated colon-targeted pellets of indomethacin," *J. Drug Target.*, vol. 15, no. 2, pp. 123–131, Jan. 2007.
[58] M. Suhail, P.-C. Wu, and M. U. Minhas, "Development and characterization of pH-sensitive chondroitin sulfate-co-poly(acrylic acid) hydrogels for controlled release of diclofenac sodium," *J. Saudi Chem. Soc.*, vol. 25, no. 4, p. 101212, Apr. 2021.
[59] S.-W. Song, K. Hidajat, and S. Kawi, "pH-Controllable drug release using hydrogel encapsulated mesoporous silica," *Chem. Commun.*, no. 42, p. 4396, 2007.
[60] BASF Pharma, "Brand Family: Kollicoat ®," 2023. [Online]. Available: https://pharma.basf.com/product-families/kollicoat. [Accessed: 14-Jun-2023].
[61] L. Palugan, M. Cerea, L. Zema, A. Gazzaniga, and A. Maroni, "Coated pellets for oral colon delivery," *J. Drug Deliv. Sci. Technol.*, vol. 25, pp. 1–15, Feb. 2015.
[62] C.-H. Yang *et al.*, "Core-shell structure microcapsules with dual pH-responsive drug release function," *Electrophoresis*, vol. 35, no. 18, pp. 2673–2680, Sep. 2014.
[63] D. Thomas, M. S. Latha, and K. K. Thomas, "Synthesis and in vitro evaluation of alginate-cellulose nanocrystal hybrid nanoparticles for the controlled oral delivery of rifampicin," *J. Drug Deliv. Sci. Technol.*, vol. 46, pp. 392–399, Aug. 2018.
[64] H. H. Gadalla, I. El-Gibaly, G. M. Soliman, F. A. Mohamed, and A. M. El-Sayed, "Amidated pectin/sodium carboxymethylcellulose microspheres as a new carrier for colonic drug targeting: Development and optimization by factorial design," *Carbohydr. Polym.*, vol. 153, pp. 526–534, Nov. 2016.
[65] H. H. Gadalla, G. M. Soliman, F. A. Mohammed, and A. M. El-Sayed, "Development and in vitro/in vivo evaluation of Zn-pectinate microparticles reinforced with chitosan for the

colonic delivery of progesterone," *Drug Deliv.*, vol. 23, no. 7, pp. 2541–2554, Sep. 2016.
[66] G. K. Vinner, G. T. Vladisavljević, M. R. J. Clokie, and D. J. Malik, "Microencapsulation of Clostridium difficile specific bacteriophages using microfluidic glass capillary devices for colon delivery using pH triggered release," *PLoS One*, vol. 12, no. 10, p. e0186239, Oct. 2017.
[67] J. Gan *et al.*, "Orally administrated nucleotide-delivery particles from microfluidics for inflammatory bowel disease treatment," *Appl. Mater. Today*, vol. 25, p. 101231, Dec. 2021.
[68] M. M. Hasani-Sadrabadi *et al.*, "Microfluidic Manipulation of Core/Shell Nanoparticles for Oral Delivery of Chemotherapeutics: A New Treatment Approach for Colorectal Cancer," *Adv. Mater.*, vol. 28, no. 21, pp. 4134–4141, Jun. 2016.
[69] P. Shrimal, G. Jadeja, and S. Patel, "Ultrasonic enhanced emulsification process in 3D printed microfluidic device to encapsulate active pharmaceutical ingredients," *Int. J. Pharm.*, vol. 620, p. 121754, May 2022.
[70] B. Homayun, A. Kumar, P. T. H. Nascimento, and H.-J. Choi, "Macropored microparticles with a core–shell architecture for oral delivery of biopharmaceuticals," *Arch. Pharm. Res.*, vol. 41, no. 8, pp. 848–860, Aug. 2018.
[71] P. C. Naha, V. Kanchan, P. K. Manna, and A. K. Panda, "Improved bioavailability of orally delivered insulin using Eudragit-L30D coated PLGA microparticles," *J. Microencapsul.*, vol. 25, no. 4, pp. 248–256, Jan. 2008.
[72] M. K. Chourasia and S. K. Jain, "Design and Development of Multiparticulate System for Targeted Drug Delivery to Colon," *Drug Deliv.*, vol. 11, no. 3, pp. 201–207, Jan. 2004.
[73] S. K. Umadevi, R. Thiruganesh, S. Suresh, and K. B. Reddy, "Formulation and evaluation of chitosan microspheres of aceclofenac for colon-targeted drug delivery," *Biopharm. Drug Dispos.*, vol. 31, no. 7, pp. 407–427, Sep. 2010.
[74] A. vaidya, A. Jain, P. Khare, R. K. Agrawal, and S. K. Jain, "Metronidazole loaded pectin microspheres for colon targeting," *J. Pharm. Sci.*, vol. 98, no. 11, pp. 4229–4236, Nov. 2009.
[75] S. A. Kleinubing *et al.*, "Gastro-resistant controlled release of OTC encapsulated in alginate/chitosan matrix coated with acryl-EZE® MP in fluidized bed," *J. Appl. Polym. Sci.*, vol. 131, no. 12, p. n/a-n/a, Jun. 2014.
[76] M. S. Crcarevska, M. G. Dodov, G. Petrusevska, I. Gjorgoski, and K. Goracinova, "Bioefficacy of budesonide loaded crosslinked polyeletrolyte microparticles in rat model of induced colitis," *J. Drug Target.*, vol. 17, no. 10, pp. 788–802, Dec. 2009.
[77] P. C. Ferrari *et al.*, "Development and in vitro evaluation of coated pellets containing chitosan to potential colonic drug delivery," *Carbohydr. Polym.*, vol. 91, no. 1, pp. 244–252, Jan. 2013.
[78] Y. Xu, F. Qu, Y. Wang, H. Lin, X. Wu, and Y. Jin, "Construction of a novel pH-sensitive drug release system from mesoporous silica tablets coated with Eudragit," *Solid State Sci.*, vol. 13, no. 3, pp. 641–646, Mar. 2011.
[79] K. Dewettinck and A. Huyghebaert, "Fluidized bed coating in food technology," *Trends Food Sci. Technol.*, vol. 10, no. 4–5, pp. 163–168, Apr. 1999.
[80] A. Sattari and P. Hanafizadeh, "Controllable preparation of double emulsion droplets in a dual-coaxial microfluidic device," *J. Flow Chem.*, vol. 11, no. 4, pp. 807–821, Dec. 2021.
[81] Y. Liu *et al.*, "A review on emulsification via microfluidic processes," *Front. Chem. Sci. Eng.*, vol. 14, no. 3, pp. 350–364, Jun. 2020.

[82] F. M. White, *Fluid Mechanics*, 8th ed. McGraw Hill Education, 2016.
[83] T. M. Squires and S. R. Quake, "Microfluidics: Fluid physics at the nanoliter scale," *Rev. Mod. Phys.*, vol. 77, no. 3, pp. 977–1026, Oct. 2005.
[84] P. Zhu and L. Wang, "Passive and active droplet generation with microfluidics: a review," *Lab Chip*, vol. 17, no. 1, pp. 34–75, 2017.
[85] S. Okushima, T. Nisisako, T. Torii, and T. Higuchi, "Controlled Production of Monodisperse Double Emulsions by Two-Step Droplet Breakup in Microfluidic Devices," *Langmuir*, vol. 20, no. 23, pp. 9905–9908, Nov. 2004.
[86] C.-X. Zhao, "Multiphase flow microfluidics for the production of single or multiple emulsions for drug delivery," *Adv. Drug Deliv. Rev.*, vol. 65, no. 11–12, pp. 1420–1446, Nov. 2013.
[87] V. Barbier, M. Tatoulian, H. Li, F. Arefi-Khonsari, A. Ajdari, and P. Tabeling, "Stable Modification of PDMS Surface Properties by Plasma Polymerization: Application to the Formation of Double Emulsions in Microfluidic Systems," *Langmuir*, vol. 22, no. 12, pp. 5230–5232, Jun. 2006.
[88] A. R. Abate, A. T. Krummel, D. Lee, M. Marquez, C. Holtze, and D. A. Weitz, "Photoreactive coating for high-contrast spatial patterning of microfluidic device wettability," *Lab Chip*, vol. 8, no. 12, p. 2157, 2008.
[89] W.-A. C. Bauer, M. Fischlechner, C. Abell, and W. T. S. Huck, "Hydrophilic PDMS microchannels for high-throughput formation of oil-in-water microdroplets and water-in-oil-in-water double emulsions," *Lab Chip*, vol. 10, no. 14, p. 1814, 2010.
[90] M. Zhang *et al.*, "Controllable microfluidic strategies for fabricating microparticles using emulsions as templates," *Particuology*, vol. 24, pp. 18–31, Feb. 2016.
[91] E. E. Ekanem, Z. Zhang, and G. T. Vladisavljević, "Facile microfluidic production of composite polymer core-shell microcapsules and crescent-shaped microparticles," *J. Colloid Interface Sci.*, vol. 498, pp. 387–394, Jul. 2017.
[92] W. Li *et al.*, "Microfluidic fabrication of microparticles for biomedical applications," *Chem. Soc. Rev.*, vol. 47, no. 15, pp. 5646–5683, 2018.
[93] P. Garstecki, M. J. Fuerstman, H. A. Stone, and G. M. Whitesides, "Formation of droplets and bubbles in a microfluidic T-junction—scaling and mechanism of break-up," *Lab Chip*, vol. 6, no. 3, p. 437, 2006.
[94] P. Zhu, T. Kong, Z. Kang, X. Tian, and L. Wang, "Tip-multi-breaking in Capillary Microfluidic Devices," *Sci. Rep.*, vol. 5, no. 1, p. 11102, Sep. 2015.
[95] B.-U. Moon, N. Abbasi, S. G. Jones, D. K. Hwang, and S. S. H. Tsai, "Water-in-Water Droplets by Passive Microfluidic Flow Focusing," *Anal. Chem.*, vol. 88, no. 7, pp. 3982–3989, Apr. 2016.
[96] A. R. Abate and D. A. Weitz, "High-Order Multiple Emulsions Formed in Poly(dimethylsiloxane) Microfluidics," *Small*, vol. 5, no. 18, pp. 2030–2032, Sep. 2009.
[97] T. Fu, Y. Wu, Y. Ma, and H. Z. Li, "Droplet formation and breakup dynamics in microfluidic flow-focusing devices: From dripping to jetting," *Chem. Eng. Sci.*, vol. 84, pp. 207–217, Dec. 2012.
[98] S. L. Anna and H. C. Mayer, "Microscale tipstreaming in a microfluidic flow focusing device," *Phys. Fluids*, vol. 18, no. 12, p. 121512, Dec. 2006.
[99] P. Zhu, X. Tang, and L. Wang, "Droplet generation in co-flow microfluidic channels with vibration," *Microfluid. Nanofluidics*, vol. 20, no. 3, p. 47, Mar. 2016.
[100] S. Bazban-Shotorbani, E. Dashtimoghadam, A. Karkhaneh, M. M. Hasani-Sadrabadi, and

K. I. Jacob, “Microfluidic Directed Synthesis of Alginate Nanogels with Tunable Pore Size for Efficient Protein Delivery,” *Langmuir*, vol. 32, no. 19, pp. 4996–5003, May 2016.
[101] Z.-Z. Li, L.-X. Wen, L. Shao, and J.-F. Chen, “Fabrication of porous hollow silica nanoparticles and their applications in drug release control,” *J. Control. Release*, vol. 98, no. 2, pp. 245–254, Aug. 2004.
[102] X. Qi, L. Wang, J. Zhu, Z. Hu, and J. Zhang, “Self-double-emulsifying drug delivery system (SDEDDS): A new way for oral delivery of drugs with high solubility and low permeability,” *Int. J. Pharm.*, vol. 409, no. 1–2, pp. 245–251, May 2011.
[103] L.-Y. Chu, A. S. Utada, R. K. Shah, J.-W. Kim, and D. A. Weitz, “Controllable Monodisperse Multiple Emulsions,” *Angew. Chemie Int. Ed.*, vol. 46, no. 47, pp. 8970–8974, Dec. 2007.
[104] W. Yu, B. Li, X. Liu, and Y. Chen, “Hydrodynamics of triple emulsion droplet generation in a flow-focusing microfluidic device,” *Chem. Eng. Sci.*, vol. 243, p. 116648, Nov. 2021.
[105] M. Jeyhani, R. Thevakumaran, N. Abbasi, D. K. Hwang, and S. S. H. Tsai, “Microfluidic Generation of All-Aqueous Double and Triple Emulsions,” *Small*, vol. 16, no. 7, p. 1906565, Feb. 2020.
[106] H. Chen, J. Li, J. Wan, D. A. Weitz, and H. A. Stone, “Gas-core triple emulsions for ultrasound triggered release,” *Soft Matter*, vol. 9, no. 1, pp. 38–42, 2013.
[107] M. G. Bulmer, *Principles of Statistics* . Edinburgh: Oliver & Boyd, 1965.
[108] Stan Brown, “Measures of Shape: Skewness and Kurtosis,” 17-Mar-2022. [Online]. Available: https://brownmath.com/stat/shape.htm. [Accessed: 12-Jul-2023].
[109] M. Danaei *et al.*, “Impact of Particle Size and Polydispersity Index on the Clinical Applications of Lipidic Nanocarrier Systems,” *Pharmaceutics*, vol. 10, no. 2, p. 57, May 2018.
[110] G. Bradski, “The OpenCV Library,” *Dr. Dobb’s Journal of Software Tools*. 2000.
[111] E. Jones and T. E. Oliphant, “SciPy: Open Source Scientific Tools for Python.” 2001.
[112] C. R. Harris, K. J. Millman, and S. J. Van der Walt, “Array programming with NumPy,” *Nature*, vol. 585, pp. 357–362, Sep. 2020.
[113] J. D. Hunter, “Matplotlib: A 2D Graphics Environment,” *Comput. Sci. Eng.*, vol. 9, no. 3, pp. 90–95, 2007.

# Appendix A: Spot Plating Protocol

Protocol by: Juan Burckhardt (UBC)

## Materials:

- Overnight culture of your bacteria of interest (**You want your bacteria to be in the stable phase after overnight incubation**)
- Media that supports the growth of your bacteria (LB for *E. coli*)
- Plates that support the growth of your bacteria (LB-agar plates)
    - To make LB agar plates: Mix LB powder with agar (15g/L), add stirring bar and mix well (remove all clumps), autoclave (Liquid 30), slowly stir after autoclaving until media bottle can be handled, pour plates aseptically and allow to dry overnight before storing at 4°C.
- Sterile PBS
- Multichannel pipette (2-20uL and 20-200uL) – **if available**
- 20-200uL pipette
- Pipette tips (10uL tips and 200uL tips)
- Reservoir
- Incubator at 37°C
- Spectrophotometer

# Protocol:

**Day 1:**

1. Inoculate a colony of your bacterium of interest in media that will support its growth. Incubate overnight in the required growth conditions (37°C for *E. coli*)
    - It would be best to inoculate in an appropriate volume such that you have enough volume of culture to subculture the next day (5mL is usually okay).
    - You should allow the bacteria to grow completely to a stable phase of growth.

**Day 2:**

Before starting your experiment, plan out how many timepoints you will need to do. Usually, you will need timepoints that will tell you about each phase of growth. For fast-growing bacteria, timepoints every 30-60 minutes should be fine! (For *E. coli,* I would recommend: 1h, 2h, 3h, 4h, 6h, 8h, 20h)

1. Using a multichannel pipette (20-200uL) and a reservoir fill up two 96-well plate with 180uL of sterile PBS per well. These plates will be used for your **10-fold serial dilutions and your spot plating**.
    - In one of the plates, you will run you *E. coli* control (base media) and in the other the your treatment group (If you had more than one condition, you could use more plates)
2. Subculture your overnight culture sufficiently diluted so that your bacterium of interest is able to go through every phase of growth (lag phase, exponential phase and stable phase). **Typically, you would do a 1:10-1:100 dilution.** Incubate at 37°C while shaking.
    - Subculture into enough volume as you will be taking aliquots from this same culture throughout the whole day (anywhere from 20-50mL should be fine).
    - Plate the media you are be using to grow your bacterium into a plate that will support the growth of your bacterium to check for contamination! Do this after you have filled your 96-well plate.
3. **For Spot plating:** From your subculture, take a 20uL sample and use the 96-well plate you filled in step 1 to do 10-fold dilutions of that sample in the first column of your plate (20uL into 180uL). Do the dilutions column-wise (Not in a row). **When making your serial dilutions make sure to pipette at least 10 times up and down to make sure the well is completely mixed and change pipette tips after every dilution step!**
4. Using the 2-10uL multichannel pipette, spot-plate 5ul (depending on the space you have) of the column of your 10-fold dilutions into a labelled plate in duplicates or triplicates (See diagram). Allow the plate to dry before flipping it over (agar-side up) and incubating until you are able to see well-defined colonies (**Most of the time, this is overnight)**.
    - Once you spot plate, don't move the plate aggressively!

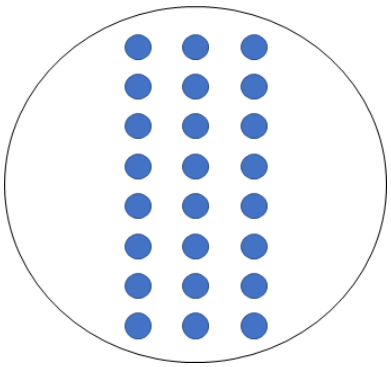

5. **For OD600 readings:** From your subculture, take a 200uL aliquot and dispense it onto an empty well of a 96-well plate (**Not the one you filled in step 1**). In that same 96-well plate, dispense 200uL of media into another empty well (you will subtract the OD600 of the media well from your sample reading to account for the background of the media).
    - Use a plate reader to read the absorption (OD600) of the blank media and your sample well.
    - Subtract your blank sample from your media to get your OD reading.
    - **Note:** If plate reader nor available, use a spectrophotometer
    - **Note:** If the OD600 of your sample is **higher than 0.5**, dilute your sample into another well (1:2-1:10) and re-read that well. This will help you get a more accurate read.

**NOTE:** When you do steps 4-6, **quickly** take the aliquots you need from your subculture and put the subculture back into the incubator (**You want to disrupt the growth of your bacteria as least as possible**).

6. Incubate your sample until another timepoint is met and repeat steps 4-6. **Once you reach higher timepoints you will probably need to do more dilutions (up to 10^-9 or 10^-10). You can do these dilutions in the empty 96-well plate you are using to do your OD600 reading (i.e. do the initial 10^-1 dilution on a well of the empty plate and then use that dilution to do your 10-fold dilutions on your spot plate)**
7. The next day (**or once you have defined colonies in your plate**) count the colonies in the lowest dilution where there is a range of **5-50 colonies**, average your replicates and calculate CFU/mL.
    - The following link explains you how to calculate CFU per mL from a dilution: https://sciencing.com/measure-bacterial-growth-petri-dishes-5837896.html
    - **Example:** For timepoint 3, you plated 10uL of your 10-fold serial dilutions and after 1 day you saw countable colonies in row 4 of your spot plates (which is 1:10000).
        i. **Replicate 1:** 10 colonies
        ii. **Replicate 2:** 14 colonies
        iii. $\frac{CFU}{mL} = \frac{\frac{Replicate\ 1 + Replicate\ 2}{2}}{Volume\ plated\ in\ mL * dilution} = \frac{\frac{10\ CFU + 14\ CFU}{2}}{0.010\ mL * 0.0001} = 12x10^6\ CFU/mL$

8. Graph OD600 and CFU/mL vs. time

# Appendix B : Microparticle Detection Python Code

## B.1: Particle Counting Function

```python
import cv2
import numpy as np
import matplotlib.pyplot as plt
import sys
from scipy.ndimage import gaussian_filter


def count_particles_gen(file,smin,smax, droplet_area, examined_area, particle_weight,t_l,t_h,kern):

    #Read in image
    img = cv2.imread(file)

    #Convert image to grayscale
    gray_image = cv2.cvtColor(img, cv2.COLOR_BGR2GRAY)
    count = 0

    #Crop image to a 468x468 pixel square and reverse grayscale values
    cropped_image = 255-gray_image[1100:1568,1400:1868]

    #Subtract off the median value of the image to better define the particles against the background
    cropped_image = np.array(cropped_image,dtype=np.float64)
    cropped_image -= np.median(cropped_image)

    #Smooth image, subtract off any brighter regions to generate relative brightness of particles, further define particles
    cropped_image_temp = gaussian_filter(cropped_image, kern,truncate=100)
    cropped_image -= cropped_image_temp
    cropped_image = gaussian_filter(cropped_image, 0.85,truncate=100)

    #set threshold values to convert to binary image and isolate particles
    th, threshed = cv2.threshold(cropped_image, t_l, t_h,cv2.THRESH_BINARY)

    # Set up the detector with default parameters.
    im = np.uint8(255-threshed.copy())
    detector = cv2.SimpleBlobDetector()

    # Set up the SimpleBlobDetector with default parameters
    params = cv2.SimpleBlobDetector_Params()

    # Set the threshold
    params.minThreshold = 0
    params.maxThreshold = 256
```

```python
    # Filter by Area
    params.filterByArea = True
    params.minArea = 1
    params.maxArea = 100

    # Filter by Circularity
    params.filterByCircularity = True
    params.minCircularity = 0.1

    # Filter by Convexity
    params.filterByConvexity = True
    params.minConvexity = 1e-5

    # Filter by Inertia
    params.filterByInertia = True
    params.minInertiaRatio = 1e-5

    # Define minimum distance between blobs
    params.minDistBetweenBlobs = 1

    # Create detector using parameters defined above
    detector = cv2.SimpleBlobDetector_create(params)

    # Detect blobs
    keypoints = detector.detect(im)

    #outline particles detected in threshold binary image
    im_with_keypoints = cv2.drawKeypoints(im, keypoints, np.array([]), (256,0,0), cv2.DRAW_MATCHES_FLAGS_DRAW_RICH_KEYPOINTS)

    print(len(keypoints))

    #calculation of 100% conc. particles
    conc_stock = 4.55e10
    conc_polymer_stock = conc_stock*0.05
    total_conc = particle_weight*conc_polymer_stock
    particles_per_area_100p = total_conc*(0.2e-3)*(examined_area/droplet_area)

    #calculation of conc. in area of droplet
    final_conc = (len(keypoints)/particles_per_area_100p)*100

    return final_conc
```

## B.2: Snippet of Function Call

```
import cv2
import numpy as np
import matplotlib.pyplot as plt
import sys
from Count_particles_pipeline_v2 import count_particles_gen
from scipy.ndimage import gaussian_filter
from tqdm.notebook import tqdm

#examined area in mm2
examined_area = (200e-3)**2
#droplet volume in ml
droplet_vol = 0.2e-3

#weight of particles added to each tube
acidic_weight = 0.0418
neutral_weight = 0.0576

#thresholding values and kernel for smoothing images
t_l = 10
t_h = 255
kern  =25

#surface areas of flattened droplets
acidic_area_mins = [[4.592, 7.311, 6.685] , [10.086, 19.83, 14.137]]
acidic_area_hrs = [[4.516, 6.832, 6.014], [5.479, 5.636, 20.769], [11.957, 7.027, 10.106], [8.287, 11.668, 11.286], [7.563, 4.397,
12.361], [2.389, 8.296, 9.497]]
neutral_area_mins = [[5.063, 8.662, 4.663] , [20,10.26,18.597]]
neutral_area_hrs = [[6.5, 8.279, 15.345], [7.058,4.716,7.399], [2.957, 8.478, 3.411], [8.149, 6.647, 11.151], [5.587, 10.951,
6.975], [9.325, 13.7, 13.339]]

#computing average surface area
combined_all = np.vstack([acidic_area_mins, acidic_area_hrs, neutral_area_mins, neutral_area_hrs])
mean_surf_area = np.mean(combined_all)

#initializing for loop for hour measurements
percent_n_hrs = np.zeros((6,9))#[]
percent_a_hrs = np.zeros((6,9)) #[]

#for loop to calculate number of particles detected in 9 images for each time point (hours)
for i in tqdm(range(1,7)):
    ind = 0
    for j in range(1,4):
        for k in range(1, 4):
            #neutral
            filename_n ='071723 neutral '+str(i)+' hr drop '+str(j)+'_000'+str(k)+' Annotated 1_jpg_oaf.JPG'
            temp_area_n = mean_surf_area
            percent_n_hrs[i-1,ind] = count_particles_gen(filename_n, temp_area_n, examined_area, neutral_weight, t_l, t_h, kern)
            #acidic
            filename_a ='071723 acidic '+str(i)+' hr drop '+str(j)+'_000'+str(k)+' Annotated 1_jpg_oaf.JPG'
            temp_area_a = mean_surf_area
            percent_a_hrs[i-1,ind] = count_particles_gen(filename_a, temp_area_a, examined_area, acidic_weight, t_l, t_h, kern)
            print(i, j, k, percent_n_hrs[i-1,ind])
            ind+=1

```

## B.3: Example of Particle Detection

The data shown in the following example was from the 5-hour time point of the basic data set in trial 3 (see Chapter 4). Note that the purple and orange colouring is simply a change in colour scale to improve visibility over the original green and black.

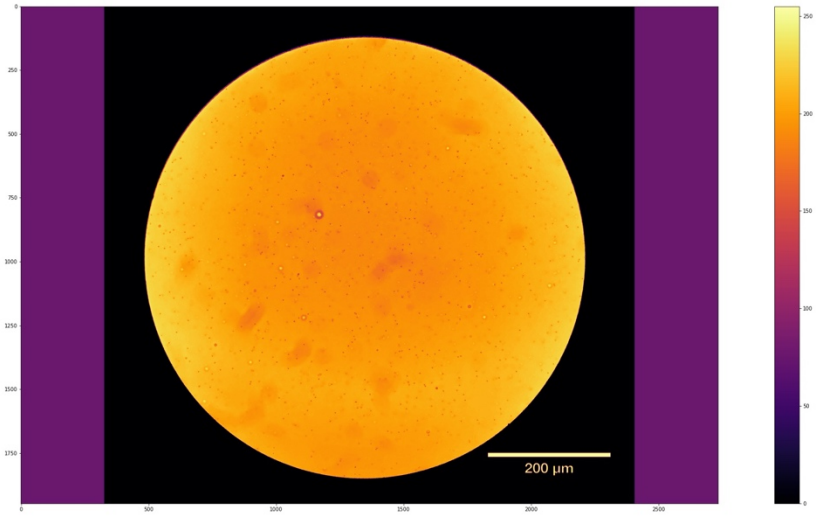


*Figure B 1: Full-size image*

Figure B1 shows the full-size image as taken on the microscope. The color scale has been changed to enhance visibility.

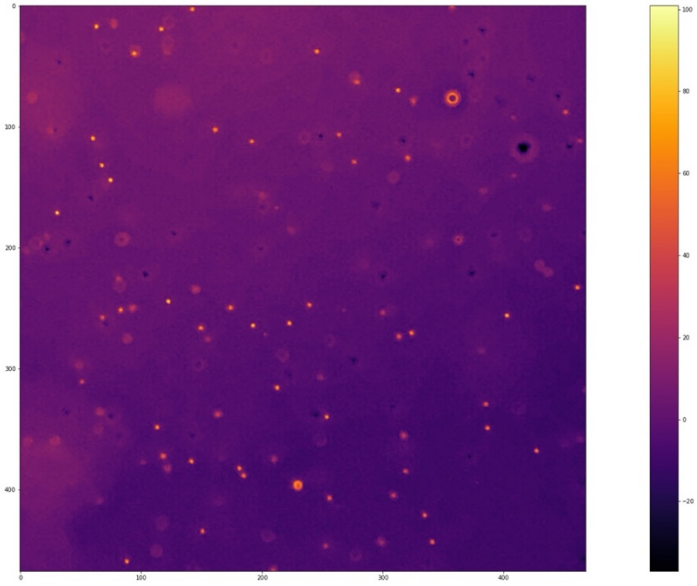

*Figure B 2: Cropped image*

Figure B2 shows the same image, cropped to an area of 200x200 µm, or 468x468 pixels. These values were chosen based on the scale bar in Figure B1.

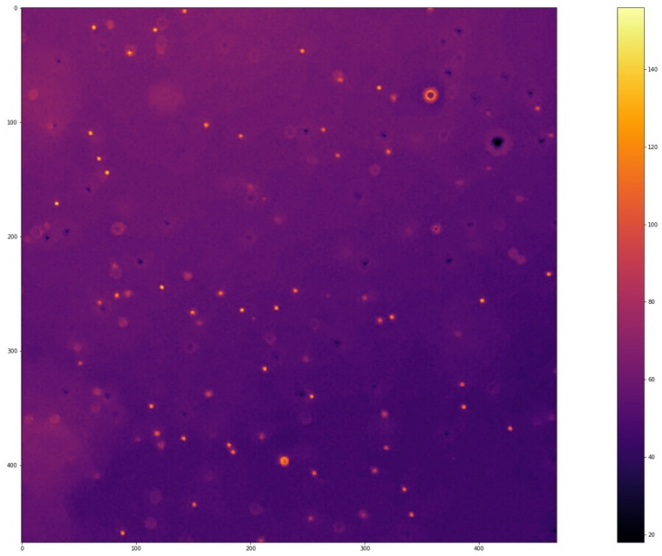

*Figure B 3: Cropped image with median brightness subtracted off*

Figure B3 shows the cropped image with the median brightness of the image subtracted off. It is a minor change in this case, but the difference can be distinct in images with more background noise.

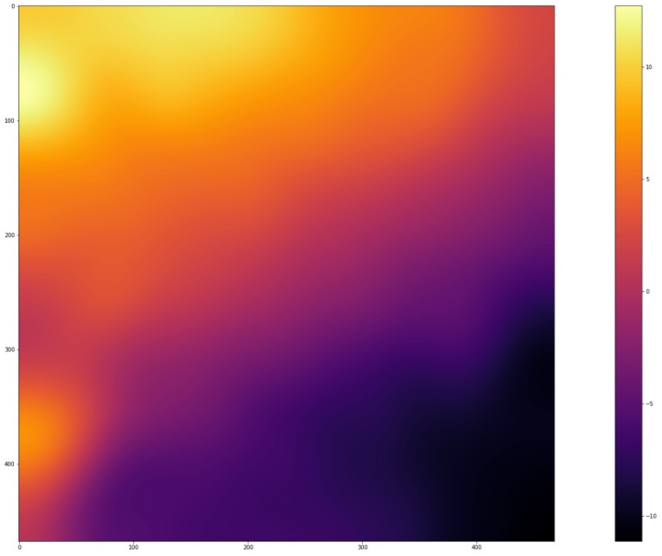

*Figure B 4: Gaussian smoothing to generate relative brightness*

Figure B4 shows the Gaussian smoothing that is subtracted off from the final image. Utilizing this smoothing step helps to define a relative brightness from which particles can be identified, as opposed to absolute values. This is important as particles that are located in areas of less contrast may not otherwise be identified.

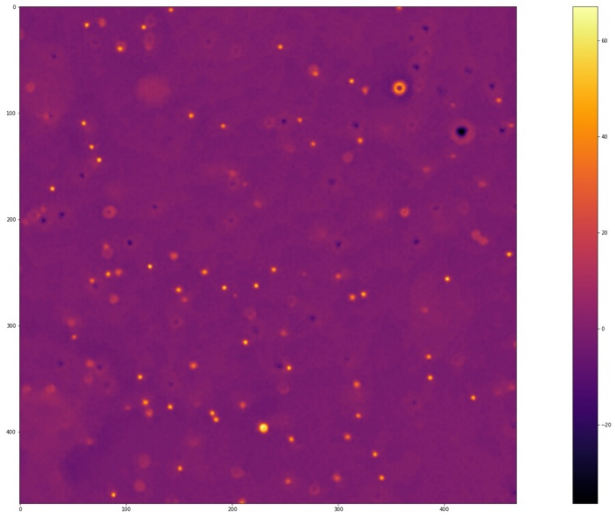

*Figure B 5: Image with Gaussian blur removed*

Figure B5 shows the cropped image after the Gaussian smoothing has been applied (and subtracted off). Note the consistent shade of the background compared to the gradient in Figure B3.

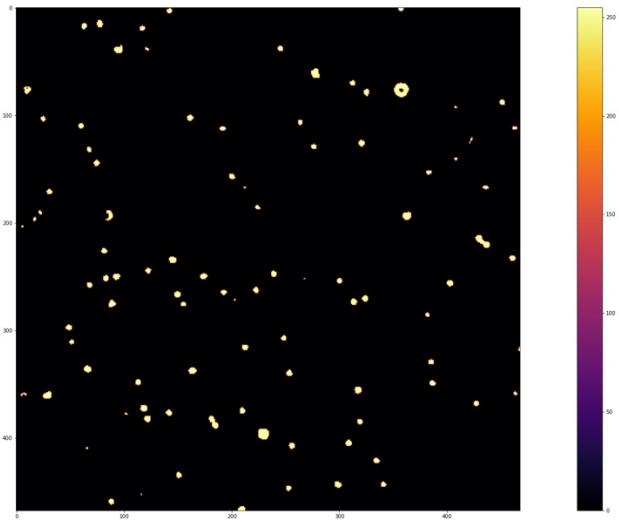

*Figure B 6: Binary image with detected particles based on threshold*

Figure B6 shows the image converted to binary, after thresholding has been applied. Gold dots in this image represent all particles (or bubbles) that have a binary value higher than 10.

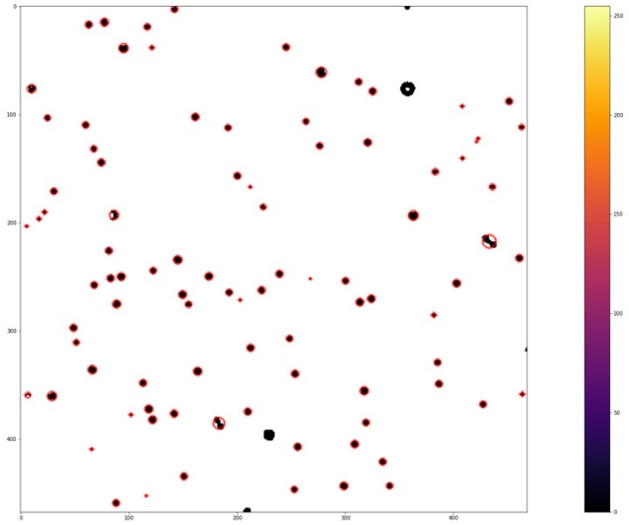


*Figure B 7: Detected particles (circled in red) based on size and shape parameters*

Finally, Figure B7 shows the particles in the binary image that are counted by the algorithm. All black dots that are outlined in red are particles that are added to the count. The algorithm filters by size to avoid counting bubbles.